

POLITECNICO DI TORINO

Collegio di Ingegneria Chimica e dei Materiali

**Corso di Laurea Magistrale
in Ingegneria Chimica e dei Processi Sostenibili**

Tesi di Laurea Magistrale

The role of zinc oxide nanostructures as antimicrobial and biocompatible agents



Relatore

Prof. Valentina Alice Cauda

Candidato

Pasquale Sanvitale

Correlatori

Prof. Montserrat Colilla

Prof. Isabel Izquierdo Barba

Marzo 2018

Table of contents

Riassunto	VI
1 Introduction	1
1.1 Bone implants: introduction to the problem.....	2
1.2 Pathogenesis of implant infections	2
1.3 Solutions for implant infections	2
1.4 Nanomaterials for infection control.....	3
1.5 Antibacterial nanostructures.....	3
1.6 Inorganic nanostructures	4
1.7 ZnO introduction and properties.....	5
1.8 ZnO Synthesis Techniques.....	6
1.9 ZnO nanostructures.....	6
1.10 ZnO applications.....	7
1.11 ZnO biocompatibility and osseointegration properties.....	7
1.12 ZnO antimicrobial activity	8
2 Materials and Methods	10
2.1 Materials.....	10
2.1.1 Preparation of ZnO NPs via Microwave synthesis	10
2.1.2 Functionalization.....	10
2.1.3 Preparation of Nanoparticles suspensions	11
2.1.4 Preparation of porous ZnO thin film.....	11
2.2 Morphological and structural characterization.....	13
2.2.1 X-Ray Diffraction –XRD	13
2.2.2 Analysis of colloidal stability	13
2.2.3 Transmission electron microscope -TEM	14
2.2.4 X-ray diffraction for ZnO Porous Film.....	15
2.2.5 Field emission scanning electron microscopy - FESEM.....	15
2.3 Cellular studies	16
2.3.1 Cell culture conditions.....	16
2.3.2 Cell trypsinization	16
2.3.3 Cytotoxicity	18
2.3.4 Cytotoxicity test-LDH.....	18
2.3.5 Mitochondrial activity – MTT	19
2.3.6 Cell morphology studies.....	19
2.3.7 Differentiation assay: Alkaline phosphatase activity – ALP.....	19

2.3.8	Differentiation assay: Total protein content	21
2.4	Antibacterial Studies	23
2.4.1	Bacteria culture conditions	23
2.4.2	CFU counting method	23
2.4.3	Preparation of Agar plates	24
2.4.4	Preparation of bacteria suspensions	24
2.4.5	CFU counting method procedure	24
2.4.6	Bacterial Adhesion and biofilm formation	25
2.4.7	Morphologies studies-SEM	25
2.4.8	Biofilm assay	26
2.4.9	Statistical analysis	26
3	Results and discussion	27
3.1	Morphological and structural characterization of ZnO NPs	27
3.1.1	X-Ray diffraction	27
3.1.2	Analysis of colloidal stability	28
3.1.3	Transmission electron microscope –TEM.....	29
3.2	Morphological and structural characterization of porous ZnO film.....	31
3.2.1	X-ray diffraction	31
3.2.2	Field-emission scanning electron microscopy	31
3.3	Cellular studies	34
3.3.1	Cytotoxicity test-LDH.....	34
3.3.2	Cell proliferation.....	35
3.3.3	ZnO film biocompatibility.....	37
3.3.4	Cell proliferation at 70% of confluence	38
3.3.5	Cell morphology studies.....	40
3.3.6	Differentiation assay: Alkaline Phosphatase	42
3.3.7	Total protein content and cell morphology.....	43
3.3.8	Differentiation assay for porous ZnO film: Alkaline phosphatase and total protein content.....	47
3.4	Antibacterial studies.....	49
3.4.1	CFU counting method	49
3.4.2	Biofilm assay	53
3.4.3	Bacterial adhesion and biofilm formation	55
	Conclusions.....	58
	Bibliography	60
	Ringraziamenti.....	64
	List Of Figures	65

List Of Tables 68

Riassunto

Introduzione

Durante il ventesimo secolo, le infezioni erano la causa maggiore di morte al mondo. L'introduzione degli antibiotici nei primi anni del 1900 ha portato ad un notevole miglioramento delle condizioni di vita. Nonostante ciò, negli ultimi anni si è manifestata una preoccupante resistenza agli antibiotici. In particolare, la maggior parte degli *Stafilococchi aureus* è resistente alla Meticillina, mentre una piccola quantità di loro risulta resistente anche alla Vancomicina, che rappresenta l'antibiotico più avanzato per questo tipo di infezioni. Inoltre, in Germania è stato isolato un nuovo ceppo di *Escherichia coli* che ha mostrato caratteristiche infettive mai viste prima. Oltre al problema della resistenza agli antibiotici, le infezioni croniche come quelle polmonari e quelle associate a innesti ossei rappresentano un grave pericolo per la salute dell'uomo. Negli ultimi anni infatti, è sempre più pratica comune ridurre le fratture per via chirurgica ricorrendo a protesi oppure viti, perni per fissare i lembi di osso fratturato. Nonostante il notevole miglioramento degli standard di sterilità e l'impiego di personale altamente specializzato, si registrano ancora numerosi casi di infezione che oscillano in range tra lo 0,5 il 5 % del totale delle operazioni.

Riguardo il meccanismo infettivo, l'introduzione di un corpo estraneo e i micromovimenti di esso, rendono debole il tessuto e le cellule circostanti, abbassando le difese immunitarie e creando terreno fertile per un'infezione da parte di batteri contenuti nella pelle e nella mucosa. Inizialmente, questi microrganismi si assorbono passivamente sulla superficie dell'osso ma col passare del tempo riescono a formare una matrice di polisaccaridi chiamata biofilm.

Il biofilm protegge i batteri al suo interno, ostacolando l'azione degli antibiotici. Le infezioni da biofilm sono causate per il 34% dallo *Stafilococco aureus*, il 32 % dallo *Stafilococco epidermidis* e il resto da altri ceppi batterici. Pertanto, è lampante la dipendenza di queste dal ceppo degli Stafilococchi, che risultano essere, quindi, tra gli organismi più resistenti al trattamento antibiotico. Tutte queste caratteristiche rendono molto difficile il trattamento delle Osteomeliti (infezioni ossee). Le conseguenze sono molto serie e si traducono in una prolungata ospedalizzazione, con aumento del trauma e dei costi sanitari per il paziente. Inoltre, nei casi più gravi, è necessario rimuovere la protesi o l'impianto per sradicare l'infezione. Per questo, negli ultimi anni, sono stati fatti numerosi sforzi per trovare nuovi materiali e nuove terapie da impiegare per far fronte al problema. Le strategie per più utilizzate, implicano l'utilizzo di materiali capaci di favorire le funzioni esplicate degli osteoblasti e sfavorire l'adesione dei batteri sulla sua superficie.

In particolare, è di vitale importanza il processo di osteointegrazione. Esso coinvolge numerosi aspetti ed è governato dagli osteoblasti, i quali prima devono aderire alla superficie, poi proliferare ed infine differenziarsi per depositare il contenuto di calcio necessario per la rigenerazione dell'osso. Per favorire questo processo, il biomateriale deve presentare particolari caratteristiche chimiche e topografiche. Riguardo le caratteristiche chimiche, i metalli (titanio, CoMoCr), i polimeri ed i ceramici (allumina, titania, idrossipatite) mostrano proprietà molto interessanti. A queste però devono essere aggiunte particolari caratteristiche topografiche, quali la microrugosità, che permettano di migliorare le performance biologiche. Tra le varie proprietà che un materiale deve possedere, non si può non citare la dimensione di essi. I biomateriali devono avere dimensioni del nanometro perché i componenti naturali dell'osso come minerali, fosfato di calcio e collagene sono molto piccoli, appunto dell'ordine del nanometro. Pertanto, le dimensioni svolgono un ruolo fondamentale, in quanto nanomateriali possono simulare meglio i componenti dell'osso e favorire la sua ricrescita. Visto quanto sopra,

progettare un materiale per queste applicazioni (scaffold) richiede numerosi proprietà tra cui sicuramente biocompatibilità, caratteristiche antibatteriche e facilità di manipolazione.

Nanoantibiotici

Negli ultimi anni, numerosi scaffold ibridi sono stati progettati combinando polimeri, metalli e ceramici in forma di nanomateriali.

Secondo la IUPAC e la FDA, per definire un nanomateriale, esso deve mostrare almeno una dimensione inferiore ai 100 nanometri. Questa caratteristica implica un'ampia area superficiale specifica e quindi un maggior numero di atomi esposti in superficie. Il loro impiego in campo medico è assai diffuso ed il settore dove trovano maggiore applicazione è l'oncologia, seguito poi dalla cura delle infezioni ed infine trattamento di malattie cardiovascolari e Alzheimer.

I Nanoantibiotici, oltre ad avere un'elevata area superficiale specifica, presentano numerosi vantaggi. Infatti, essi possono essere ingegnerizzati e liberare il farmaco o l'agente antibatterico una volta arrivato a destinazione, grazie a stimoli quali pH, ultrasuoni, calore, ecc. Inoltre, presentano minori effetti collaterali in confronto ai normali antibiotici e possono consentire una prolungata circolazione del farmaco, migliorando i target terapeutici e consentendo un rilascio controllato di esso. In ultimo, sono facili da preparare e poco costosi cosa che li rende particolarmente interessanti. Nonostante tutti questi vantaggi, essi presentano anche degli svantaggi. In particolare, la limitata conoscenza della loro tossicità nei confronti di cellule, tessuti e organi, rende il loro impiego lento per la necessità di eseguire test di biocompatibilità. L'accumularsi di nanoparticelle nei tessuti e negli organi rappresenta un ulteriore problema poiché il corpo umano non sempre è in grado di smaltire queste sostanze. I Nanomateriali usati come nanoantibiotici, possono essere organici ed inorganici. Per quanto concerne gli organici, essi sono quelli più studiati e racchiudono liposomi, nanoparticelle polimeriche e micelle polimeriche. Il vantaggio delle particelle organiche è rappresentato da un'elevata biodegradabilità e biocompatibilità. Per quanto concerne le particelle inorganiche composte da metalli o ossidi metallici presentano dimensioni più piccole rispetto a quelle inorganiche e possono essere caricate con grandi quantità di farmaco. Le nanostrutture inorganiche presentano una notevole attività antimicrobica perché riescono a produrre per via fotocatalitica i ROS (reactive oxygen species) che danneggiano le cellule, compromettendo la membrana cellulare dei batteri, inibendo l'attività enzimatica e la sintesi del DNA. In aggiunta, particelle metalliche possono rilasciare ioni metallici, i quali danneggiano il nucleo e i mitocondri della cellula. Argento, ossido di titanio, ossido di zinco, oro e silice sono i materiali inorganici più usati in questo tipo di applicazioni. In particolare, la silice, grazie all'elevata biocompatibilità ed alla possibilità di poter trasportare ingenti quantitativi di farmaco è particolarmente interessante in ambito medico.

Le nanoparticelle di argento sono note già da anni e sono state utilizzate negli impianti dentali. A tale proposito sono utilizzati argento metallico, nitrato di argento. L'azione combinata dell'argento e degli antibiotici ha mostrato risultati promettenti nei confronti di batteri come *Escherichia coli* and *Staphylococcus aureus*.

Nanoparticelle di oro possono essere funzionalizzate facilmente ed accoppiate con un gran numero di antibiotici in un'ottica di terapia combinata. Esse inoltre possono assumere differenti morfologie come nanorods, nanoshells e nanocages.

Ossido di titanio e ossido di zinco mostrano un'attività fotocatalitica che porta alla produzione di ROS come radicali idrossili e perossidi. L'ossido di titanio è specialmente adatto per gli innesti ossei in quanto ostacola l'adesione dei batteri sulla superficie.

L'ossido di zinco trova già largo impiego nei cosmetici come creme da sole e il suo aspetto antimicrobico sta suscitando molto interesse nell'ambiente scientifico.

ZnO proprietà, sintesi e applicazioni

L'ossido di zinco è un semiconduttore del gruppo II-VI con una band gap di 3,37 eV a temperatura ambiente. L'ossido di zinco presenta tre strutture cristalline, chiamate rispettivamente zinc blend, rock salt e wurtzite. A temperatura e pressione ambiente la forma stabile è la wurtzite che risulta anche la più comune. La wurtzite presenta una forma tetraedrica con lo zinco al centro e l'ossigeno ai quattro angoli come indicato in figura 1.2. Le nanostrutture di ZnO sono sintetizzate attraverso vari approcci. Il metodo "sol gel" è uno dei più utilizzati a causa dell'elevata versatilità, basse temperature e costi e sfrutta precursori come nitrato di zinco o acetato di zinco. Altro metodo largamente utilizzato è la deposizione chimica o fisica in fase vapore per l'eccellente controllo del livello di cristallinità. Differenti morfologie si possono ottenere in base al metodo di sintesi utilizzato. Tra cui troviamo sicuramente nanorods, nanowires, nanoflowers and nanoparticles. L'ossido di zinco presenta notevoli applicazioni. E' usato come catalizzatore nella sintesi del metanolo, trova impiego come materiale anticorrosivo ed è presente in molte creme da sole e per bambini. Inoltre, le sue proprietà piezoelettriche lo rendono molto interessante nel settore energetico, in particolare nella produzione di energia elettrica.

Infine, esso, mostra spiccate caratteristiche per applicazioni biologiche, quali infezioni, biosensori, tumori e per sta suscitando molto interesse negli addetti ai lavori.

Biocompatibilità e proprietà antibatteriche dell'ossido di zinco

L'ossido di zinco è riconosciuto come "GRAS material" (generally recognized as safe) dalla FDA, ma questa etichettatura si riferisce al materiale in scala del micron o maggiore. Per questo motivo è necessaria una profonda valutazione della citotossicità sia in vitro che in vivo per capire effettivamente la sua biocompatibilità.

Tuttavia, lo zinco ha un ruolo chiave nella crescita dell'osso in quanto l'85 % dello zinco presente nel corpo umano è localizzato proprio nell'osso. Inoltre, influenza fattori metabolici quali l'ormone della crescita ed è capace di attivare processi di sintesi delle proteine negli osteoblasti. Numerosi articoli scientifici indicano che lo zinco è un promotore della differenziazione degli osteoblasti, regolando collagene, ALP, osteopontina e osteocalcina mentre deficienze di zinco indicano ritardi e problemi nella crescita ossea. Viste tutte queste proprietà, lo zinco è un componente fondamentale nell'osteointegrazione, ovvero la rigenerazione ossea. Riguardo sempre l'osteointegrazione tra i vari composti dello zinco, ha suscitato notevole interesse l'ossido di zinco. Infatti, si è osservato un aumento della proliferazione cellulare e dell'attività dell'ALP in occasione di coating superficiali contenenti ossido di zinco.

Come già enunciato prima l'attività antimicrobica riveste un ruolo fondamentale nelle infezioni ossee e l'ossido di zinco mostra proprietà a riguardo.

Le proprietà antibatteriche sono influenzate dalla dimensione e dalla concentrazione delle nanoparticelle di ossido di zinco. Si è riscontrato che l'attività aumenta al diminuire della dimensione poiché vi è un maggiore esposizione di atomi in superficie ed una migliore internalizzazione e produzione di radicali. L'effetto della concentrazione è invece direttamente proporzionale all'effetto antimicrobico. In aggiunta a queste, la morfologia delle nanostrutture può rivestire un ruolo importante. Studi scientifici hanno tentato di spiegare i meccanismi responsabili dell'attività antimicrobica e hanno evidenziato che i principali meccanismi sono la produzione di ROS, rilascio di ioni zinco e azione nanoantibiotica. I ROS vanno a danneggiare la membrana del batterio irreversibilmente mentre gli ioni zinco si assorbono sulla superficie di esso, causando la perdita dell'equilibrio di carica e la conseguente deformazione della cellula. In aggiunta, lo zinco può penetrare nella membrana e interagire con gruppi funzionali. Questa interazione porta ad uno squilibrio nel metabolismo che conduce alla morte cellulare.

Infine, l'azione da nanoantibiotico, la sua elevata area superficiale specifica ed energia superficiale, può penetrare e disorganizzare la membrana. Pertanto, viste i numerosi vantaggi di usare l'ossido di zinco come papabile candidato nelle infezioni ossee, si è deciso di analizzare le performance dell'ossido di zinco in vitro sia dal punto di vista della biocompatibilità che da quello antibatterico.

L'obiettivo di questo lavoro di tesi, quindi, è stato di esaminare l'attività antibatterica dello ZnO nei confronti di *Escherichia coli* e *Stafilococcus aureus* in stato planctonico e nel biofilm. In parallelo a questo studio, è stata esaminata la biocompatibilità dell'ossido di zinco nei confronti dei pre-osteoblasti provenienti da ossa parietali e occipitali di topo. La sintesi delle nanostrutture è stata fatta via microonde per le nanoparticelle e via sputtering per i film porosi. La biocompatibilità è stata studiata analizzando il lattato deidrogenasi per quanto concerne la citotossicità e l'attività mitocondriale per la proliferazione cellulare. Per una maggiore completezza è stato studiato anche il processo di differenziazione attraverso la fosfatasi alcalina.

Materiali e metodi

Sintesi delle nanoparticelle di ossido di zinco

Le nanoparticelle di ossido di zinco sono state sintetizzate attraverso una sintesi solvotermale assistita al microonde. L'utilizzo del microonde permette di avere uniformità di riscaldamento in tutto il mezzo, nucleazione istantanea e quindi cinetiche di reazioni velocissime. I precursori usati sono acetato di zinco e idrossido di potassio in proporzione 1:2 e come solvente invece è stato utilizzato il metanolo. Una prima soluzione è stata preparata dissolvendo idrossido di potassio in metanolo. Una seconda soluzione contenente acetato di zinco e metanolo è stata preparata direttamente nel vessel del reattore. Una volta ultimate le dissoluzioni, le soluzioni sono state miscelate e messe in un forno a microonde a 60 °C e pressione massima 10 bar per 30 minuti. Successivamente per separare il prodotto, dal metanolo e dalle impurità, il tutto è stato centrifugato per 10 minuti a 5000 RPM. Una volta terminata l'operazione, lo ZnO è stato sospeso in etanolo e centrifugato di nuovo per eliminare ulteriormente le impurità. Quest'ultima operazione è stata ripetuta ancora una volta ed infine si sono ottenute delle nanoparticelle di ossido di zinco, cristalline, sferiche e con dimensione compresa tra 16 e 25 nm in una sospensione con etanolo. Inoltre, parte di queste particelle sono state funzionalizzate con gruppi ammino (NH₂) tramite la reazione con APTMS 3-aminopropyltrimethoxysilane. Si è pertanto analizzata la differenza tra ZnO puro e funzionalizzato.

Per utilizzare l'ossido di zinco in ambiente biologico, le nanoparticelle sono state centrifugate e riospese in acqua ultrapura, perché l'etanolo è tossico per le cellule e per i batteri.

Sintesi di film di ossido di zinco

Il film sono stati sintetizzati tramite deposizione sputtering. Lo sputtering è una deposizione fisica in fase vapore e sfrutta un plasma come fonte di energia per estrarre atomi e molecole da un materiale solido chiamato target, e depositarli su un substrato. Un sistema per lo sputtering è dotato di una camera di deposizione in acciaio stainless steel, di un generatore di potenza e da una coppia di elettrodi. Il catodo è l'alloggiamento del target mentre l'anodo è rappresentato dal supporto del substrato. La camera per la deposizione è mantenuta sotto vuoto e la scarica al plasma è data dalla ionizzazione di un gas inerte tramite una polarizzazione degli elettrodi. In questo lavoro di tesi l'ossido di zinco è stato depositato su dei vetrini da laboratorio. Inizialmente si è assicurato un alto grado di vuoto tramite l'utilizzo di una pompa rotativa e di una pompa turbomolecolare. Successivamente è stato depositato lo zinco metallico a temperatura ambiente, sfruttando un generatore di frequenza per creare la scarica al plasma, e

un target di zinco metallico. La deposizione dura circa due ore e la potenza del generatore di frequenza, la pressione parziale dell'argon e la portata sono i parametri più importanti del processo in quanto influenzano la morfologia finale del film. L'ultima fase riguarda l'ossidazione in forno a 380 °C per 2 ore in modo da convertire lo zinco metallico in ossido di zinco.

Caratterizzazione morfologica e strutturale

I campioni di nanoparticelle sono stati caratterizzati tramite TEM (Transmission Electron Microscopy) e XRD (X Ray Diffraction), mentre la Dynamic Light Scattering è stata usata per analizzare la stabilità colloidale.

L' XRD permette di avere informazione riguardo la struttura cristallina, fase, dimensioni dei cristalliti di campioni solidi. Il TEM invece permette di ottenere informazioni aggiuntive, quali morfologia, forma e dimensioni delle nanoparticelle. La DLS dal canto suo provvede informazioni sulla stabilità colloidale come il raggio idrodinamico.

Per quanto concerne i film porosi si sono utilizzate XRD e Field-Emission Scanning Electron Microscopy (FESEM). Il FESEM in particolare mette in risalto la morfologia del film, permettendo inoltre lo studio del suo spessore.

Studio di biocompatibilità

L'ossido di zinco in forma di nanomateriale è stato sottoposto ad uno studio di biocompatibilità nei confronti della linea cellulare MC3T3-E1. Le cellule sono provenienti da ossa del cranio di topo e sono state coltivate in vitro utilizzando come medio di coltura α -MEM completo. Le condizioni di coltura sono 37 °C e un'atmosfera avente il 5 % di CO₂. Inoltre, due volte a settimana, sono state tripsinizzate per rallentare la crescita cellulare in una "Flask". In occasione delle prove sperimentali, oltre alla tripsinizzazione, le cellule dopo essere state contate, sono state sospese nel medio con una concentrazione di 10⁴ cellule/ml e poi spostate in 24 well plates. In particolare, due tipi di esperimenti sono stati portati avanti per quanto riguarda la biocompatibilità. Nel primo le cellule sono state coltivate in presenza dell'ossido di zinco già da subito in modo da simulare la situazione in cui cellule staminali e agente antimicrobico arrivano allo stesso momento.

Nel secondo invece, le cellule sono state coltivate fino al 70 % di confluenza e poi aggiunto l'ossido di zinco in modo da studiare l'interazione con un tessuto osseo già pre-formato. Le concentrazioni di ZnO e ZnO-NH₂ utilizzate sono 5 µg/ml, 10 µg/ml, 25 µg/ml, 50 µg/ml, 100 µg/ml.

Riguardo la citotossicità, è stata monitorato il rilascio del lattato deidrogenasi (LDH), un enzima che viene liberato dalla membrana cellulare in seguito a rottura. A tale proposito, le cellule sono state incubate per 3 giorni in presenza di ZnO e poi la misura della LDH è stata fatta tramite uno spettrofotometro grazie ad un kit commerciale.

Sempre riguardo la biocompatibilità, è stata esaminata la proliferazione cellulare. Per monitorarla, si è studiata l'attività mitocondriale delle cellule in incubazione con il nanomateriale per 3 giorni, e poi successivamente sfruttando il protocollo dell'MTT, si è misurata l'attività.

Per avere un quadro generale più completo, le cellule inoltre sono state esaminate al microscopio a fluorescenza per capire la morfologia e per avere un'ulteriore conferma del loro comportamento.

Tra questi studi rientra anche il monitoraggio del processo di differenziazione degli osteoblasti. Gli osteoblasti derivano da cellule mesenchimali, chiamate pre-osteoblasti che hanno la capacità di trasformarsi in cellule specializzate (osteoblasti) attraverso il processo di differenziazione. Il processo di ricostruzione ossea si articola in tre step, osteogenesi, modellazione e rimodellazione e tali passaggi sono governati da osteoblasti e osteoclasti.

Riguardo il processo di differenziazione, esso è regolato da regolatori trascrizionali, in particolare il RunX2. L'attivazione di questo regolatore è un processo fondamentale perché permette la conversione dei pre-osteoblasti. Dopodiché i pre-osteoblasti si differenziano in tre stage. Il primo stage è caratterizzato da una pronunciata proliferazione cellulare. Nel secondo stage le cellule iniziano a differenziarsi maturando la matrice ossea con ALP e collagene. L'ultimo step riguarda la mineralizzazione della matrice caratterizzata da alti livelli di osteocalcina e dalla caratteristica forma cuboidale degli osteoblasti.

Nel nostro caso, il processo di differenziazione è stato studiato monitorando l'attività della fosfatasi alcalina (ALP), un enzima presente in grandi quantità nel tessuto osseo, e il contenuto totale di proteine. A tale proposito le cellule sono state incubate per 10 giorni in presenza dell'ossido di zinco. Successivamente si è misurato il contenuto di fosfatasa alcalina e proteine per via spettrofotometrica tramite un kit commerciale distribuito dalla Spinreact.

Studio dell'attività antibatterica

L'attività antibatterica dell'ossido di zinco è stata provata nei confronti di batteri in stato planctonico e nel biofilm. I batteri utilizzati sono *Escherichia coli* e *Stafilococco aureus* in modo da esaminare due differenti morfologie. Infatti, l'*E. coli* è un batterio gram positivo, aerobico o anaerobico, e presenta una forma allungata a bastoncino. *E. coli* è l'organismo procariote più studiato in laboratorio perché impiega solo 20 minuti per riprodursi in condizioni favorevoli ed è molto facile da coltivare. La maggior parte dei ceppi di *E. coli* sono poco pericolosi e si possono trovare facilmente nella flora batterica dei mammiferi. Tuttavia, alcuni ceppi stanno dimostrando caratteristiche preoccupanti e riescono a partecipare alla formazione del biofilm. Per quanto concerne, *lo Stafilococco aureus*, esso è un batterio gram negativo dalla forma rotonda. Rispetto all'*Escherichia coli*, è molto più pericoloso perché può causare infezioni croniche ed è il maggiore responsabile della formazione di biofilm nelle operazioni chirurgiche per traumi ossei.

I batteri sono stati coltivati nel medio Todd Hewitt Broth a 37 °C. I medi utilizzati per esplicitare gli esperimenti sono stati sterilizzati in autoclave a 121 °C per 20 min. In ogni esperimento è stata utilizzata una concentrazione di 10⁶ batteri/ml

Come primo esperimento si è verificata l'attività in stato planctonico. Anche in questo caso il range di concentrazioni usato va da 5 µg/mL a 100 µg/mL. A tale proposito, sono stati impiegati dei piatti Petri contenenti un medio chiamato Tryptic Soy Agar, perché permettono di contare le colonie di batteri formatesi.

Nel CFU counting method, sia l'*Escherichia coli* che *Stafilococco aureus* sono stati tenuti in incubazione con le nanoparticelle di ossido di zinco per un giorno, e successivamente le sospensioni sono state poste in contatto con i piatti contenenti l'Agar.

Dopo averne testata l'efficienza in stato planctonico, si è proceduto ad analizzare l'attività nei confronti del biofilm. La formazione del biofilm procede attraverso vari step, tra cui l'adesione dei batteri alla superficie. L'adesione batterica è un passo fondamentale nella formazione del biofilm in quanto i batteri provenienti dal bulk del liquido, possono adsorbirsi o meno alla superficie. Una volta adsorbiti, inizia la cosiddetta lag phase dove le interazioni e la crescita fanno sì che si viene a formare una struttura a fungo che permette il passaggio dei nutrienti all'interno del biofilm prematuro. Successivamente c'è la fase esponenziale caratterizzata da una forte crescita del numero di batteri e dall'escrezione della matrice di polisaccaridi. Dopo questa fase, c'è la formazione finale del biofilm maturo che conferisce una spiccata protezione ai batteri al suo interno.

Rispetto al caso precedente, i batteri vengono sospesi in THB con il 4% di saccarosio per favorire la crescita del biofilm. Successivamente la sospensione batterica viene posta in un well plate e lasciata in incubazione per 48 ore per permettere appunto la formazione del biofilm. Le nanoparticelle vengono poi aggiunte ed incubate un'ora. Infine, l'attività antibatterica è stata

poi monitorata al microscopio confocale utilizzando un kit di coloranti che colora in verde i batteri vivi, in rosso quelli morti ed in blu i biofilm.

Riguardo i film porosi, sono stati testati ponendoli in contatto con la sospensione batterica per 24 ore e anche in questo caso sono stati poi esaminati al microscopio confocale confrontandoli con dei vetrini senza rivestimento di ossido di zinco.

Inoltre, i film porosi sono stati sottoposti prima ad una analisi preliminare al SEM per valutare l'interazione con le sospensioni batteriche e per osservare come cambia la morfologia, confrontandoli con i film tal quali.

Risultati e discussione

Caratterizzazione morfologica e strutturale

La tecnica dell'XRD permette di identificare la struttura cristallina, la dimensione dei cristalliti analizzando la larghezza dei picchi ottenuti e confrontandoli con un database di composti noti. Nella figura 3.1 e 3.2 sono mostrati i risultati dell'XRD. Le nanoparticelle di ossido di zinco presentano picchi a 31.9° , 34.4° , 36.4° , 47.6° , 56.7° e confrontandoli con la letteratura, risultano essere i picchi tipici della wurtzite. Inoltre, tramite la formula di Scherrer, è stato possibile ottenere la dimensione dei cristalliti che è risultata di 17 nm per lo ZnO puro e 15 nm per lo ZnO funzionalizzato.

In figura 3.5 e 3.6 mostrano le immagini al TEM di entrambi i tipi di nanoparticelle e si può osservare che le particelle mostrano una forma poligonale e dimensioni tra 20 e 25 nm. Inoltre, il campione delle nanoparticelle funzionalizzate presenta un'aggregazione maggiore.

I risultati dell'analisi di stabilità colloidale tramite DLS sono mostrati in figura 3.3 e 3.4 ed evidenziano la presenza di un picco ben definito e centrato a 59 nm per lo ZnO e a 122 nm per lo ZnO-NH₂. La presenza di un unico picco dimostra che il campione non è aggregato ed è monodisperso.

I film sono stati caratterizzati tramite XRD e FESEM. Anche in questo caso, il pattern dell'XRD in figura 3.7 evidenzia che i picchi sono corrispondenti alla wurtzite.

La FESEM invece fornisce informazioni sulla morfologia del film. Nell'immagine 3.9 si può osservare lo spessore del film che risulta poco superiore a 3,5 micrometri. Invece nella figura 3.8 è possibile apprezzare la struttura porosa del film, con una struttura simile ad una spugna. Inoltre, è evidente la rete porosa formata da nanocristalli di ossido di zinco. Dal confronto con immagini dello zinco metallico si evidenzia che il processo di ossidazione termica non cambia la morfologia del film.

Studio di biocompatibilità

La combinazione dei risultati di citotossicità (LDH) e proliferazione cellulare (MTT) mostra un quadro generale della biocompatibilità delle nanostrutture di ossido di zinco. Per quanto concerne la citotossicità, le nanoparticelle funzionalizzate e tal quali non presentano differenze importanti. Riguardo la citotossicità in funzione della concentrazione di esse, si può osservare in figura 3.10 e 3.11, che la quantità di LDH rilasciata è simile al controllo eccetto per 100 µg/ml. Infatti, in corrispondenza di questo valore, si registra un quantitativo doppio di tale enzima (rispetto al controllo) e ciò implica un effetto citotossico.

La proliferazione cellulare presenta un andamento simile. Come osservato precedentemente, non ci sono differenze tra l'ossido di zinco tal quale e funzionalizzato. L'attività mitocondriale decresce leggermente all'aumentare della concentrazione, tranne per la concentrazione più alta dove si rilevano diminuzioni del 70 % rispetto al controllo.

Nel secondo esperimento di biocompatibilità dove si simulava un tessuto osseo già formato, si è monitorata la proliferazione cellulare e la morfologia delle cellule. In figura 3.16 e 3.17 si

osserva che la proliferazione è molto buona e si registrano anche dei piccoli aumenti rispetto al controllo fino alla concentrazione di 25 µg/ml dopodiché, la proliferazione inizia a diminuire e si registra il valore più basso per 100 µg/ml. È interessante notare che le funzionalizzate presentano una buona proliferazione anche in corrispondenza della concentrazione più alta.

Gli studi riguardanti la morfologia, hanno confermato i precedenti risultati, evidenziando la caratteristica morfologia degli osteoblasti per le cellule in contatto con concentrazioni non superiori a 50 µg/ml (figure 3.18 e 3.19). Dall'altro lato, pre-osteoblasti in contatto con nanoparticelle di ossido di zinco alla concentrazione di 100 µg/ml, presentano una morfologia sferica e una minore confluenza. Le cellule in contatto con le nanoparticelle funzionalizzate presentano tutte la morfologia tipica ma a 100 µg/ml si registra una notevole diminuzione delle cellule.

I film porosi sono stati analizzati con i medesimi esperimenti. Purtroppo, mostrano una notevole citotossicità e una minore proliferazione con valori molto simili alla concentrazione più alta di nanoparticelle. Questo effetto è probabilmente dovuto al rilascio ed alla dissoluzione di ossido di zinco non controllato.

Riguardo la differenziazione degli osteoblasti, si è monitorata la fosfatasi alcalina e la quantità di proteine. Le nanoparticelle di ossido di zinco tal quali hanno fatto registrare una diminuzione della fosfatasi alcalina all'aumentare della concentrazione mentre le nanoparticelle funzionalizzate mostrano un comportamento completamente diverso. Infatti, non ci sono apprezzabili differenze con il controllo, dimostrando quindi una maggiore affinità verso il processo di differenziazione (figura 3.21).

In figura 3.22 sono mostrati i risultati relativi al quantitativo di proteine. Si può vedere benissimo che l'andamento è molto simile a quello della fosfatasi alcalina sia nel caso delle nanoparticelle tal quali e funzionalizzate.

Per una maggiore completezza sono state effettuate delle foto al microscopio ottico per valutare la morfologia delle cellule differenziate. Le foto presenti in figura 3.24 e 3.25 mostrano la tipica morfologia degli osteoblasti fino a 50 µg/ml di ZnO. Come al solito, la concentrazione di 100 µg/ml mostra una morfologia sferica. Inoltre, il grado di confluenza va progressivamente diminuendo all'aumentare della concentrazione. Le cellule coltivate in presenza di nanoparticelle funzionalizzate presentano tutte la morfologia tipica e il grado di confluenza diminuisce leggermente all'aumentare della concentrazione di esse.

I film porosi mostrano invece una netta diminuzione della fosfatasi alcalina e delle proteine con valori sempre comparabili alla concentrazione più alta di nanoparticelle di ossido di zinco. Le immagini al microscopio, evidenziano una morfologia sferica e un quantitativo di cellule molto basso.

Studio dell'attività antimicrobica

I risultati dell'attività antibatterica nei confronti dei batteri in stato planctonico sono stati ottenuti tramite CFU counting method. Le nanoparticelle di ossido di zinco tal quali e funzionalizzate hanno mostrato un'ottima efficienza verso l'*Escherichia coli*, risultando in una completa inibizione della crescita a qualsiasi concentrazione.

I risultati per lo *Stafilococco aureus* sono differenti e qui l'effetto della concentrazione è abbastanza rimarchevole. Infatti, si è registrato un aumento della attività all'aumentare della concentrazione con un picco in corrispondenza di 25 µg/ml. In corrispondenza di concentrazioni superiori, l'attività decresce probabilmente per la presenza di PBS che causa l'aggregazione delle particelle, e tale effetto risulta più marcato a concentrazioni maggiori. Particelle più grandi espongono un numero minore di atomi in superficie che si traduce in un minore quantitativo di agente antimicrobico. Lo stesso effetto non è stato riscontrato con *Escherichia coli* perché presenta una forma allungata e quindi una maggiore interazione con le particelle sferiche.

Visti i risultati in stato planctonico, si è proceduto ad analizzare il comportamento nei confronti dei batteri nel biofilm. Tuttavia, si è utilizzata solo la concentrazione di 25 µg/ml perché ha mostrato il miglior comportamento antimicrobico ed una buona biocompatibilità. Le immagini derivanti dal microscopio confocale (figura 3.34) esibiscono una buona attività antimicrobica già dopo un'ora di incubazione. Nonostante ciò, è necessario un'analisi più approfondita con tempi di incubazione più lunghi per verificare l'efficienza di questo materiale nei confronti del biofilm.

Per quanto concerne i film porosi, inizialmente si è analizzata la loro interazione con i batteri attraverso il SEM. Le immagini al SEM (fig 3.35) hanno evidenziato un profondo cambiamento della struttura, dovuto alla dissoluzione dell'ossido di zinco nel medio di coltura batterico, e dimostrano l'adesione dei batteri sul film poroso.

Successivamente si è esaminato il comportamento al microscopio confocale nei confronti di *S aureus* e *Escherichia coli*. Dalla figura 3.36 è possibile osservare che in presenza del film la quantità di batteri è notevolmente più bassa rispetto al controllo, simbolo di una diminuzione della proliferazione e di una minore adesione.

Conclusioni

Negli ultimi anni, l'uso dei nanomateriali in campo medico ha trovato largo impiego. Tra gli svariati campi della medicina, sono molto interessanti le applicazioni dei nanomateriali per infezioni come quelle ossee. Come già scritto precedentemente, questo tipo di infezioni sono molto difficili da curare perché sono causate da batteri fortemente resistenti agli antibiotici ed inoltre prevedono lo sviluppo del biofilm. I nanomateriali studiati per questo tipo di applicazioni sono essenzialmente nanostrutture inorganiche, composte da metalli o da ossidi di metalli. Tra questi, un promettente candidato è sicuramente l'ossido di zinco. Per questo motivo, lo scopo di questo lavoro di tesi è stato analizzare il comportamento delle nanostrutture di ossido di zinco nei confronti di batteri in stato planctonico e in stato di biofilm. Inoltre, si è effettuato uno studio di biocompatibilità nei confronti dei pre-osteoblasti provenienti da ossa di topo. Sono state sintetizzate e testate due differenti morfologie: nanoparticelle sferiche e film porosi di ossido di Zinco. In aggiunta parte delle nanoparticelle sono state funzionalizzate per vedere se la funzionalizzazione potesse avere degli effetti diversi.

I risultati hanno evidenziato una buona biocompatibilità delle nanoparticelle fino alla concentrazione di 50 µg/ml e ciò è confermato sia dalla non citotossicità che da una buona proliferazione cellulare. Dall'altro lato, i film porosi e la concentrazione di 100 µg/ml hanno mostrato un effetto tossico. Lo studio di biocompatibilità è stato completato con l'analisi del processo di differenziazione. Le particelle funzionalizzate hanno dimostrato avere un comportamento migliore perché presentavano valori di ALP molto simili al controllo. Invece le nanoparticelle tal quali mostrano una diminuzione di tale enzima all'aumentare della concentrazione. I film sono risultati poco adatti a favorire tale processo perché presentano valori di ALP molto bassi confrontabili con la concentrazione più alta di nanoparticelle di ZnO. Per quanto concerne l'attività antimicrobica, l'ossido di zinco si è mostrato un ottimo materiale. Infatti, dai primi studi in fase planctonica si è visto che Nanoparticelle di ossido di zinco tal quali e funzionalizzate anche con concentrazioni molto basse hanno la capacità di inibire completamente la crescita dell'*Escherichia coli*. L'attività nei confronti dello *Stafilococcus aureus* è leggermente diversa e risulta dipendente dalla concentrazione di ossido di zinco. In particolare, si è registrata la massima attività alla concentrazione di 25 µg/ml mostrando una inibizione della crescita batterica pari al 97 %. Successivamente si è analizzata l'attività dell'ossido di zinco nei confronti del biofilm e si è visto che dopo solo un'ora d' incubazione vi è già una notevole diminuzione del numero di batteri vivi. Riguardo i film porosi, si è analizzata l'adesione batterica e la formazione del biofilm. Dai risultati ottenuti si evince che i

film porosi presentano una minore adesione batterica ed ostacolano la proliferazione di essi. Per concludere e visti i risultati, il miglior candidato per le infezioni ossee risulta essere l'ossido di zinco funzionalizzato, in un range di concentrazioni da 5 a 25 $\mu\text{g/ml}$. Questi risultati pertanto incoraggiano l'applicazione di ossido di zinco ad esempio negli scaffold o come nanoantibiotico. Tuttavia, sono necessari dei test un più approfonditi riguardo la differenziazione e la formazione del biofilm, perché sono dei processi molto complessi governati da numerosi fattori. Inoltre, siccome è stata condotta solo una analisi in vitro, per uno studio più approfondito è necessaria un'analisi in vivo.

1 Introduction

During the 20th century, infections were the major cause of death worldwide. Thanks to the introduction of antimicrobial agents, there was a strong decrease of mortality from infection diseases. However, nowadays, the resistance to antibiotics is reaching critical levels, and most of the antimicrobial drugs used in clinics do not have the desired effect. The infections due to both gram positive and negative pathogens, are growing and developing an evolved antimicrobial resistance, making human health in serious danger in case of compromising infections. Regarding this, it is worth to notice that the 40 % of *Staphylococcus aureus* collected from the hospitals is Methicillin-resistant and sometimes even resistant to Vancomycin, the most advanced antibiotic for *S. aureus* infections. Moreover, in Germany during the last years, 1500 people have been infected by a new strain of *Escherichia coli* which led to fatal cases. Another big problem is treating chronic infections like cystic fibrosis and pulmonary infections, because they necessitate a high intravenous administration of antibiotics with serious side effects [1]. Bone infections related to the failure of orthopaedic implants is also an important challenge. In particular during the insertion of orthopaedic implant, bacteria from patient's skin or mucosa can enter and adhere to the surface of implant and start to produce an extracellular matrix called biofilm. Biofilm is made of polysaccharide matrix which is able to host and protect bacteria from antibiotics because their penetration or diffusion is impeded. This phenomenon results in osteomyelitis, localised bone destruction, that leads to prolonged hospitalisation and intense antibiotic treatment and in serious cases to the substitution of the prosthesis. [2]

For these reasons it is necessary to explore new pathways and new antibiotics to solve bacterial resistance. Unfortunately, there is no certainty about the effectiveness of new antimicrobial drugs because bacteria can develop resistance in a timely manner. A new approach to overcome this challenging and dynamic infectious disease could be the use of nanomedicine. In the recent years, numerous efforts were made to investigate the behaviour of nanomaterials, because bacteria should not be able to show resistance against these materials. Using an antimicrobial nanomaterial gives several advantages such as reduced toxicity, overcoming resistance and lower cost. Nanomaterials are also used as carriers for antibiotics to improve pharmacokinetics and accumulation, and to reduce side effects.

Nanotechnology has shown promising approaches in biomedical applications. In fact, there are promising results in using nanostructures for the determination of susceptibility and resistance of antimicrobial drugs due to their unique electrical, magnetic and catalytic properties. Other fields are vaccination and prevention of infections, because NPs can be used as adjuvants and colloidal vaccine. Nevertheless, the most interesting feature is the antimicrobial actions of nanomaterials and thus their use in treatment of infectious illnesses. In this subject, metal and metal oxide are the most studied because of their ability to produce reactive oxygen species under ultraviolet UV light. In particular, nanostructure of silver, gold, zinc, titanium, titanium dioxide and zinc oxide (ZnO) are effective in inactivating numerous pathogens. [1]

Among them, ZnO is one of the most promising inorganic antimicrobial material for tissue regeneration. [3]

Consequently, the aim of this Master Thesis project was to analyse the behaviour of ZnO nanostructures for bone implants applications. In fact, it was tested the antimicrobial activity against Gram positive and negative bacteria such as *Escherichia coli* and *Staphylococcus aureus*. Moreover, its biocompatibility, related to pre-osteoblasts cells from mouse calvaria,

was investigated. In more detail the antibacterial behaviour was analysed both at the planktonic stage and in forming the biofilm. Regarding the biocompatibility, in-vitro assays were performed to study the cytotoxicity using lactate dehydrogenase (LDH) method, proliferation via MTT tests and differentiation from Alkaline Phosphatase (ALP) activity.

1.1 Bone implants: introduction to the problem

In the last years, surgical implant procedures represent an important solution to restore the function of fractured bone segments and impaired limbs. The advent of modern standard in control of sterility and highly trained surgeons, has reduced a lot the risk of infections. However, in the US, infections are present in a range of 0,5 -5 % for the total joint replacements, and the consequences are very serious [2]. In fact, the treatment with antibiotics are not always effective on this type of infections and in more serious cases it is necessary the prosthesis removal. This drastic solution means prolonged trauma for the patient and the increase of hospital stay with important economic consequences (infected arthroplasty costs around 50'000 \$). Therefore, new strategies in the prevention of infection, and in the last 20 years many efforts have been done to better understand both the pathogenesis and the epidemiology of infections, especially related to implant materials.

1.2 Pathogenesis of implant infections

The Research has highlighted that regions, surrounding prosthetic implants, are characterised by an immune depression and are more susceptible to the instauration of infections. In these zone, the critical dose required to start an infection is much lower. This behaviour is mainly due to the micro-movements of prostheses inserted in the hard tissue, which determines a damage in the tissue surrounding the implant, leading to minor immune defences and creating the perfect conditions for pathogens attack. The Microorganism involved in this process are Gram positive and negative bacteria, which initially are adsorbed passively on biomaterial surfaces. However, successively thanks to their adhesins, receptorial proteins, they are able to mediate cell anchorage and form a complex polysaccharide matrix called biofilm. Biofilm gives protection to bacteria from antibiotic treatments and it is one of the problem related to antibiotic resistance. Moreover, in orthopaedics implants, it is estimated that 34 % of infections is caused by *Staphylococcus aureus* and 32 % by *Staphylococcus epidermidis* and only a very few proportion is represented by other bacteria like *Pseudomonas* 8%, *Enterococcus* 5%, *Escherichia* 2%, *Streptococcus* 2 % etc [2]. Therefore, taking a look at the data, the major responsible for infections are *staphylococci*, in particular *Staphylococcus aureus*. *S. aureus* is very harmful when the host defences are weak, it has the ability to form biofilm and it is one of most resistant bacteria regarding antibiotic resistance. Therefore, for all the reasons mentioned above, it is clear the difficulty to treat infections related to bone implants.

1.3 Solutions for implant infections

The strategies to solve the problem of implant related infections are a lot and they include materials that are able to increase osteoblasts functions and decrease bacteria adhesion and action. Firstly, it is mandatory to understand the mechanism that regulate the growth of the new bone in order to design an optimal implant.

Osseointegration is the adhesion of osteoblasts, including their proliferation and differentiation into calcium-depositing cells, and represent the first decisive step. On the other hand, fibroblasts adhesion and production of soft connective tissue between the bone and the implant are recognized as undesired event because they hinder the osteoblasts activities. However, the presence of substance such as Fibronectin and Vitronectin can increase osteoblasts adhesion and reduce fibroblast adhesion. Particular surface chemistry and topography can also enhance osteoblast adhesion. All these benefits can be induced by nanomaterials.

For these reasons, design of an implant is a challenging process that involves a lot of factors like bacterial adhesion, chemistry of materials, surface topography, nanoscale dimensions. Bacterial adhesion is a crucial step, therefore numerous efforts have been done to find coating materials with the aim to create adhesion resistant or bacteria repellent surfaces. The Chemistry of materials is important because certain substances can show properties for osseointegration, promoting osteoblast adhesion and differentiation. The best material chemistry for bone regeneration has been not found yet but there are promising materials such as metals (titanium or metal alloys as CoMoCr), ceramics (alumina, hydroxyapatite, titania) and polymers. The surface topography also represents a very relevant feature and can improve the biological performance of the employed material in the implant. In particular micro-roughness can facilitate osteoblast activity, included cell proliferation and differentiation. Finally, the nanoscale is the gold standard for bone regeneration because natural bone structures and mineral components such as calcium phosphate crystals and Type I collagen are nanostructures. Therefore, the nanoscale size can mimic the dimensions of constituent of natural bone and better promote tissue regeneration. For these reasons a scaffold has the scope to help the bone regeneration, forming a bridge between the bone and the graft material. It needs to be biocompatible, easy to manipulate, antimicrobial and promoter of new bone formation. In the recent years, hybrid scaffolds made of polymers and nanoceramics have shown excellent characteristics regarding this field, such as pure ceramics and biopolymers materials. Among them, an important role can be represented by ZnO because it is a very interesting candidate for inclusion in these hybrid scaffold. [8]

1.4 Nanomaterials for infection control

Nanoantibiotics are nanomaterials which show an antimicrobial activity. According to the FDA and IUPAC, nanomaterials are defined such as structures or materials with almost one dimension less than 100 nm. Among them, there are substances which exhibit a great antibacterial action and their behaviour in controlling infections in vivo and in vitro was deeply studied in the last years. Many antimicrobial agents of this type are used in clinics and they offer multiple pathways in treatment of infections. The main biological investigated area of using nanostructure is oncology, the second one corresponds to infection illnesses and also other area are investigated like cardiovascular or Alzheimer diseases.

Regarding the infections, the research is focusing the attention on their use against different pathogens, multi drug resistant strains and biofilms.

1.5 Antibacterial nanostructures

Antimicrobial NPs can exploit several clinical advantages. Firstly, they can be engineered in order to be activated by stimuli like pH, ultrasound, heat etc light etc and reach a targeted delivery of ions and drugs. Secondly, nanocarriers show lower side effects related to traditional antibiotics thanks to an improved stability and solubility. In addition, they have promising features to overcome the bacterial resistance to normal antibiotics. Other advantages include the prolonged drug circulation when the drug is carried in the nanomaterial, improving therapeutic index in order to achieve a controlled release. Last but not least antimicrobial nanoparticles (NPs) can show a low cost of preparation and administration. Although nanoantibiotics benefits, there are some disadvantages that make challenging their employment. Actually, it is necessary to evaluate the interaction of nanomaterials with living cells, tissues and organs and in consequence to recalibrate dose and administration in a desired therapy. Further investigations are needed to understand the nanomaterial toxicity and accumulation in tissues, organs and bone marrow. [1]

Antibacterial NPs can be organic and inorganic. The organic nanomaterials, are the most studied and includes liposomes, polymeric nanoparticles (NPs), polymeric micelles and solid

lipid NPs. Their main advantage is biodegradability and biocompatibility, but on the other side they show a low loading efficacy of potentially carried drugs and drug loss during storage. Inorganic nanostructures consist of metal and metal oxides and they have different sizes, shapes and long-term stability. Compared with the organic ones, they exhibit smaller dimensions and a better drug loading efficacy. On the other hand, they can show problem of aggregation, metabolization, accumulation and less homogeneity or stability in biological solutions. [6]

1.6 Inorganic nanostructures

Inorganic NPs made of both metals and metal oxides are the most used as antimicrobial nanostructure due to their incredible properties.

They are characterised by high surface area to volume ratio and easy method for synthesis. Typically, the chemical reduction of metallic salts is often used to synthesise metal NPs, while hydrolysis of inorganic salt precursors is used for metal oxide nanoparticles. The final product depends on the synthesis condition like temperature, pH, reduction time, presence of surfactant or capping agents etc. They have unique chemical and physical characteristics for an effective antimicrobial activity. First of all, they exploit the photocatalytic production of reactive oxygen species (ROS) to damage cellular components and compromise the bacteria cellular membrane. Moreover, ROS can interrupt the energy transduction and inhibit enzyme activity and DNA synthesis. In addition, both metal and metal oxides particles are able to release metal ions, so they can damage the nucleus and mitochondria of bacteria cell. The most important antibacterial nanomaterials are Silver (Ag), ZnO, Titania (TiO₂), Silica (SiO₂) and other inorganic compound made of platinum, copper, palladium and iron.

The antibacterial properties of Ag NPs are famous since ancient times and it is used in wound treatment, dental implants and bacterial infection control. The type of silver utilised are metallic silver, silver nitrate and silver sulfadiazine [1]. In addition, its action combined with antibiotics was investigated and it results an advanced and efficient treatment against *Escherichia coli* and *Staphylococcus aureus* [6]. Gold NPs can be easily functionalized and thus they can be coupled with a big number of drug molecules or biological moieties. This characteristic makes Au NPs suitable as adjuvants for antibiotics therapy in order to have lower antibiotics dosage and minor side effects. Au NPs present different morphologies such as nanorods, nanoshells and nanocages which are able to treat infections using irradiation with focused laser pulses of suitable wavelength [6]. Silica also represents an important material and it is used as carriers because can carry large amounts of drugs due to its highly biocompatibility and easy synthesis. ZnO and TiO₂ NPs show a photocatalytic antimicrobial activity due to production of ROS as free hydroxyl radicals and peroxide. In fact, they are able to generate very strong radicals upon receiving irradiation with near UV light and then, these radicals attack microorganism damaging the cellular membrane. TiO₂ NPs has also showed promising results in decreasing bacterial adhesion for bone implants. [1]

Zinc oxide NPs have been utilized in cosmetic industry, as antibacterial creams and medical filling materials. Recently ZnO is investigated as antimicrobial agent and it has demonstrated a good action against food pathogen like *Escherichia coli*, so it is auspicious its employment in preserving food. In addition, great results were obtained in nano-ZnO multilayer deposited on cotton fabrics, exhibiting an excellent activity against *S. aureus* [1].

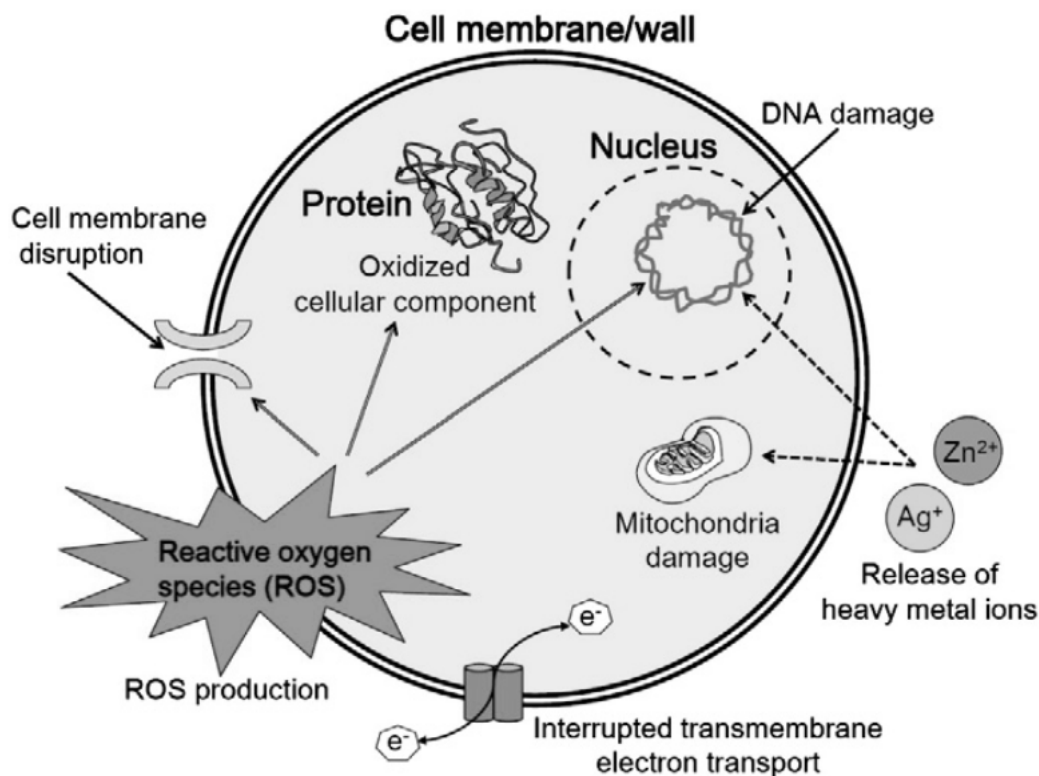


Figure 1.1 Antimicrobial mechanisms of inorganic nanostructures (modified from [1])

1.7 ZnO introduction and properties

ZnO is a metal oxide semiconductor of group II–VI, it exhibits large band gap (3.37 eV) and large exciton-binding energy (60 meV) at ambient temperature. The absorption of UV light is in the range of 200–350 nm and emission in the near UV and visible range from 500 to 600 nm. The crystalline structures featured by ZnO are three and called respectively rock salt, zinc blende and wurtzite. However, under ambient conditions the most thermodynamically stable, is the wurtzite crystalline structure, which is also the most common one. The wurtzite is constituted by tetrahedral units having the zinc atom at the centre and the oxygen atoms at the four corners as showed in figure below. The orientation of all tetrahedra is in one direction, and their stacking produces a hexagonal symmetry. Thanks to its crystalline structure, ZnO is a pyro- and piezoelectric material. In fact, under mechanical stress or temperature, the tetrahedron shows a deformation that leads to formation of dipole moment because of no longer coincidence of positive and negative centres. ZnO nanomaterials are synthesized easily and it is easy to find raw materials and precursors. Today, ZnO nanostructures are object of study in a lot of applications, from piezoelectric sensing or energy harvesting devices to photovoltaic solar cells, to photocatalytic energy conversions and to biomedical materials for both imaging and therapeutic purposes. [4]

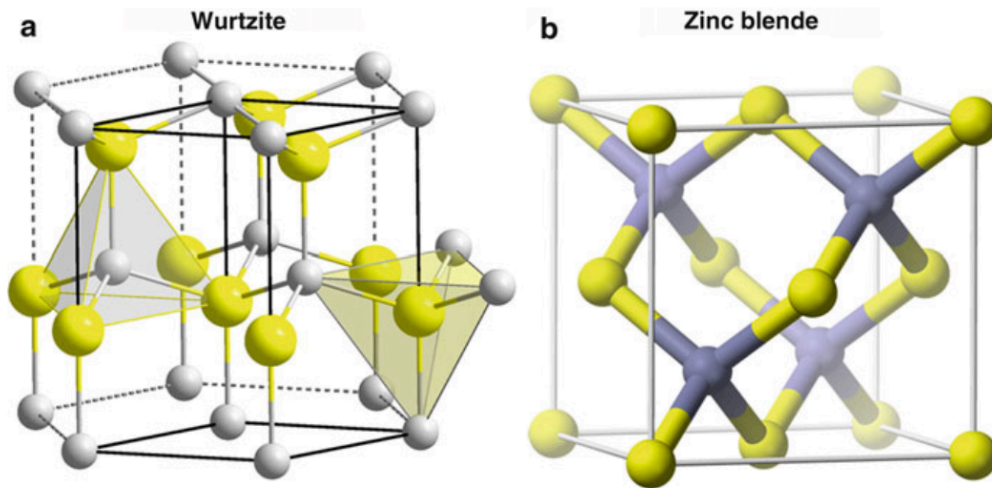


Figure 1.2 ZnO crystal structures [4]

1.8 ZnO Synthesis Techniques

Several research efforts have been done in studying various preparation procedures for ZnO nanomaterials. Wet chemical approaches, like sol-gel methods, are often adopted due to their high versatility, low temperatures and cost. Metal or metalloid element surrounded by various ligands are used as the precursors in this method. The most common precursors for zinc oxide are inorganic salts like zinc nitrate $\text{Zn}(\text{NO}_3)_2$ and organic compounds such as zinc acetate $\text{Zn}(\text{OOCCH}_3)_2$ (often written as $\text{Zn}(\text{OAc})_2$) which is a carboxylate, the type of precursors most used in sol-gel research. Sol-gel method are divided in three main families: solution growth, for nano-sized powders or colloids; hydrothermal or aqueous chemical growth, that permits an anisotropic growth of vertically oriented nanowires on a substrate; template-based growth, exploiting a porous matrix for the growth of nanostructures.

On other hand, dry methods exhibit a high quality and excellent control over the level of crystallinity of the synthesized ZnO structures, minimised level of contamination and high purity of the final product. The exposure of substrates to chemical precursors in the vapor phase, that react and decompose on their surface to obtain the final product, is typical of Chemical Vapor Deposition CVD methods. There are different CVD methods and they are classified for the source of energy employed. Among them, thermal CVD, plasma-enhanced CVD (PECVD), spray pyrolysis and atomic layer deposition (ALD) are the main investigated methods for the growth of ZnO nanostructures. Physical Vapor Deposition (PVD) methods, that involves sputtering and evaporation, partially solve the problem of using high working temperatures typical of many CVD approaches, and they are greatly employed too mainly for the preparation of films of nanostructured ZnO.

1.9 ZnO nanostructures

The different final ZnO nanostructures, from the morphological point of view, depends on the synthesis method. In particular, nanostructures can be represented into four basic classes: 0D (i.e., nanoclusters and nanoparticles), 1D (i.e., nanotube, nanowires, nanorods, and nanobelts), 2D (i.e., nanoplates and layers), and 3D (i.e., nanotetrapods, nanoflowers). [11]

Using chemical growth and CVD methods, it is possible to synthesize 0 D and 1 D nanostructures such as nanoparticles, nanowires and nanorods that are particularly suitable for

biomedical applications, solar cells and gas sensors. Among ZnO morphologies, ZnO porous dense thin film are also very important and have interesting applications. They are synthesized by chemical or physical synthesis routes, and a usual method can be the sputtering deposition. These unique electrical and optical properties of porous ZnO thin films or well dispersed ZnO nanoparticles or nanowires, in addition to the possibility to expose high surface area to air or different types of chemical or biological solutions, means that ZnO structure is a great candidate for a wide range of applications. [4]

1.10 ZnO applications

The combination of different properties, with the easy and high versatile synthesis, make ZnO a promising material for a lot of potential applications. For example, the selective oxidation of involving oxygenates and methanol synthesis are using ZnO nanostructures as catalyst. This material is also largely employed as protective, and anticorrosion layer in galvanized steel products. Furthermore, its biocompatibility represents a great quality in cosmetic applications. In fact, it is used in commercial formulations of baby and sun-creams. In addition, the unique combination of piezoelectric and semiconducting properties, make ZnO suitable for new research field for energy harvesting application. ZnO nanomaterials can be indeed utilized as nanogenerators, able to convert the mechanical deformation from the surrounding environment into electrical energy. Photoanodes in dye-sensitized solar cells (DSSCs) are also fabricated with ZnO nanostructure because of its high surface area. ZnO was successfully employed in the fabrication of biosensors. Last but not least, nanostructured ZnO-based materials have attracted the attention of biomaterial scientists and surgeons because of their unique properties. Actually, the combination of excellent catalytical, antimicrobial characteristics and biocompatibility makes ZnO nanostructures promising materials for tissue regeneration, bacterial resistance, wound dressing and healing, and as therapeutic tool against oncological pathologies [5]

1.11 ZnO biocompatibility and osseointegration properties

ZnO is considered to be a 'GRAS' (generally recognized as safe) material by the FDA. However, the GRAS designation refers to materials in the micrometer to larger size scale. For this reason, these substances when reduced to the nanoscale can show new actions of toxicity therefore, a detailed evaluation of nanomaterial toxicity in both in vitro and in vivo systems is necessary. [12]

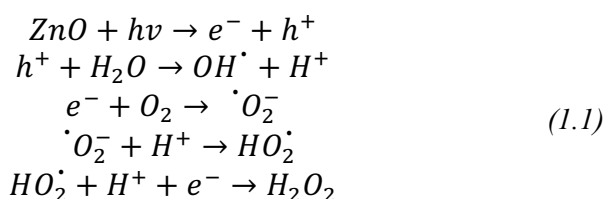
Zinc has a key role in bone growth, and 85 % of the total body zinc is in the bone. Furthermore, it affects the bone metabolic factors like growth hormone (GH), insulin-like growth factor 1 (IGF-I) and it is able to activate the protein synthesis in osteoblast cells and increase ATPase activity. Moreover, numerous papers indicate that Zn is a promoter of osteoblast differentiation and in particular ALP activity of stromal cells increases with it. Numerous genes relative to transcription of osteoblastic differentiation, such as collagen I, ALP, osteopontin and osteocalcin are regulated by Zn. Furthermore, Zn deficiency means a retardation and failure of bone growth in mammals [3]. These qualities encourage the use of Zinc compound in osseointegration and bone regeneration. Especially ZnO nanostructures show some interesting results in this area. According to Memarzadeh [10], ZnO can provide a suitable substrate for osteoblast growth, adhesion and metabolic activity. Moreover, osteoblasts seeded on NP surface coatings have demonstrated an increase in proliferation and alkaline phosphatase release with higher ZnO percentages. Colon et al [9] have analyzed nanophases ZnO on *S. Epidermidis* adhesion and osteoblasts functions. The results of this study provided the first

evidence of significantly greater osteoblast adhesion, alkaline phosphatase activity, and calcium mineral deposition on nanophase ZnO with a reduction of *S. epidermidis* adhesion as well.

1.12 ZnO antimicrobial activity

ZnO nanostructures are one of the most promising materials for tissue regeneration, because of their great antibacterial properties. Important roles in ZnO NPs antimicrobial activity are represented by their size and concentration. It is crucial to control the particles' size because the antibacterial activity increases by decreasing the particles' size. Small particles have a higher surface area in consequence a better surface area to volume ratio and a larger amount of hydroxyl radical produced is observed from them. The effect of concentration has been studied in literature, and in most cases an increase in concentration has a consequent rise in antimicrobial activity. Furthermore, ZnO morphology can play a relevant role. The morphology depends on the synthesis conditions as mentioned above. Some few articles show an effect regarding the internalization of ZnO in various morphologies into bacterial cells. Another possible strategy to improve the activity could be a surface modification by thermal annealing. The oxygen annealing improves the amount of oxygen atoms on the surface and as a consequence there is a bigger formation of ROS species.

To better understand the ZnO antimicrobial activity it is useful to analyse the mechanisms involved. The antibacterial activity of ZnO nanostructures are related to three phenomena: ROS generation, release of Zn²⁺ cations and nanoantibiotic action. ROS generation is the predominant mechanism. ROS are created by photocatalytic reactions with UV-Vis light (even from ambient illumination and consist in hydroxyl radicals, singlet oxygen and superoxide radicals. Their generation happens via the following reactions:



A photoenergy equal or major to the band gap energy (3.3 eV in ZnO) is necessary to move electrons from the valence band to the conduction band of this semiconductor. When the electron leaves the band gap, it creates a hole h^+ in the valence band. Then h^+ interacts with water at material surface to produce hydroxyl radicals and e^- reacts with oxygen to generate a superoxide anion radical. Successively superoxide anion radical can interact with H^+ previously generated to produce HO_2^\cdot which is able to combine with H^+ and interfere with the electron generated to give hydrogen peroxide molecules. Hydroxyl radicals are the most reactive species and they can quickly interact with every type of biological molecules. However, superoxides and hydroxyl radicals cannot penetrate into the cell membrane because they have a negative charge instead of peroxides molecules can pass through the bacterial cell wall and damage the cell irreversibly, leading to cell death.

The Release of Zn²⁺ ions from ZnO nanostructures is another important mechanism in antibacterial activity of ZnO. The zinc positive ions can adsorb to the bacteria surface (negatively charged) through electrostatic forces. This interaction leads to the loss of the charge balance and deformations of the cell occurs with consequent bacteriolysis. Moreover, other zinc ion can penetrate the cell membrane and interact with functional groups like sulphate groups, phosphate groups etc. This interaction results lethal for bacteria because a change in the structure and the performance of proteins, leads to death for unbalanced metabolism.

Finally, the penetration and disorganisation of the membrane is another mechanism to take into account. This phenomenon is due to the high specific area and surface energy of ZnO. Actually, bacteria can adsorb the ZnO nanostructure and because of their accumulation in the membrane and cytoplasm, a lack of normal metabolism occurs. The disorganisation of the cell membrane leads to bacterial death.

These are the most probable mechanisms of the ZnO action against bacteria, but they are also affected by the medium components or different chemical conditions, so the real antimicrobial mechanisms are still under investigation and have to be proved depending to ZnO morphology, chemical reactivity and bacteria cell type [3], [7].

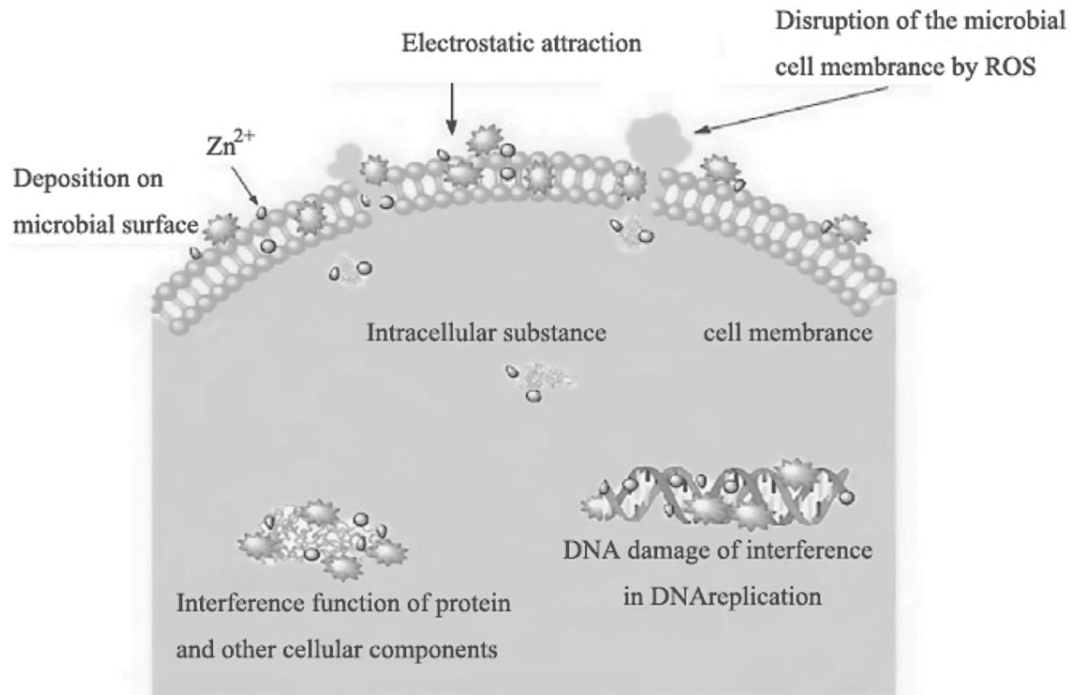


Figure 1.3 Antimicrobial mechanisms of ZnO nanostructures

2 Materials and Methods

2.1 Materials

2.1.1 Preparation of ZnO NPs via Microwave synthesis

Microwave assisted solvothermal synthesis shows various advantages such as short reaction time, rapid heating, low reaction temperature, simultaneous nucleation and low pressure. [13] ZnO powders were synthesized through a microwave assisted solvothermal synthesis by using zinc acetate and potassium hydroxide (Sigma Aldrich) in 1:2 proportions, as precursors and methanol as solvent. In more detail, a first solution was prepared by dissolving in a beaker potassium hydroxide in methanol, and in order to help the dissolution, the solution was mixed via ultrasonic bath. A second solution containing zinc acetate in methanol was prepared directly in the reactor vessel and the solution was stirred, during this process a little bit of double distilled water was added to help nucleation. When the potassium hydroxide dissolution was completed, the final solutions were mixed together in the reactor vessel. The resulting mixture was put into microwave oven for 30 min under control of pressure and temperature ($T=60\text{ }^{\circ}\text{C}$, P max admitted 10 bar). After this time, the product was centrifuged for 10 minutes at 5000 RPM, in order to separate methanol and reaction residuals from ZnO. Top was removed and precipitate was dispersed in 15 mL of ethanol in order to wash NPs, the solution was then stirred via ultrasonic bath and successively it was centrifuged for 10 min at 5000 RPM. A second washing step with ethanol was performed and after that the bottom was suspended in fresh ethanol. So by Using this procedure, it is possible to obtain single crystal ZnO nanoparticles, with special spherical morphology, with a size between 16 and 25 nm, stable in suspension in ethanol.

2.1.2 Functionalization

The functionalization of ZnO NPs with amino groups (NH_2) was obtained combining nanoparticles with APTMS 3-aminopropyltrimethoxysilane, (97% Sigma Aldrich). In more detail, from the reaction of pristine zinc oxide nanocrystals and 3-aminopropyltrimethoxysilane (APTMS) is possible to obtain the amino-propyl functionalized sample (ZnO-NH_2 NCs). The procedure is as follows: 100 mg (1.23 mmol) of ZnO NPs, dispersed in ethanol, were heated to $78\text{ }^{\circ}\text{C}$ in a 100 mL flask under continuous stirring and a nitrogen gas flow. 15 minutes later, $21.4\text{ }\mu\text{L}$ of APTMS was added to the solution; this volume of functionalizing agent represents 0.123 mmol (22.05 g), corresponding to 10 mol % of total ZnO amount. The obtained mixture was refluxed under a nitrogen gas flow for 6 h and successively washed two times to remove the unbound APTMS molecules. [14]

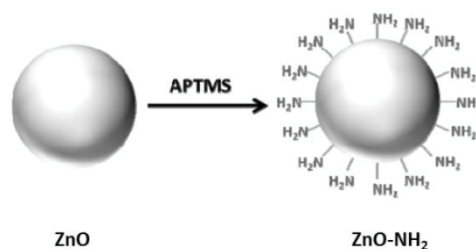


Figure 2.1 ZnO functionalization with amino groups (modified from [15])

2.1.3 Preparation of Nanoparticles suspensions

For biological assays ZnO NPs suspended in ethanol are not suitable because of the toxicity of ethanol towards cells and bacteria. For this reason, it is necessary to separate and eliminate the ethanol and to suspend the particles in a biocompatible solvent, that in our case, is Milli Q Water. Therefore, ZnO NPs suspended in ethanol were centrifuged at 10000 RCF for 15 minutes in order to separate ZnO nanoparticles to ethanol. Then nanoparticles were suspended in Milli Q Water and centrifuged another time to eliminate any trace of ethanol. After that the precipitate was recovered and NPs were suspended once again in Milli Q Water to be used in the biological assays.

2.1.4 Preparation of porous ZnO thin film

Sputtering is a Physical Vapor Deposition (PVD) method and dealing with the use of a plasma discharge as the source of energy to extract atoms and/or molecules, from a solid source material (target), to be deposited onto arbitrary substrates. The main components of a basic sputtering system are the stainless steel deposition chamber, an electric signal generator and a couple of electrodes, the cathode where the target is clamped and the anode represented by the substrate holder. The overall deposition chamber is maintained under high-vacuum conditions. The plasma discharge is formed by the ionization of an inert gas (argon, Ar) injected into the deposition chamber. The ionization process is obtained by applying a polarization voltage between the electrodes and by properly adjusting the Ar gas pressure. Depending on the considered sputtering system and target material, both direct-current or radio frequency (RF) signals can be used for generation of the plasma discharge. [15]

In this thesis work, porous ZnO thin films are deposited on cover glasses by following a synthesis method involving the following steps:

- 1) cleaning of the cover glasses;
- 2) room-temperature deposition of metallic Zn films by RF sputtering;
- 3) calcination of the prepared Zn films at 380 °C in air for 2 h, to convert the starting Zn films into ZnO (thermal oxidation).

Cleaning of the substrates: The cover glasses were washed in ultrasonic bath with acetone (10 min) and ethanol (10 min) and finally dried with nitrogen flow

Deposition of porous Zn films: The deposition of metallic zinc films was performed at room temperature in a pure Ar atmosphere. A RF generator at a working frequency of 13.56 MHz was used to generate the plasma while a 4"-diameter metallic zinc target (purity 99.99%) was used as the source material. The target-to-substrate distance was fixed at about 8 cm. Before starting the deposition, high-vacuum conditions (base pressure ~ 10⁻⁷ Torr) were obtained within the deposition chamber to avoid the presence of impurities contaminating thin films during sputtering. This was achieved with a two-stage pumping system, made of a rotary and turbomolecular pumps connected in series and with the deposition chamber. The RF power, Ar partial pressure and flow values are the main deposition parameters affecting the final thin film morphology and were set according to Table 2.1 and were previously optimized to get Zn films with a porous nanostructure. A previous optimization was needed in order to obtain a porous film with a specific thickness and morphology. The deposition lasts 2 hours after a phase of pre-sputtering where some wings were closed to avoid to cover the substrate with impurities.

Conversion of porous Zn films into ZnO. : The porous Zn films deposited on cover glasses were calcined in a muffle furnace working in air at 380 °C for 2 h. This thermal oxidation allowed to convert metallic Zn into ZnO, preserving the porous morphology of the starting Zn films.

Sputtering conditions	
Number of cover glass ϕ 1,2 cm	20
Base pressure	$4,6 \cdot 10^{-6}$ Torr
Ar flow	10 sccm
Ar pressure	$5 \cdot 10^{-3}$ millitorr
RF power	30 W
Substrate emperature	21 °C
Pre-sputtering time	10 min
Deposition time	2 h

Table 2.1 – Sputtering synthesis conditions

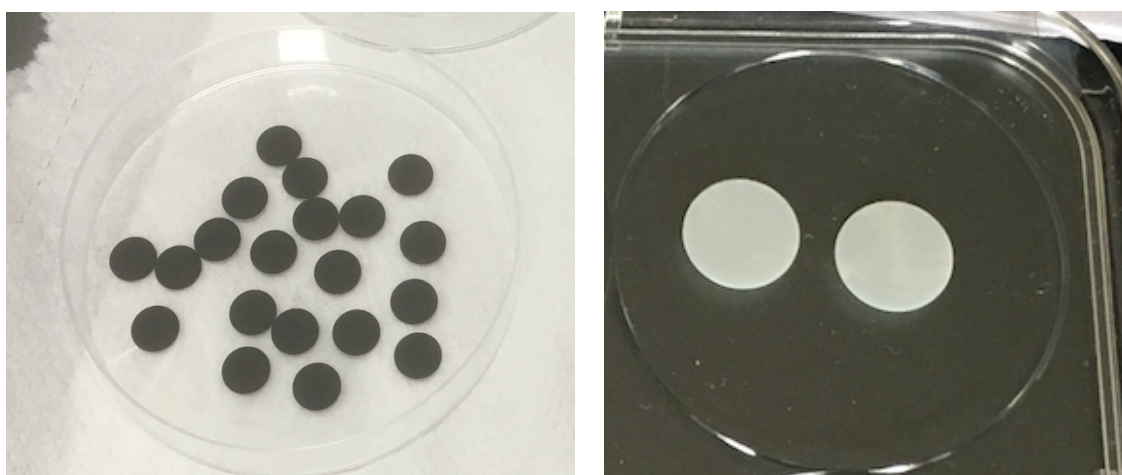


Figure 2.2 Cover glasses of ZnO film before (left) and after thermal oxidation (right)

2.2 Morphological and structural characterization

The ZnO nanoparticles obtained from microwave assisted synthesis were characterised by comparing data from different batches in order to verify the synthesis' repeatability. In particular, samples were analysed by TEM (Transmission Electron Microscopy) and XRD (X Ray Diffraction) in order to detect morphologies features such as shape, dimensions and crystalline structure. Dynamic Light Scattering was used to analyse the colloidal stability. The morphology and crystal structure of porous ZnO films were analysed by means of Field-Emission Scanning Electron Microscopy (FESEM) and X-Ray Diffraction (XRD), respectively. [M1]

2.2.1 X-Ray Diffraction –XRD

The crystallographic structure of materials is detected via X-Ray Diffraction. This particular technique of characterization can provide accurate information on the crystallographic phase of solid samples.

In particular, the sample is irradiated with a beam of monochromatic x-rays over a variable incident angle range. Interaction with atoms in the sample results in diffracted x-rays when the Bragg equation is satisfied. This law relates the wavelength of electromagnetic radiation to the diffraction angle and the lattice spacing in a crystalline sample according to the following formula:

$$n\lambda = 2d \sin \theta \quad (2.1)$$

where n is a positive integer, λ wavelength of incident wave, d lattice spacing, θ diffraction angles. Resulting spectra are characteristic of chemical composition and phase and they are compared with spectra of material databank.

The technique uniquely supplies information about phase identification, along with phase quantification, % crystallinity, crystallite size and unit cell size. [17]

To perform X-Ray diffraction a Panalytical X'Pert diffractometer in configuration 0-2 θ Bragg-Brentano was employed. This instrument uses a source of radiation Cu-K α ($\lambda=1.54 \text{ \AA}$, 40 kV e 30 mA) .

In the case of ZnO NPs, the samples were prepared by deposit drop to drop on silicon wafer in order to have a sufficiently thick layer of nanoparticles and XRD analysis has been carried out with step size of 0.02° (2 θ), 2 θ range of 20°–70° with acquisition time of 100 s. Using the Debye–Scherer formula it was possible to estimate the particle size of each sample from the peak width at half height. The formula is:

$$D = \frac{K\lambda\beta}{\cos \theta} \quad (2.2)$$

where K is a factor that depends on particles' shape, θ is the Bragg's angle, β the width at half height of peak, λ wavelength of incident radiation, D the dimension of crystallite.

2.2.2 Analysis of colloidal stability

In order to study the behavior of nanoparticles in solution, DLS (Dynamic Light Scattering) was used. This method permits to obtain information about the aggregation of particles and colloidal stability of the system. In particular, the interactions between particles in suspension

are determined by the balance of Van Der Waals forces and electrostatic forces which determines the formation of the double electronic layer.

The DLS technique is widely used for submicron particles and also particles with a size less than a nanometer can be detected. In fact, small particles in suspension exploit random thermal motion known as Brownian motion. This random motion is governed by the Stokes-Einstein equation:

$$dH = \frac{kT}{3\pi\eta D} \quad (2.3)$$

where k is Boltzmann constant, T temperature, η viscosity and D diffusivity.

It's important to note that dH is hydrodynamic diameter and it is the size of a sphere that diffuses the way as your particle. The basic principle is simple: A laser beam illuminates the sample and the fluctuations of the scattered light are detected at a known scattering angle θ by a fast photon detector. The scattered light is checked in small intervals of time in order to analyze the variation of the radiation and to calculate the diffusivity. Successively using the Stokes-Einstein equation it is possible to obtain the hydrodynamic diameter. [18]

In our specific case the measurements were performed with a Zetasizer Nano ZS90 (equipped with a laser He-Ne of 633nm). For the measurement, both functionalized and pristine nanoparticles were dispersed in ethanol at a concentration of 500 $\mu\text{g}/\text{mL}$. This concentration allows for good measurement quality because samples with high concentration give no accurate results due to multiple scattering and viscosity effects (too concentrated samples alter the viscosity of liquid).

In multiple scattering, the light scattered from a particle, is re-scattered by other particles present in the suspension.

2.2.3 Transmission electron microscope -TEM

TEM analysis, permits to obtain additional information about the particle's morphology.

The transmission electron microscope (TEM) utilizes the same basic principles of the light microscope but it uses electrons instead of light and for this reason a better resolution is obtained. In fact, a light microscope is limited by the wavelength of light. Using electrons as "light source" permits to utilize their much lower wavelength and resolution is a thousand times better than the normal one.

It is possible to see objects to the order of a few angstroms. For example, studying in more detail cells or different compounds down to near atomic levels. For these reasons the TEM is a valuable tool in both medical, biological and materials research.

TEM uses a "light source" at the top of the microscope which emits the electrons. At the same time, they travel through vacuum in the column of the microscope. Electromagnetic lenses are used, instead of glass lenses, to focus the electrons into a beam. Later, the electron beam travels through the material. Some of the electrons are scattered and disappear from the beam due to the density of the present material. At this point the unscattered electrons hit a fluorescent screen at the bottom of the microscope, a "shadow image" of the specimen is created with its different parts displayed in varied darkness according to their density. The operator directly can study the image or take a picture with a camera. [19]

To prepare the samples for TEM, they were diluted in ethanol up to a concentration of 200 $\mu\text{g}/\text{ml}$ and then some drops were deposited on a square mesh support grid copper-carbon for TEM analysis.

The measurement was performed with JEM 2100HT (JEOL) multipurpose analytical high resolution transmission electron microscope (accelerating voltage of 200 kV and point

resolution of 0.25 nm with an energy dispersive system X-ray microanalysis system EDX, OXFORD INCA). TEM images were saved using a charge coupled device camera.

2.2.4 X-ray diffraction for ZnO Porous Film

XRD patterns were collected by using a Panalytical X'Pert diffractometer working in θ - 2θ Bragg-Brentano configuration, equipped with a Cu K_{α} radiation ($\lambda=1.54 \text{ \AA}$, 40 kV e 30 mA). XRD patterns were collected in the 2θ range of 20° – 70° , with a step size of 0.02° (2θ), and an acquisition time of 10 min

2.2.5 Field emission scanning electron microscopy - FESEM

Field-Emission Scanning Electron Microscopy (FESEM) is a powerful method to get information about the morphology and elemental composition of a material's surface, with magnifications ranging from 10x to 300,000x, and with a virtually unlimited depth-of-field. Therefore, FESEM is able to produce clearer and less electrostatically-distorted images with a better resolution than the conventional scanning electron microscopy.

A field emission source frees the electrons which are accelerated in a high electrical field gradient. These are focused into a narrow primary electron beam in a high vacuum column with the aim of electromagnetic lenses. The primary electrons and electronic lenses produce a narrow scan beam that bombards the object. Upon interaction of the primary electron beam with the sample surface, emissions of secondary electrons can be obtained from each spot on the object, with an emission angle and velocity related to the surface morphology of the sample. These secondary electrons are collected by a detector and an electronic signal is produced. This signal is amplified and converted into an image which can be seen on a monitor and saved. [20]

FESEM analysis were performed in Auriga e Merlin, Carl Zeiss. The cross section image was obtained depositing porous ZnO film on Silicon wafer (cleavage procedure) in order to see it in section and estimate the thickness.

2.3 Cellular studies

In order to investigate the effect of ZnO nanostructures on pre-osteoblasts cells concerning cytotoxicity, cell proliferation and differentiation behaviors, some experiments were carried out.

2.3.1 Cell culture conditions

MC3T3-E1, pre-osteoblasts cells from mouse calvaria were used, on the basis of high alkaline phosphatase (ALP) activity in the resting state. These cells have the capacity to differentiate into osteoblasts and osteocytes and they are able to form calcified bone tissue in vitro. Cells were cultured in a P75 flask (cell growth surface area 75 cm²) at 37 °C in 5 % CO₂ atmosphere in 20 mL of complete α -modified minimal essential medium (α -MEM).

In order to complete the 500 ml of α -MEM, 5 ml of L-glutamine, 1,25 mL of penicillin/streptomycin and 50 mL (10 %) of heat inactivated fetal bovine serum were added. Cultures were trypsinized twice a week with a solution of 0.05% (w/v) trypsin and 0.02% (w/v) EDTA in sterile phosphate buffered saline. All reagents were from GIBCO ® by life technologies™.

2.3.2 Cell trypsinization

Cell trypsinization is a process of cell detachment from the flask using trypsin, a proteolytic enzyme which breaks down proteins that facilitate the adhesion of cells. This process permits the passage to a new container or in alternative reduce the degree of confluence because it decreases the percentage of cells.

The trypsinization process consists in the following step:

the culture medium was removed from the flask and the container was washed twice with Phosphate Saline Buffer (1x). Then 1,5 ml of trypsin was added and the cells were incubated at 37 °C (5% CO₂) for 5 minutes. Later, cells and trypsin were removed and added in a falcon containing 5 mL of medium. In order to separate cells from trypsin, this suspension was centrifuged at 1500 RPM for 5 minutes. At the end, cells were suspended in 20 ml of fresh medium and added in the flask or counted and seed in a plate.

In cellular studies every assay was performed following three passages:

- 1) Trypsinization
- 2) Cells count
- 3) Seeding plate

Regarding cell count, this operation was performed in an automated cell counter with a cell counting slide. In the slide, 20 μ l of cells suspension were mixed with 20 μ l of Trypan blue 0,4 %, a vital stain which is able to color dead cells or tissue in blue. After counting, plates were seeded.

In cellular assays the behavior of both ZnO pristine and ZnO-NH₂ was studied at the following concentrations: 5 μ g/mL, 10 μ g/mL, 25 μ g/mL, 50 μ g/mL, 100 μ g/mL. In the following page, the image simulates the 24 well plate used in the assay. In addition, two different experiment were performed. In the first one, cells and ZnO nanostructure were put in contact at same time, to analyse the situation when stem cells and antimicrobial agents arrive simultaneously. In the second assay, cells were cultured up to the 70 % of confluence, and then the nanoparticles were added. This procedure simulates the interaction between a pre-formed bone tissue and antibacterial agents, in order to analyze how they may affect the viability of the tissue. In the figure 2.3, the image schematizes the 24 well plates used in the assay. In addition, there are two tables regarding the composition of medium and Phosphate Saline Buffer.

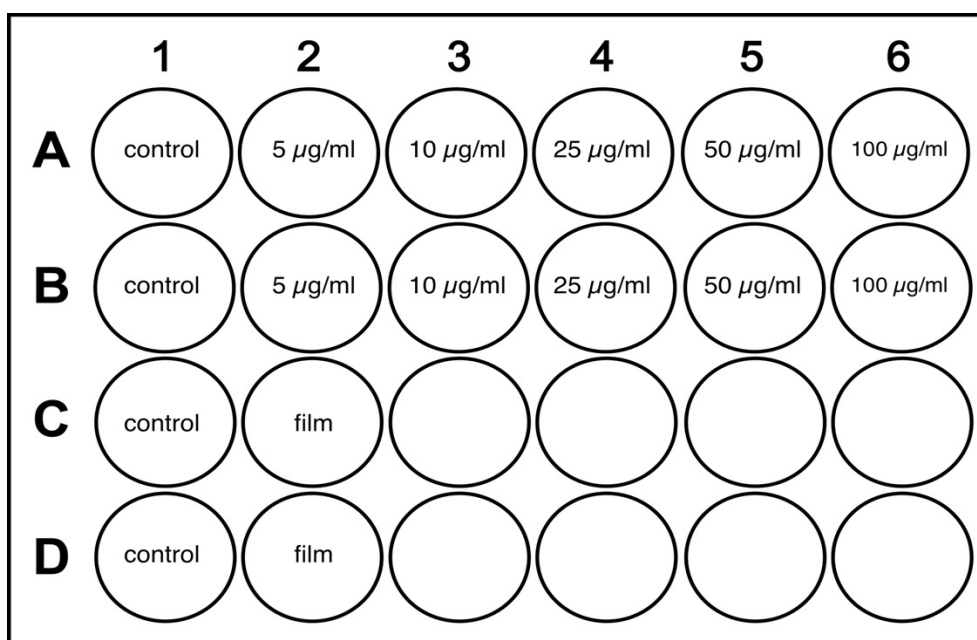


Figure 2.3 24-well plates used in the assays

Compounds	Concentration (mg/l)
Calcium Chloride (CaCl ₂) (anhyd.)	200.0
Magnesium Sulfate (MgSO ₄) (anhyd.)	97.67
Potassium Chloride (KCl)	400.0
Sodium Bicarbonate (NaHCO ₃)	2200.0
Sodium Chloride (NaCl)	6800.0
Sodium Phosphate monobasic (NaH ₂ PO ₄ -H ₂ O)	140.0
D-Glucose (Dextrose)	1000.0
Lipoic Acid	0.2
Phenol Red	10.0
Sodium Pyruvate	110.0
Amino acids	1234.4
Vitamin	59.56

Table 2.2 - Composition of α -MEM [21]

Compounds	Concentration (mg/l)
Potassium Phosphate monobasic (KH ₂ PO ₄)	144.0
Sodium Chloride (NaCl)	9000.0
Sodium Phosphate dibasic (Na ₂ HPO ₄ -7H ₂ O)	795.0
pH	7.4

Table 2.3 - Composition of PBS 1x [22]

2.3.3 Cytotoxicity

Cell cytotoxicity refers to the ability of certain substances or cells mediator cells to kill living cells. Cells exposed to a cytotoxic compound can respond in a number of different behaviors. If the insult is lethal, the cells can undergo necrosis, during which membrane integrity is lost and they die quickly. Otherwise the cells can follow other ways of cell death, like apoptosis or autophagy. Cells exposed to a sublethal compound can stop the growth and divide. This behavior can be estimated measuring various factors that include induction of superoxide, depletion of glutathione, decrease or loss of mitochondrial membrane potential, and reduction in overall viability.

2.3.4 Cytotoxicity test-LDH

Activity of LDH released by the MC3T3-E1 cells is directly related to the breakage of the plasmatic membrane (cell death) that, when broken, releases all organelles and enzymes present in the cytoplasm. For this reason this enzyme can be used as a marker of cell death. More in details, Lactate dehydrogenase (LDH) is an enzyme of living cells ant it is able to catalyze the reduction of pyruvate by NADH, according to the reaction 2.4:



The rate of decrease in concentration of NADPH, is directly proportional to the catalytic concentration of LDH present in the sample and it is measured by utilizing a spectrophotometer. Activity of the lactate dehydrogenase enzyme (LDH) was determined in the culture medium in contact with the NPs for 3 days of incubation. For this purpose, 0.750 mL of cell suspensions with a concentration of 1.33×10^4 cells/mL and 0.250 mL of NPs suspensions with 4x desired concentration were added in each plate.

After adding NPs in the cells suspensions, the well plates were left in incubation under CO₂ (5%) atmosphere at 37 °C for 3 days after which the medium was taken off and frozen at -20 °C. The frozen samples were then used for LDH measurement. After unfreezing of the samples, the commercial kit by Spinreact was employed to measure the LDH.

The kit consists of two reagents:

R1 (vial)	Imidazol 65 mmol/L Pyruvate 0,6mmol/L
R2 (tablet)	NADH 0,18 mmol/L

Table 2.4 Reagents of LDH measurement [23]

The procedure was as follows :1 mL of working reagent was mixed with 33 μL of sample and they were incubated for 1 minute. After absorbance was read in spectrophotometer at 340 nm and repeated the measure every minute for 3 minutes.

It is necessary to use the formula 2.5 to obtain the amount of LDH:

$$\frac{\Delta A}{\text{min} \times 4925} = \text{U/L LDH (25}^\circ\text{C)} \quad (2.5)$$

Regarding the unit, one international unit (IU) is the amount of enzyme that converts 1 mol of substrate per minute, in standard conditions. The concentration is expressed in units per liter of sample (U/L). [23]

2.3.5 Mitochondrial activity – MTT

Cell proliferation is a process that results in the increase of number of cells due to cell growth and division.

For evaluating cell proliferation various assay are available. Among them, the most important are: DNA synthesis, metabolic activity, antigens associated with cell proliferation and ATP concentration. The chosen option in this work is metabolic activity. The metabolic activity is monitored via mitochondrial activity of living cells, using MTT assay.

The MTT assay is a colorimetric assay for measuring cell metabolic activity. At the base of this method there is the capacity of nicotinamide adenine dinucleotide phosphate (NADPH)-enzyme to reduce the tetrazolium dye MTT to its insoluble formazan (purple color). This analysis checks cell viability in terms of reductive activity as enzymatic conversion of the tetrazolium compound to water insoluble formazan crystals. This process is due to dehydrogenase, which occur in the mitochondria of living cells. In this assay, it is necessary a solution able to dissolve the insoluble purple formazan product into a colored solution. Successively, the absorbance of this colored solution is measured at a certain wavelength by a spectrophotometer. MTT method is one of the most used methods to analyze cell proliferation and viability. However, the conversion to formazan crystals depends on metabolic rate and number of mitochondria, which are affected by many other known interferences, and for this reason further experiments like LDH are needed to check the cytotoxicity. [24]

For MTT assay, 0.750 ml of MC3T3-E1 cells in a concentration of 10^4 cells/ml in complete medium were cultured in 24-well plates in presence of 0.250 ml of ZnO and ZnO-NH₂ nanoparticles suspension at different concentrations and incubated in 5% CO₂ atmosphere at 37°C during 3 days. After this time, culture medium were substituted with 1 ml of α -MEM and 125 μ L of MTT solution (5 mg/mL in PBS 1x) was added. Samples were incubated for 4 h at 37 °C and 5% CO₂ in dark conditions. Then, media was removed and 500 μ l of HCl-isopropanol solution 0.4 M was added. At the end, absorbance at 570 nm was measured. [25]

2.3.6 Cell morphology studies

The morphology of pre-osteoblast cells MC3T3-E1 was studied in AMG EVOS fl LED Fluorescent Microscope. For this purpose, cell were cultured up to 70 % of confluence, and then the medium was taken off. Afterwards 0.750 mL of complete α MEM and 0.250 mL of NPs suspensions with 4x desired concentration were added in each plate. Samples were incubated for 4 days. After this time, adherent cells were fixed with Paraformaldehyde (4% in PBS) for 30 minutes. Then Atto 565-conjugated phalloidin and DAPI were added in each plate to stain respectively actin in red and nuclei in blue. [25]

2.3.7 Differentiation assay: Alkaline phosphatase activity – ALP

Osteoblasts develop from mesenchymal precursors called pre-osteoblasts through differentiation process. Bone is constructed in 3 processes: osteogenesis, modeling and remodeling. Osteoblasts mediates all these processes and they work in cooperation with bone resorbing osteoclasts. In fact, the bone matrix is secreted and mineralized by osteoblasts, while osteoclasts are responsible for bone modelling and remodeling.

Regarding the differentiation, transcriptional regulators govern this process. In particular, the activation of Runx2 is a fundamental step after which mesenchymal cells are converted in pre-osteoblasts. Then, pre-osteoblasts undergo a 3-stage differentiation, which leads to mature osteoblasts.

Stage 1 is characterized by cell proliferation and expression of fibronectin, collagen, TGF β receptor 1, and osteopontin.

In the Stage 2 the cells start differentiating and matrix maturation occurs with Alp and collagen.

the stage 3 matrix mineralization occurs when organic scaffold reaches great level of osteocalcin, which accelerates the deposition of mineral substance. In this final stage the osteoblasts have the characteristic cuboidal shape [26]. For evaluating the differentiation of

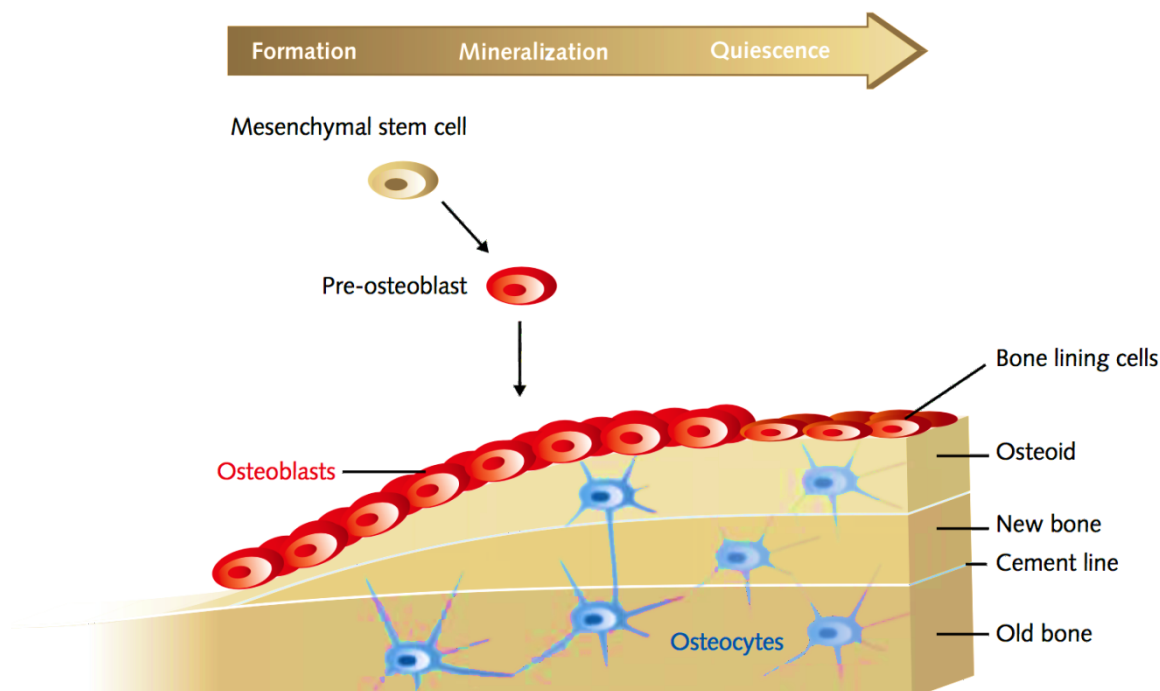
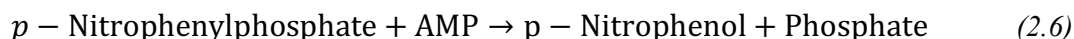


Figure 2.4 Scheme of osteoblasts differentiation and mineralization (modified from [27])

MC3T3-E1, Alkaline Phosphatase (ALP) measurements were employed. Alkaline phosphatase is an enzyme present in most of the organisms, with high quantities in bone, liver, placenta, intestine and kidney. Both rise and drop of plasma ALP values are of clinical importance.

ALP of the cells growing in contact with ZnO nanostructure was utilized as marker of cellular differentiation in the evaluation of the phenotype expression of osteoblasts. In details, Alkaline Phosphatase (ALP) catalyses the transfer of the phosphate group from p-nitrophenylphosphate to 2-amino-2-methyl-1-propanol (AMP), liberating p-nitrophenol according to the reaction 2.6:



The rate of p-Nitrophenol formation, is directly proportional to the catalytic concentration of alkaline phosphatase concentration in the sample and it is measured by utilizing a spectrophotometer.

For this purpose, MTC3T3-E1 pre-osteoblastic cells (10^4 cells/mL) were cultured directly in a 24-well plate and incubated for 10 days in contact with ZnO and ZnO-NH₂ under standard culture conditions (37 °C , 5 % CO₂) using α -MEM completed medium supplemented with b-glycerolphosphate (50 mg/ml) and L-ascorbic acid (10 mM). In particular 0.750 mL of cells suspensions with a concentration of 1.33×10^4 cells/ mL and 0.250 mL of NPs suspensions with 4x desired concentration were added in each plate. Two replicated were done for each concentration.

After incubation for 10 days, the medium was taken off and every well plate was washed twice with PBS (1x pH 7.4). Successively, samples were frozen and before the measurement they

were frozen and unfrozen for 3 times in order to break the cell membrane and release ALP. ALP was measured employing a Spinreact kit.

The kit consists of two reagents:

R1 buffer	2-Amino-2-methyl-1-propanol	0,35 mol/L
	Zinc sulfate	1 mmol/L
	Magnesium acetate	2 mmol/L
	N-hydroxyethylethylenediaminetriacetic- acid (EDTA)	2 mmol/L
R2 substrate	p-Nitrophenylphosphate (<i>p</i> NPP)	10 mmol/L

Table 2.5 Reagents for ALP measurement [28]

To obtain the working reagent, R1 and R2 were mixed, and then 1mL of working agent was put in every well plate and incubated under orbital stirring at 100 RPM at 37 °C for 30 min. Successively 200 µL di NaOH 2M were added to stop reaction and the absorbance was read in a spectrophotometer at 405 nm. [28]

2.3.8 Differentiation assay: Total protein content

Regarding the differentiation, total protein content was measured as well. The proteins are widely distributed in the organism and they are macromolecular organic compounds which act like structural and transport elements. Albumin and globulins are two types of protein contained in the serum. The determination of total proteins is useful in the detection of differentiation. The total protein content is directly proportional to the intensity of formed color when they give an intensive violet-blue complex with copper salts in an alkaline medium.

For this purpose, MTC3T3-E1 pre-osteoblastic cells (10^4 cells/mL) were cultured directly in a 24-well plate and incubated for 10 days in contact with ZnO and ZnO-NH₂ under standard culture conditions (37 °C, CO₂ 5 %) using α -MEM completed medium supplemented with b-glycerolphosphate (50 mg/ml) and L-ascorbic acid (10 mM). In particular 0.750 mL of cells suspensions with a concentration of 1.33×10^4 cells/ mL and 0.250 mL of NPs suspensions with 4x desired concentration were added in each plate. Two replicated were done for each concentration

After incubation for 10 days, the medium was taken off and every well plate was washed twice with PBS (1x pH 7.4). Successively, samples were frozen and before the measurement they were frozen and unfrozen for 3 times in order to break the cell membrane and release protein. Total protein was measured employing a Spinreact kit.

The kit consists of two reagents:

R biuret	Sodium potassium tartrate 15 mmol/L Sodium iodide 100 mmol/L Potassium iodide 5 mmol/L Copper (II) sulphate 5 mmol/L Sodium hydroxide 1000 mmol/L
T PROTEIN CAL	Bovine albumin primary standard 7 g/dL

Table 2.6 Reagents for total protein content measurement[29]

1 mL of Working reagent was added to every well plate and incubated for 5 minutes at 37 °C. Standard consist in 1 mL of working reagent and 25 µL of T Protein Cal. Later absorbance was read at 540 nm. [29] To obtain the quantitative of Total Protein, the following formula was used:

$$\frac{(A)_{sample} - (A)_{Blank}}{(A)_{standard} - (A)_{Blank}} \times 7(\text{Conc. standard}) = \frac{g}{dL} \text{ of total protein} \quad (2.7)$$

2.4 Antibacterial Studies

Bacteria are divided in Gram positive and negative. Bacteria's structure is characterised by a cell membrane, cell wall and cytoplasm. The cell wall is outside the cell membrane and is characterised by a peptidoglycan layer of amino acids and sugars. It has the function to maintain the osmotic pressure of cytoplasm and cell shape. The cytoplasm is a jelly like fluid, composed mainly of proteins, carbohydrates salts, ions and water, and it has the function to involve all cellular component except the nucleus. These components are organelles that regulate growth, metabolism, and replication. The difference between Gram positive and negative bacteria is in cytoplasmic membrane. In fact, gram positive show only one cytoplasmic membrane and a cell wall of 70-80 nm. On the other side, gram negative bacteria have two cell membranes and a plasma membrane of 7-8 nm.

The effectiveness of ZnO and ZnO-NH₂ nanoparticles against bacteria in planktonic stage have been determined and the antimicrobial activity was carried out against Gram negative and positive bacteria to see the behavior against two different bacteria morphologies

Escherichia coli is gram negative bacteria, anaerobic or aerobic, rod shaped and it is the most widely studied prokaryotic model organism. Most *E. coli* strain are not harmful, in particular this strain are part of the normal gut flora and prevent colonization of the intestine with pathogenic bacteria. It takes only 20 minutes to reproduce in favourable conditions and it is easy to culture. All these characteristics make it suitable for laboratory studies.

On the other hand, *Staphylococcus aureus* is Gram positive bacteria and the most important species of the *staphylococci*. It is round shaped and appears as grape like clusters in the microscope. Respect to *E. coli*, *S. Aureus* is an opportunistic pathogen and is more harmful. Besides its presence in normal flora bacteria in mammals, it can cause chronic infections and form biofilm on medical implants. [7]

2.4.1 Bacteria culture conditions

Escherichia coli and *Staphylococcus Aureus* were cultured in sterile Todd Hewitt Broth (THB) medium. THB medium was prepared, suspending 37 g of Todd Hewitt Broth in 1 L of Milli Q Water, mixed, stirred and at the end sterilized by autoclaving at 121 °C for 20 minutes. [30]

Compounds	Composition (g/L)
beef heart, infusion (from 500 g)	10
Peptic Digest of Animal Tissue	20
Dextrose	2
Sodium Chloride	2
Disodium Phosphate	0.4
Sodium Carbonate	2.5
Final pH at 25°C	7.8

Table 2.7 Composition of Todd Hewitt Broth [30]

2.4.2 CFU counting method

To examine the bactericidal effect of ZnO nanoparticles on bacteria, in planktonic stage, CFU counting method was used. CFU counting method is frequently used and it exploits Agar plates. Agar plates are Petri dishes containing Agar in combination with a growth medium to culture microorganisms such as bacteria. In our case the medium was Tryptic Soy Agar, and it is used for cultivation, isolation of microorganism or for maintenance of stock culture. Agar plates

permits the determination of number of colony-forming units (CFU) present after the treatment of bacteria suspension with an antimicrobial agent.

Compounds	Composition (g/l)
Casein peptone (pancreatic)	15
Soya peptone (papainic)	5
Sodium chloride	5
Agar	15
final pH at 25 °C	7.3

Table 2.8 Composition of Tryptic Soy Agar (Sigma Aldrich) [31]

2.4.3 Preparation of Agar plates

40 g of Tryptic Soy agar by Sigma Aldrich (composition in table above) were added to 1 L of Milli Q water, mixed and stirred. After, the suspension was sterilized by autoclaving at 121 °C for 20 minutes. Then Agar was cooled at 40-50 °C and was added into sterile petri dishes. [31]

2.4.4 Preparation of bacteria suspensions

Bacteria cultured in sterile THB medium, at 37 °C under orbital stirring, were taken away and 100 µL of this suspension was added in a falcon with 6 mL of THB. Two falcon tubes were made, steril and no steril. The absorbance relative to the blank (THB medium) was measured up to the value of 0,4, that means bacteria concentrations of 2×10^9 bacteria/ml. At this point, a certain amount was taken and bacteria were suspended in sterile PBS (1x) with a desired concentration. In our case 10^6 bacteria/ml was used.

2.4.5 CFU counting method procedure

In this case, the concentrations of 5 µg/mL, 10 µg/mL, 25 µg/mL, 50 µg/mL, 100 µg/mL were used. ZnO free suspensions were utilized as control. The figure 2.5 summarizes the 24 well plate used in the assay. Two replicas were done for every concentration. 0.750 mL of bacteria suspensions with a concentration of 1.33×10^6 bacteria/ mL and 0.250 mL of NPs suspensions with 4x desired concentration were added in each plate.

NPs and bacteria suspensions were incubated for 24 h under orbital stirring at 37 °C . After 24 h, severe dilutions were made in order to count CFU. 20 µL of every sample was collected and added in an agar plates, which were incubated at 37 °C for an overnight. Then CFU were counted.

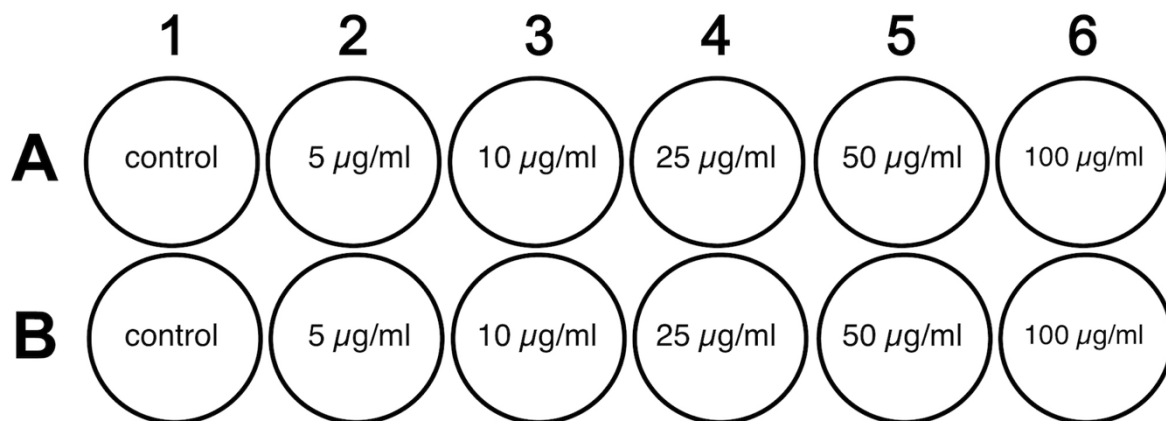


Figure 2.5 24 well-plates used in the assays

2.4.6 Bacterial Adhesion and biofilm formation

A different assay was performed to test the ZnO porous film against bacteria. This assay consists in a bacterial adhesion and biofilm formation on film surface. As seen before, bacteria adhesion is a crucial step in forming biofilm and material that inhibits their adhesion are promising candidate for bone implants. The formation of biofilms is a process of different stages. Initially bacteria, from bulk liquid, arrive on the surface material and some of them adsorb. Depending on local environmental variables and repulsive and attractive forces, bacteria can adhere to the surface or not. At the beginning bacteria are adsorbed reversibly but as time goes by, they adsorbed irreversibly. After this phase, a lag phase occurs, interactions and growth develop a mushroom structure that allows the passage of nutrients to bacteria deep within a biofilm. The lag phase is followed by an exponential phase, characterised by exponential growth and excretion of polysaccharide intercellular adhesion polymers. The final step is the formation of mature biofilm. [32]

For this purpose, ZnO films and Cover glass disks (control) were washed in ethanol and sterilized by UV-light radiation for 15 minutes. The effectiveness of ZnO film was determined against *Staphylococcus aureus* and *Escherichia coli*. Suspensions at concentration of 10^6 bacteria/ml were prepared in sterile THB medium. 1 ml of these suspensions was added in each well plate, where cover glass disks aging as control and ZnO films were localized. Well plate was incubated for 24 h and after this time, medium was removed and each plate was washed with sterile PBS. Every disk included ZnO film was stained with 3 µl/ml (in PBS) Live/Dead® Bacterial Viability Kit (Backlight TM) and 5 µl/ml (in PBS) of calcofluor solution in order to examine in confocal microscope the bacterial adhesion. Both reactants were incubated 10 minutes at room temperature.

2.4.7 Morphologies studies-SEM

SEM micrographs were carried out to study the change in morphology of ZnO porous film after the incubation with *E. coli*. The aim of this assay is to determine how bacteria interact with surface of films. ZnO films were incubated for 24 h in presence of *E. coli* suspension with a concentration of 10^6 bacteria/ml. After this time, adherent bacteria were fixed with Glutaraldehyde (2.5 % in PBS) for 40 min. Afterwards Glutaraldehyde was removed and films were washed twice with PBS. Then samples were gradually dehydrated with a series of ethanol solutions (10%, 25 %, 50 %, 70 %, 90 %, 95 %, 100 %), for 30 minutes. Later, the samples were dried into a vacuum oven at 30 °C for 7 days. Successively, films were stick onto a copper holder, metalized with gold in a metallization instrument and analysed in the scanning electron microscope JEOL 3565F.

2.4.8 Biofilm assay

The effectiveness of ZnO and ZnO-NH₂ NPs was determined against *Escherichia coli* biofilm. For this purpose, cover glass disks were washed in ethanol and sterilized by UV-light radiation for 15 minutes. Then cover glass disks were treated with Poly-lysine for 90 minutes. *Escherichia coli* was suspended in sterile THB medium with 4 % of Sucrose (> 99% by Sigma Aldrich) at concentration of 10⁶ bacteria/ml. 1 ml of these suspensions was added in each well plate, where cover glass disks were localized. Well plate were incubated for 48 h and after this time, medium was removed and each plate was washed with sterile PBS. Afterwards 0.750 ml of sterile THB medium with 4 % of Sucrose (> 99% by Sigma Aldrich) and 0.250 ml of ZnO and ZnO-NH₂ NPs at concentration of 100 µg/ml were added in each plate. ZnO free suspension were made as control. NPs and bacteria were incubated for 1 h. After this time, medium was removed and samples were stained with 3 µl/ml Live/Dead® Bacterial Viability Kit (Backlight TM) and 5 µl/ml of calcofluor solution in order to examine them in confocal microscope. Both reactants were incubated 10 minutes at room temperature.

2.4.9 Statistical analysis

Data are expressed as average/mean ± standard deviation in two experiments. The software Statistical Package for the Social Sciences (SPSS) version 11.5 was used to perform statistical analysis. the variance analysis (ANOVA) was utilized for Statistical comparatives. Scheff proof was used for the post hoc evaluation of the differences among groups. In all statistical evaluations, $p < 0.05$ was considered as statistically significant.

3 Results and discussion

3.1 Morphological and structural characterization of ZnO NPs

3.1.1 X-Ray diffraction

In order to obtain information about phase identification, along with phase quantification, % crystallinity, crystallite size and unit cell size XRD was performed. In the figures 3.1 and 3.2, the X-ray patterns of pristine ZnO NPs and ZnO-NH₂ NPs are reported. The comparison of patterns with data bank (JCPDS 36-1451) has confirmed the crystalline structure of the particle. In particular, there are peaks at 31.9°, 34.4°, 36.4°, 47.6°, 56.7°. All peaks are indexed to (100), (002), (101), (102) and (110) planes which corresponds to the Miller index of typical hexagonal wurtzite structure of ZnO according to the literature and compared with standard pattern of ZnO. By using the Scherrer formula mentioned above and considering the dominant peak, it was possible to estimate the dimension of crystallite. In our specific case the dimension of crystallite results to be around 17 nm for ZnO pristine and 15 nm for ZnO-NH₂.

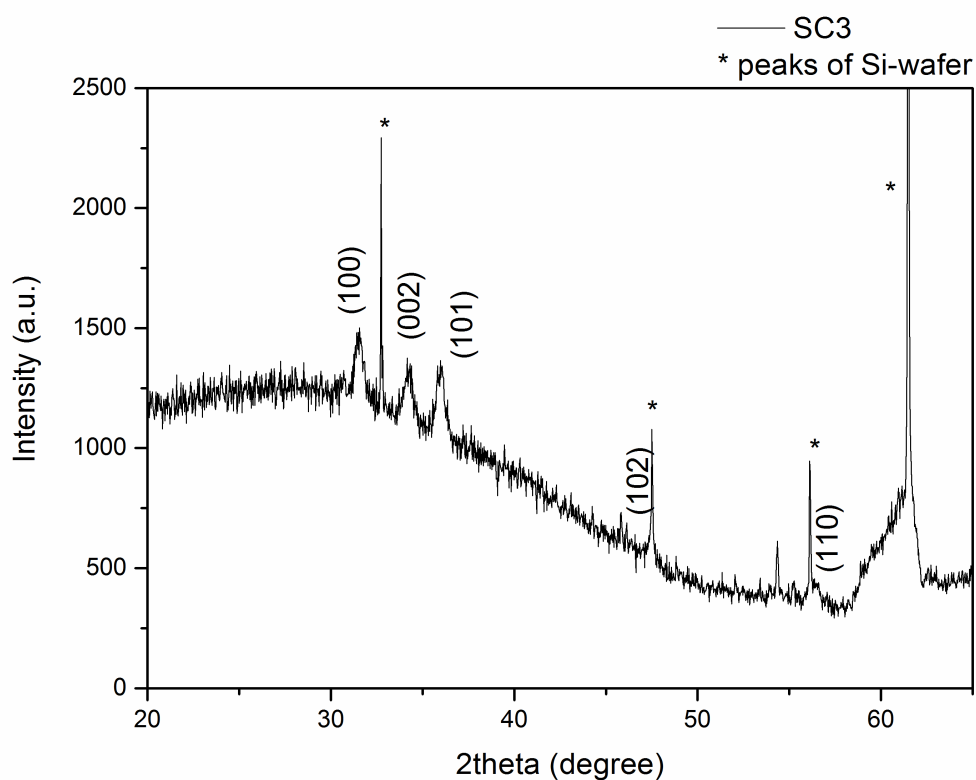


Figure 3.1 XRD pattern for ZnO NPs

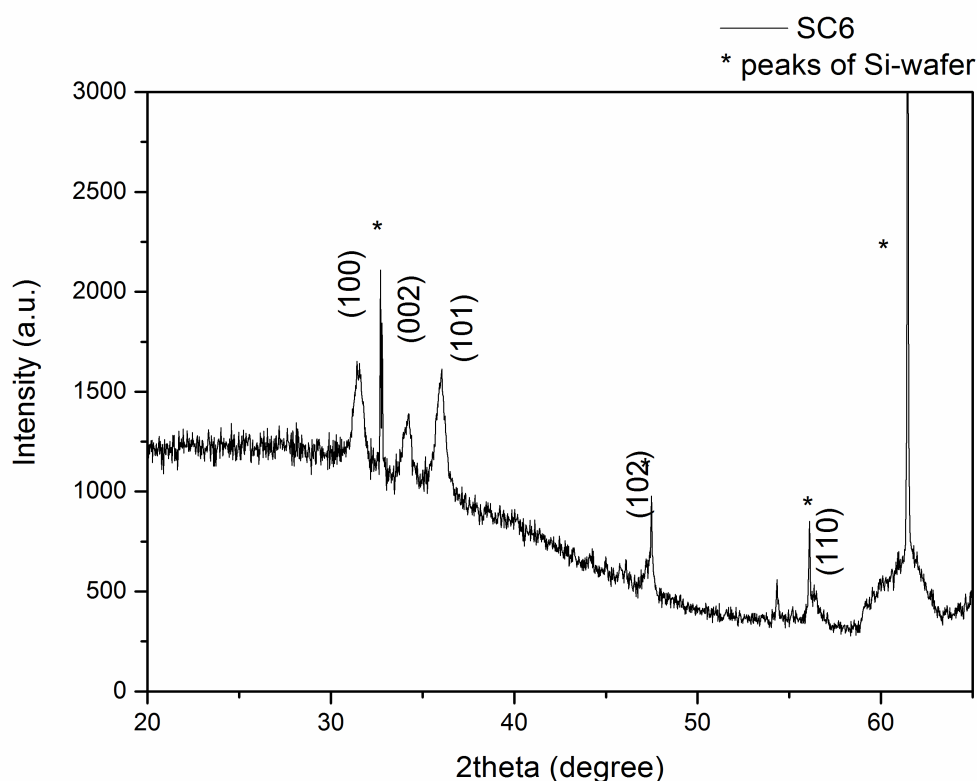


Figure 3.2 XRD pattern for ZnO-NH₂ NPs

3.1.2 Analysis of colloidal stability

In order to study the behavior of nanoparticles in solution, DLS (Dynamic Light Scattering) was used. This particular technique permits to obtain information about the aggregation of particles and colloidal stability of the system. It is very relevant to evaluate the stability in suspension for clinical applications. In fact, it is important that particles are not aggregated because they need a higher surface area to volume ratio to exhibit great activity. Moreover, a better internalization and a larger amount of hydroxyl radicals produced for antibacterial activity, is ensured by using smaller particles.

Taking a look at distribution number curve in figures 3.3 and 3.4, it is possible to observe a well defined peak, centered at 59 nm for pristine ZnO NPs and at 122 nm for functionalized ones. The presence of an only one peak means that the samples are not aggregated and well mono-dispersed. In addition, ZnO-NH₂ NPs result more aggregated because the distribution moves to higher dimensions ranges. Regarding the intensity distribution curve is well shown a very wide peak at 142 nm for pristine NPs and a thinner peak at 190 nm for functionalized ones.

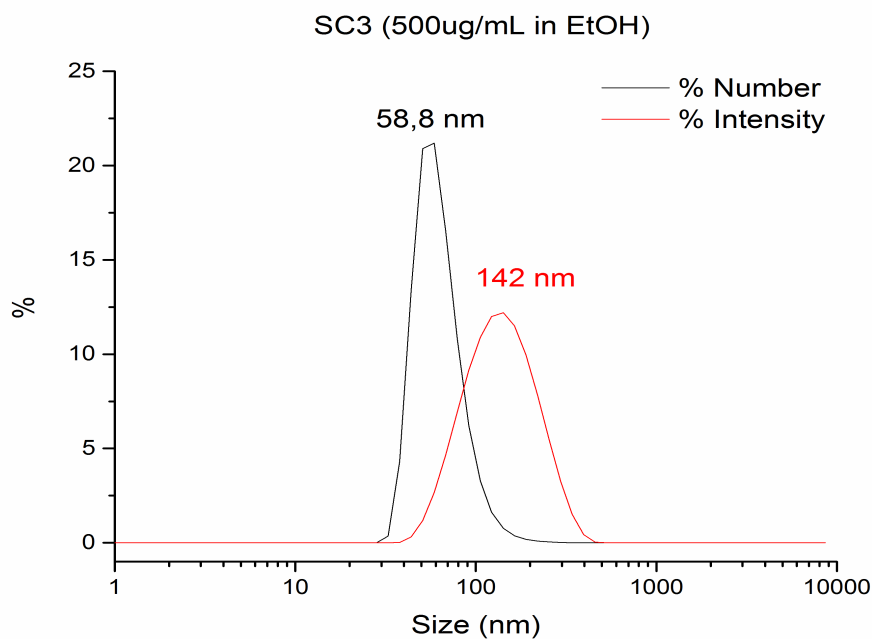


Figure 3.3 Distribution curves deriving from DLS measurement for ZnO NPs

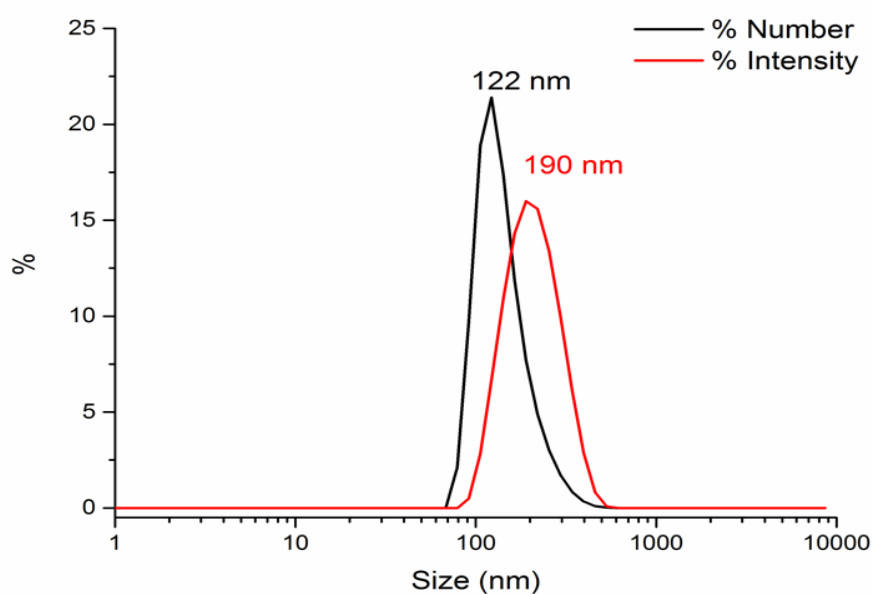


Figure 3.4 Distribution curves deriving from DLS measurement for ZnO-NH₂ NPs

3.1.3 Transmission electron microscope –TEM

TEM analysis has permitted to obtain additional information about the particle's morphology and size. Two different magnification were used and the size of the particle was detected using Image J software.

The images 3.5 and 3.6 show that the particles have a polygonal shape, typical of ZnO nanoparticles. Taking a look at TEM micrographs, functionalized nanoparticles are more aggregated than pristine nanoparticles as seen in DLS measurements. The dimensions of nanoparticles range from 20 to 25 nm both for pristine and functionalized as expected at the

beginning. The TEM micrograph confirms the obtained results from XRD and they are in agreement with the literature.

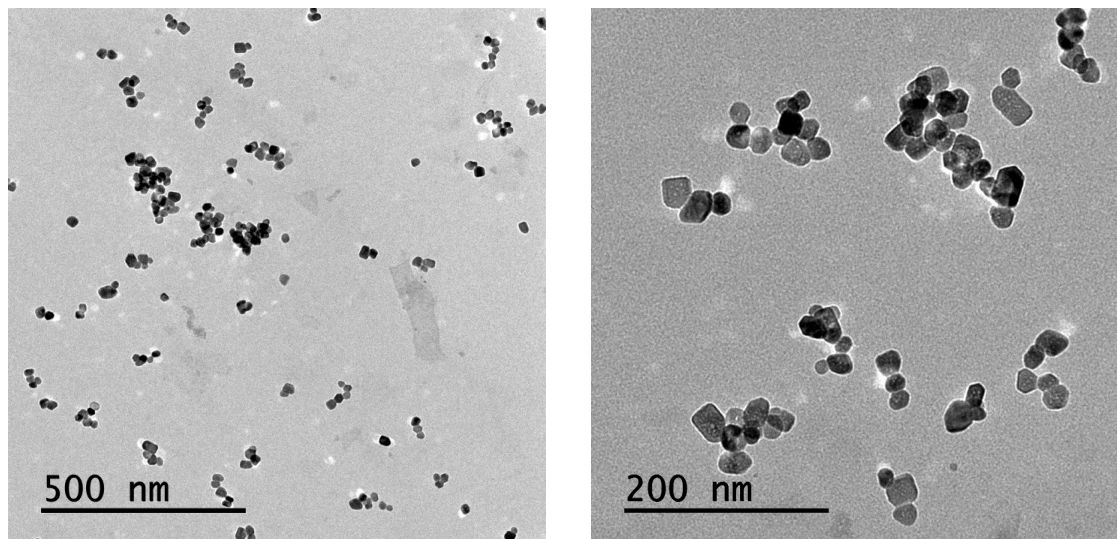


Figure 3.6 - Tem micrographs of ZnO NPs at different magnification

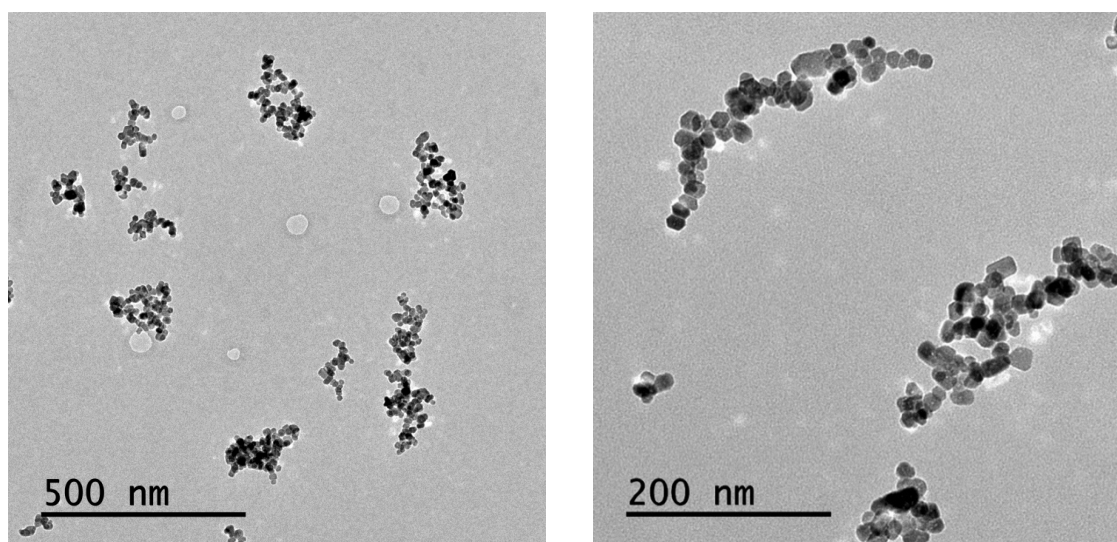


Figure 3.5 - Tem micrographs of ZnO -NH₂ NPs at different magnification

3.2 Morphological and structural characterization of porous ZnO film

3.2.1 X-ray diffraction

Figure 3.7 shows the XRD pattern representative for porous ZnO thin films deposited on cover glasses. This analysis was carried out to obtain information about the crystal structure and orientation of the porous ZnO samples. The comparison of the retrieved XRD patterns with data bank (JCPDS card no. 89-1397) confirmed the polycrystalline structure of the porous ZnO thin films. In particular, distinct diffraction peaks positioned at 31.9° , 34.5° , 36.4° , 47.7° and 56.7° were detected. According to the literature and comparing with standard reference patterns for ZnO, these peaks were assigned to (100), (002), (101), (102) and (110) planes belonging to wurtzite ZnO structure with hexagonal cell symmetry.

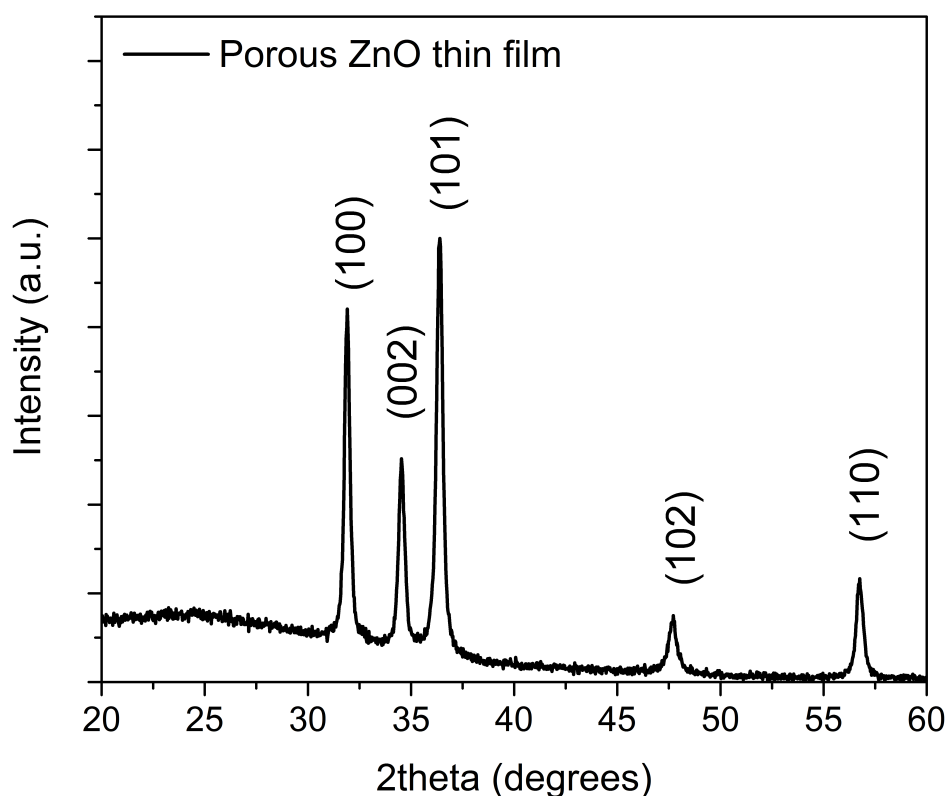


Figure 3.7 XRD pattern of porous ZnO thin film

3.2.2 Field-emission scanning electron microscopy

FESEM analyses provided information about several morphological features such as the shape and dimension of nanocrystals originating the porous ZnO thin film. The FESEM micrographs shown in Figures 3.8 highlight the presence of a sponge-like structure composed by randomly-oriented crystal grains. The surface is thus formed by a close interconnection of elongated and branched nanocrystals (average size 10-20 nm), resulting into a nanoporous network. From the comparison of the morphological characteristics between the starting Zn layer and the final ZnO thin film, no substantial changes in the nanobranched structure are observed. Therefore, the

starting porous morphology is preserved even after the thermal oxidation treatment. From cross-section FESEM imaging (figure 3.9), the average thickness of ZnO film was estimated to be around 3.5 μm .

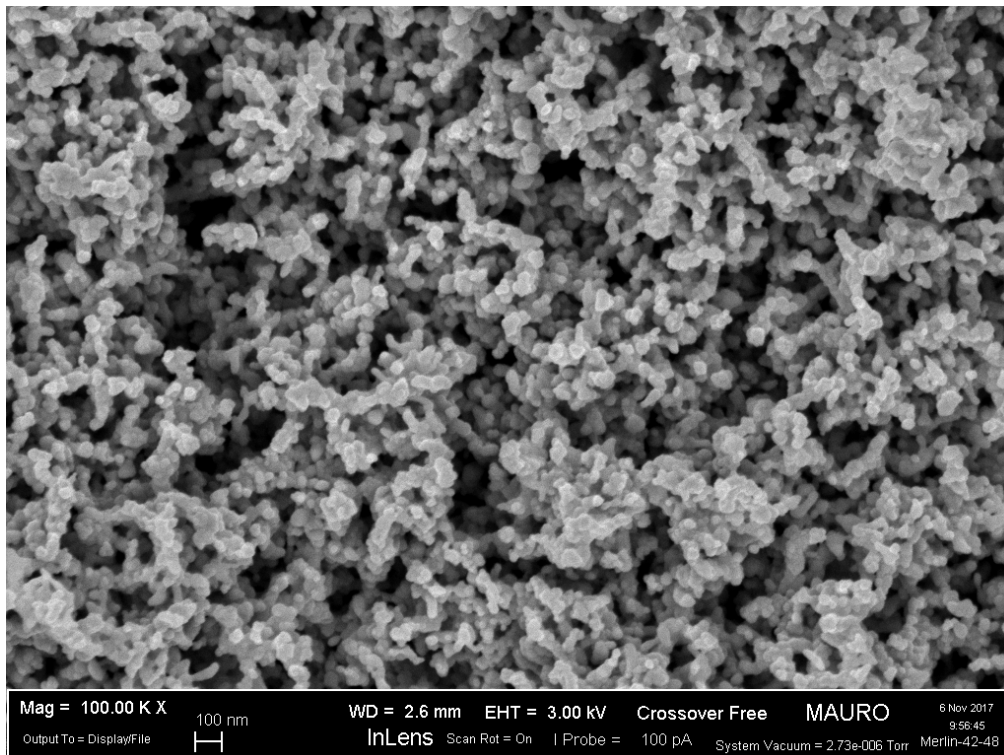
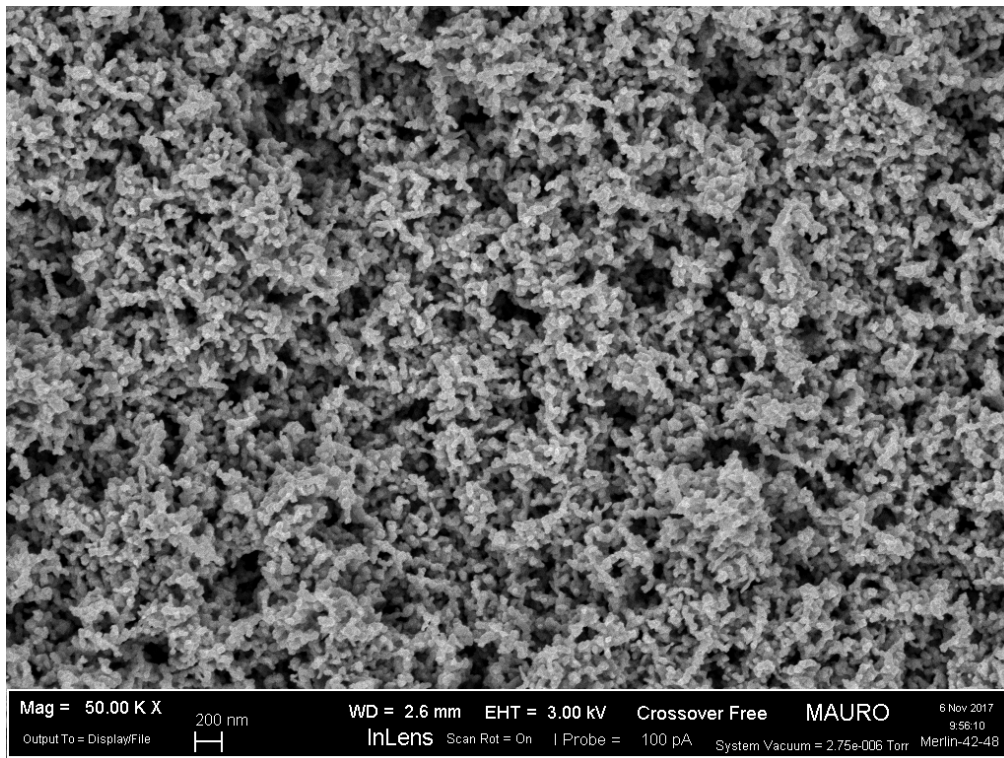


Figure 3.8 FESEM micrographs of porous ZnO thin film

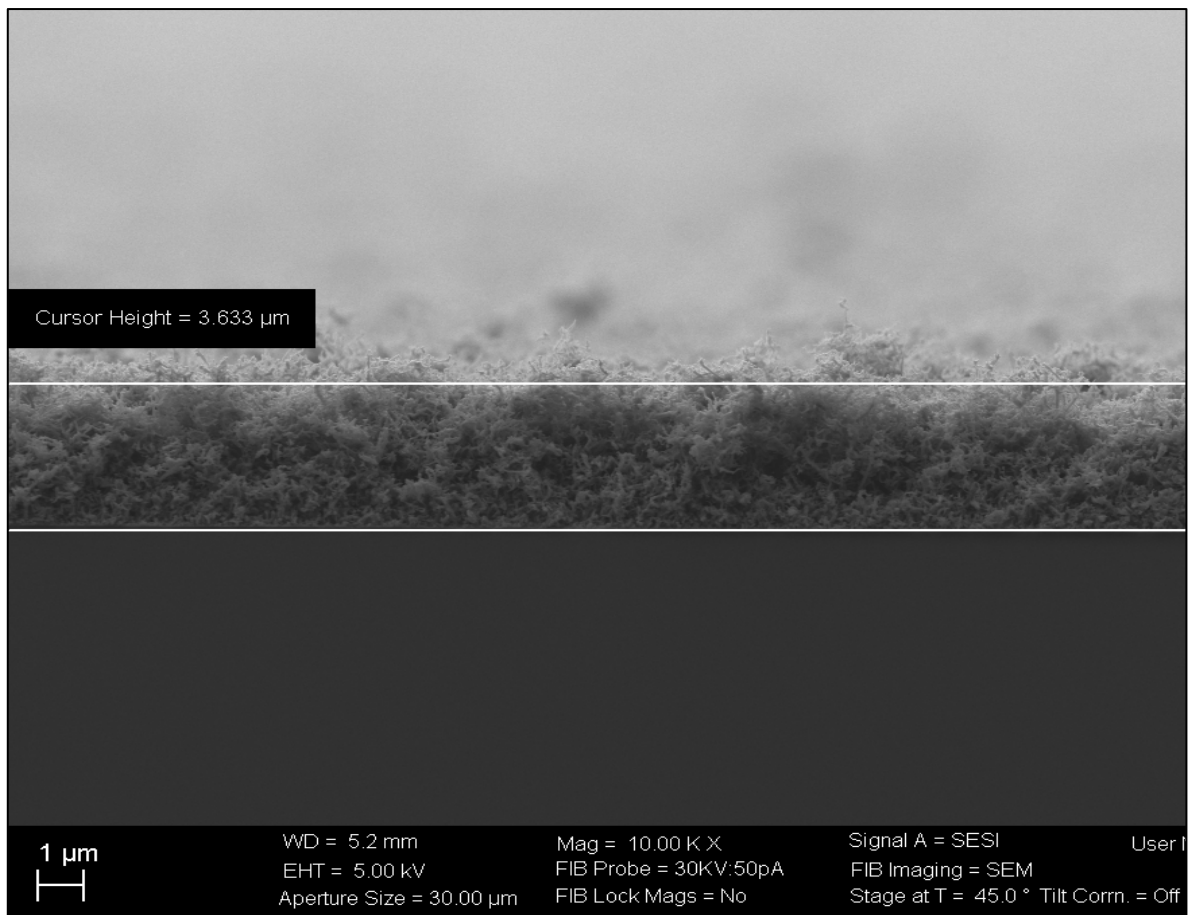


Figure 3.9 FESEM micrograph (cross section) of porous ZnO film

3.3 Cellular studies

3.3.1 Cytotoxicity test-LDH

Lactate dehydrogenase (LDH) and Mitochondrial activity (MTT) were studied to monitor the biocompatibility of both pristine ZnO and functionalized ZnO-NH₂ nanoparticles in living pre-osteoblast cells. The combination of LDH and MTT measurements gives a complete picture of the cytotoxicity and the cell proliferation behavior. The study is performed after 3 days of incubation in order to permit the cells growth in presence of nanoparticles.

Regarding the lactate hydrogenase tests reported in Figures 3.10 and 3.11, there is no cytotoxic effect up to 50 µg/ml because no significant differences were registered compared to the control in absence of nanoparticles. On the other side, the concentration of 100 µg/ml exhibits a cytotoxic effect on pre-osteoblast cells because the quantity of LDH was almost double compared to control. This trend was observed both for pristine and for functionalized nanoparticles.

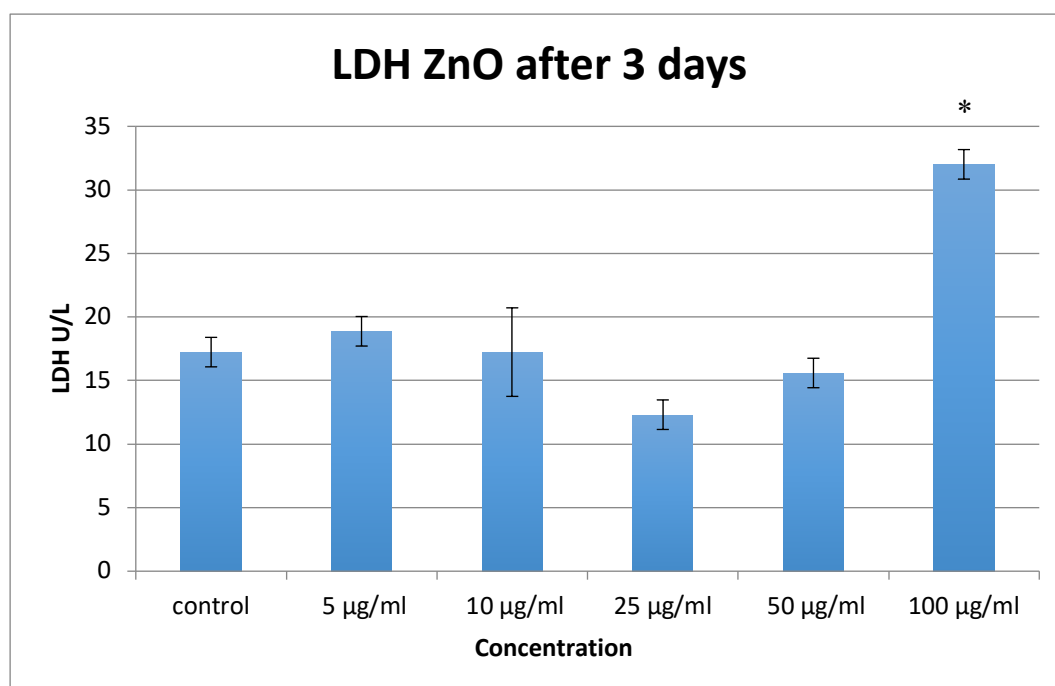


Figure 3.10 Cytotoxicity by lactate dehydrogenase (LDH) released into the medium after 3 days of incubation with different concentrations of ZnO NPs. ($p < 0.05$, significant differences compared to control denoted by an asterisk (*))

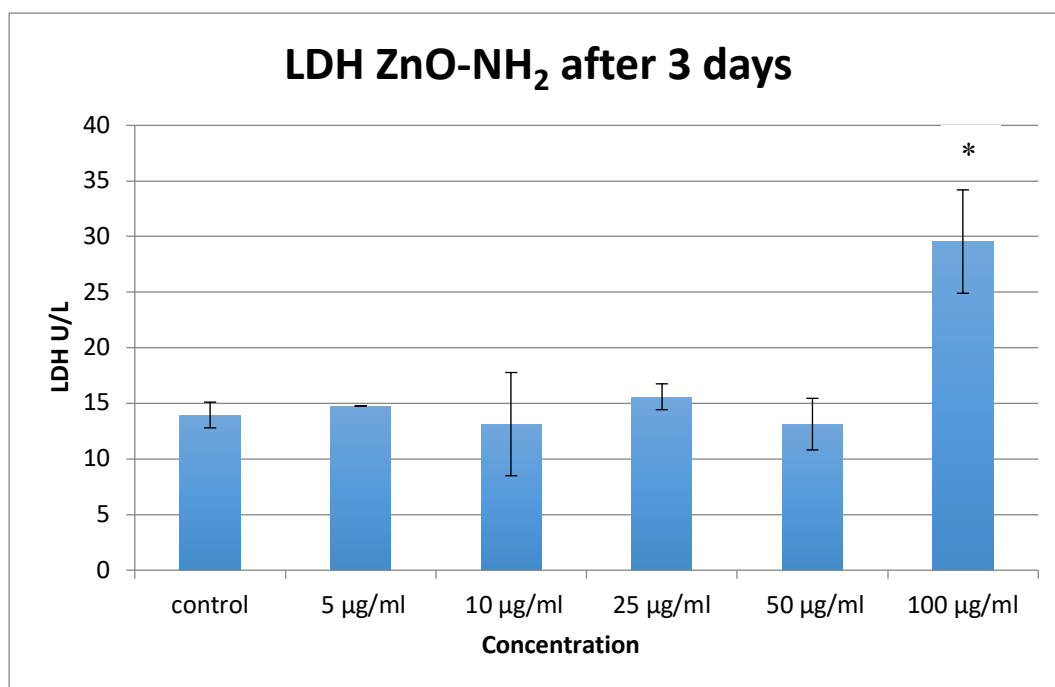


Figure 3.11 Cytotoxicity by lactate dehydrtheogenase (LDH) released into the medium after 3 days of incubation with different concentrations of ZnO-NH₂ NPs ($p < 0.05$, significant differences compared to control denoted by an asterisk (*))

3.3.2 Cell proliferation

Concerning the proliferation assay in Figures 3.12 and 3.13, there is an adequate proliferation. In particular, a slight decrease of mitochondrial activity occurs by increasing the concentration of NPs. The values of proliferation range from 90 % to 70 % up to 25 µg/ml (compared to control), then a slight decrease occurs for 50 µg/ml ($\approx 60\%$) both for pristine and functionalized NPs. Regarding the highest concentration, as observed in LDH of Figure 3.10, there is a significant change compared to control and other concentrations. In fact, the cell proliferation drops to 27 % for ZnO and 43 % for ZnO-NH₂. Therefore, the combination of results deriving from LDH and MTT assay, has highlighted the great biocompatibility of ZnO and ZnO-NH₂ up to the concentration of 50 µg/ml. On the other side the concentration of 100 µg/ml has shown a cytotoxic activity and inhibited the cell proliferation.

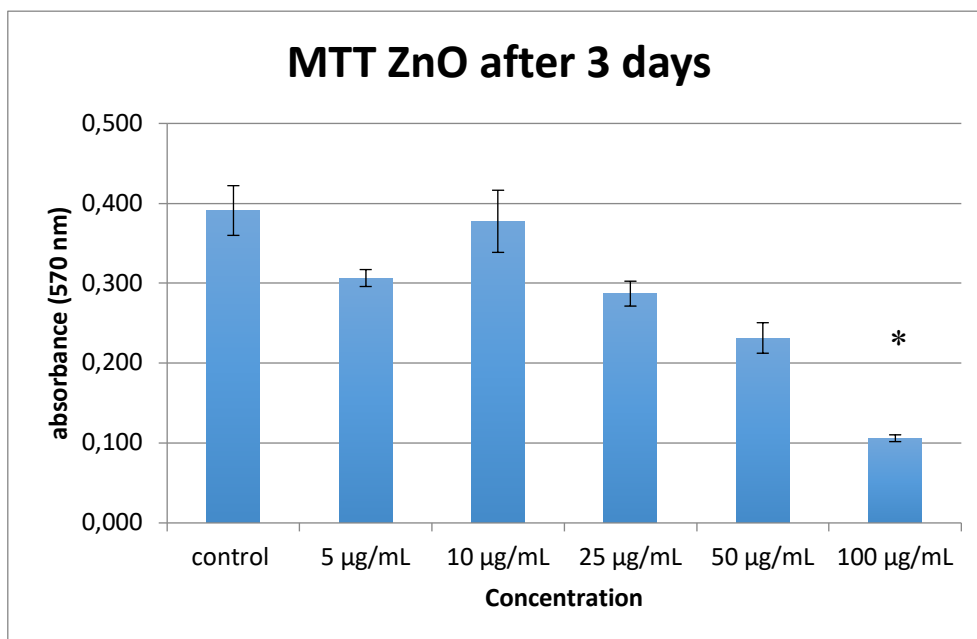


Figure 3.12 Proliferation results in terms of mitochondrial activity (MTT) after 3 days of incubation and with different concentrations of ZnO NPs. ($p < 0.05$, significant differences compared to control denoted by an asterisk (*))

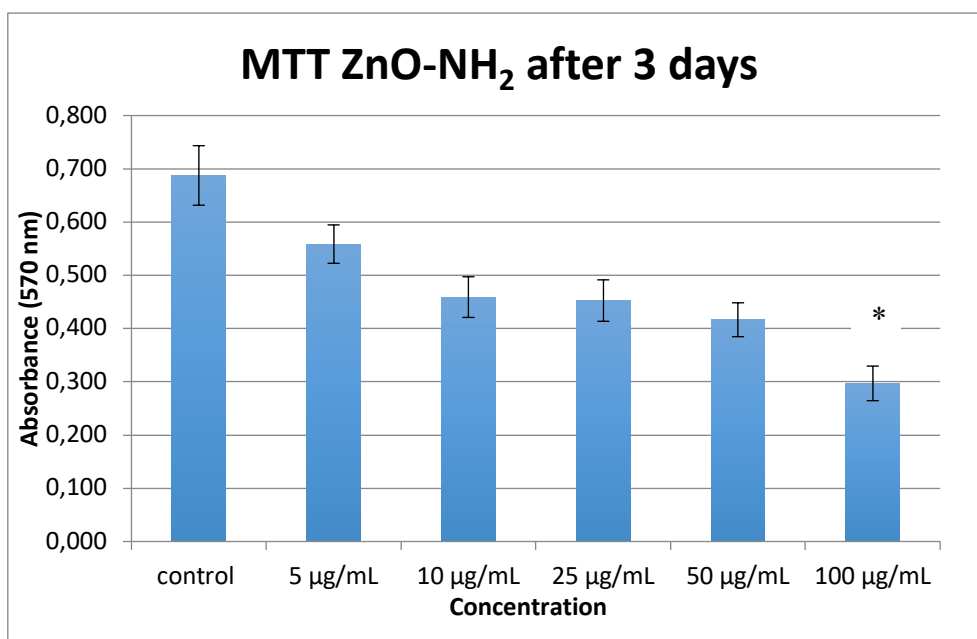


Figure 3.13 Proliferation results in terms of mitochondrial activity (MTT) after 3 days of incubation and with different concentrations of ZnO-NH₂ NPs. ($p < 0.05$, significant differences compared to control denoted by an asterisk (*))

3.3.3 ZnO film biocompatibility

In parallel to ZnO NPs biocompatibility study, the porous ZnO film biocompatibility was studied to understand how a change in morphology affects the cytotoxicity and the cell proliferation. Regarding the LDH assay in Figure 3.14, a deep difference between the control and the porous film was observed. In fact, LDH production on film sample was almost twice compared to the control. Moreover, its value is comparable to the value obtained from 100 µg/ml ZnO NPs. Therefore, it is clear the cytotoxic effect of ZnO porous film toward pre-osteoblast cells.

Taking a look at MTT assay in the figure 3.15, there was a similar trend. The decrease in proliferation compared to the control was of 41 %, comparable with 100 µg/ml. Therefore, the proliferation is hindered after 3 days in presence of ZnO film. This behavior can be explained by the fact that the porous film dissolves in the cell culture medium, and the amount of ZnO released is similar to the concentration of NPs of 100 µg/ml. For this reason, a possible solution could be a barrier layer which limits the release of ZnO.

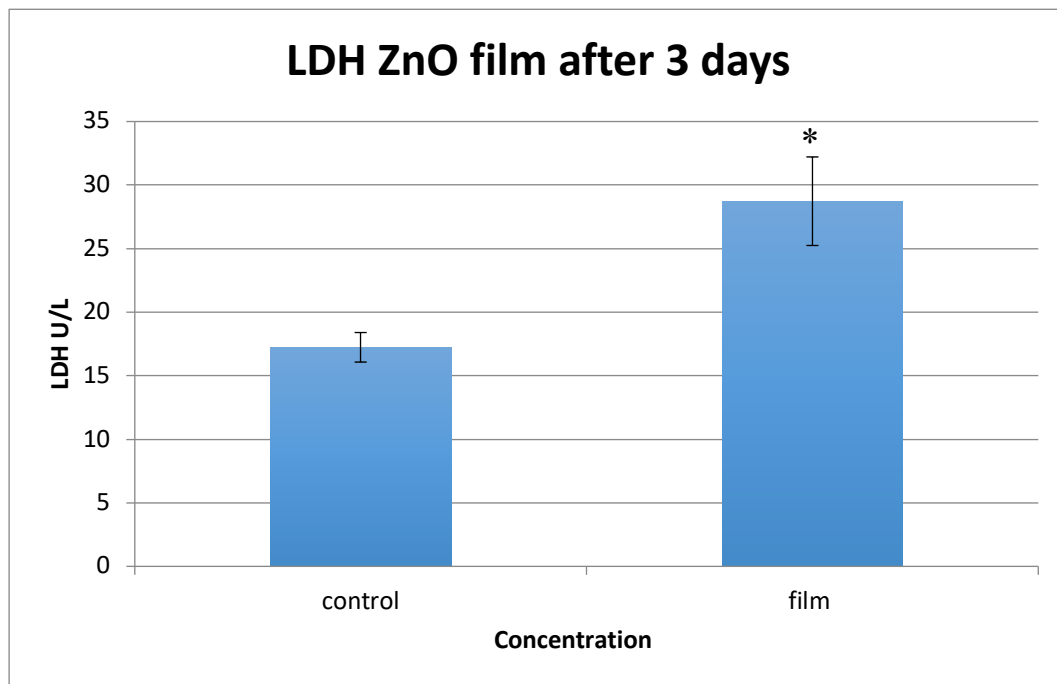


Figure 3.14 Cytotoxicity by lactate dehydrogenase (LDH) released into the medium after 3 days of incubation with porous ZnO film. ($p < 0.05$, significant differences compared to control denoted by an asterisk (*))

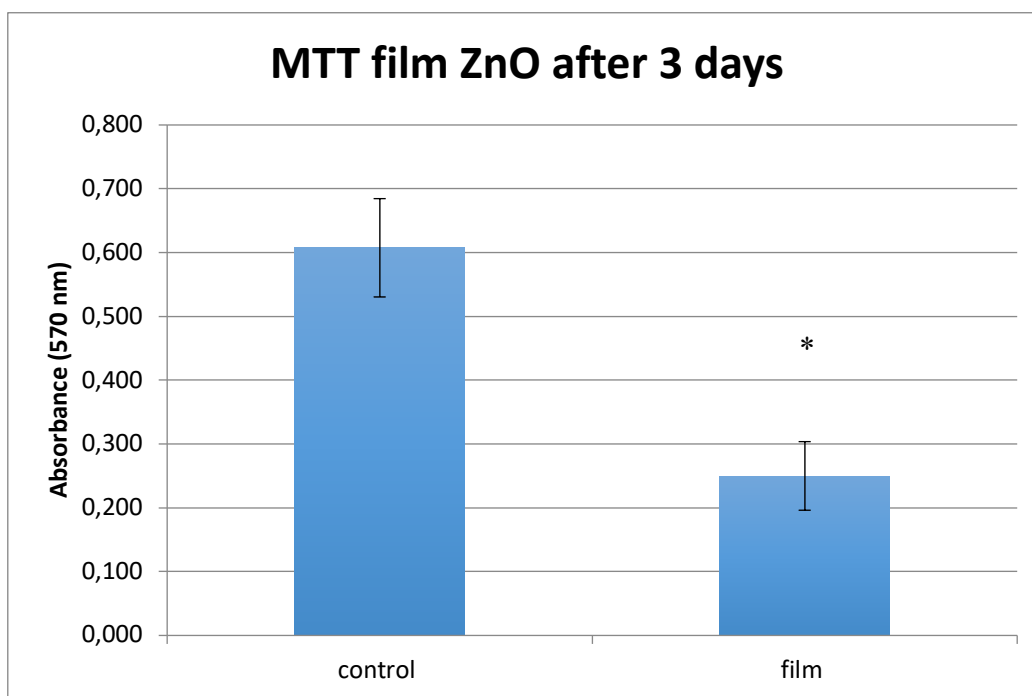


Figure 3.15 Proliferation results in terms of mitochondrial activity (MTT) after 3 days of incubation with porous ZnO film. ($p < 0.05$, significant differences compared to control denoted by an asterisk (*))

3.3.4 Cell proliferation at 70% of confluence

In this assay, the cells were cultured up to the 70 % of confluence, and then nanoparticles were added. This procedure was necessary to simulate the interaction between a pre-formed bone tissue and antibacterial agents, in order to analyze how they may affect the viability of the tissue. In this case, the proliferation via MTT was measured after 24 h of incubation and the cell morphology was studied under fluorescent microscope after 4 days of incubation (Figure 3.18 and 3.19). The values of MTT tests are of the same order of the control up to a concentration of 50 $\mu\text{g/ml}$ for pristine ZnO. Actually, the mitochondrial activity is around 100 % or higher compared to the control with a peak of mitochondrial activity for the concentration of 25 $\mu\text{g/ml}$, where the proliferation is increased up to 130 %. Unfortunately, a significant decrease occurs in correspondence of the concentration 100 $\mu\text{g/ml}$ where mitochondrial activity drops down to 41 %.

The results about ZnO-NH₂ are similar with just few differences. The best proliferation value is obtained for the concentration of 25 $\mu\text{g/ml}$, but the peak is less pronounced. Interestingly, the concentration of 100 $\mu\text{g/ml}$ does not show significant differences and the mitochondrial activity is still close to control. This result highlights the first difference between pristine and functionalized ZnO nanoparticles.

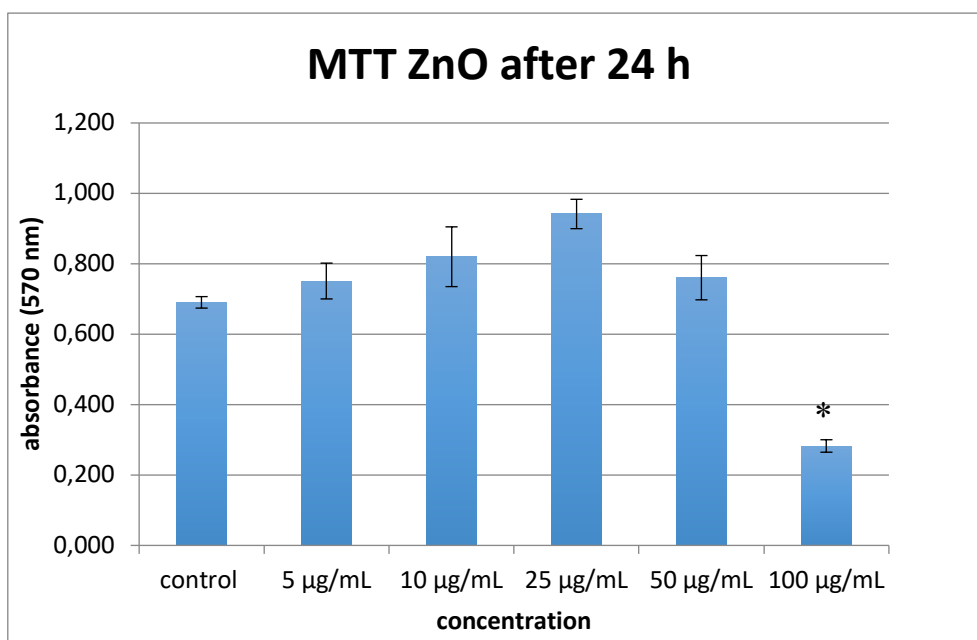


Figure 3.16 Proliferation results in terms of mitochondrial activity (MTT) of MC3T3-E1 (at 70% of confluence) and incubated for 1 day with different concentrations of ZnO NPs. ($p < 0.05$, significant differences compared to control denoted by an asterisk (*))

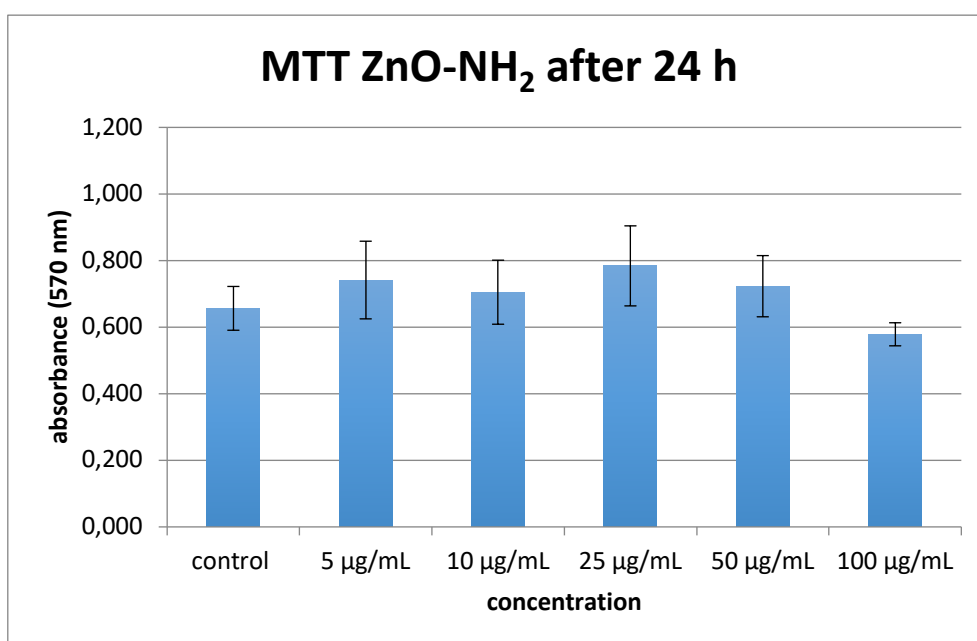


Figure 3.17 Proliferation results in terms of mitochondrial activity (MTT) of MC3T3-E1 (at 70% of confluence) and incubated for 1 day with different concentrations of ZnO-NH₂ NPs. ($p < 0.05$, significant differences compared to control denoted by an asterisk (*))

3.3.5 Cell morphology studies

Fluorescence microscope images give further information and permit to investigate the cell morphology after ZnO nanoparticle incubation and internalization. Actin was stained with Atto 565-conjugated phalloidin (red) and nuclei stained with DAPI (blue). Images in Figures 3.18 show the typical well-spread morphology of osteoblasts up to a concentration of 50 $\mu\text{g/ml}$. The cells related to pristine ZnO at a concentration of 100 $\mu\text{g/ml}$ exhibit a spherical morphology and minor confluence, that means a cytotoxic effect of this concentration.

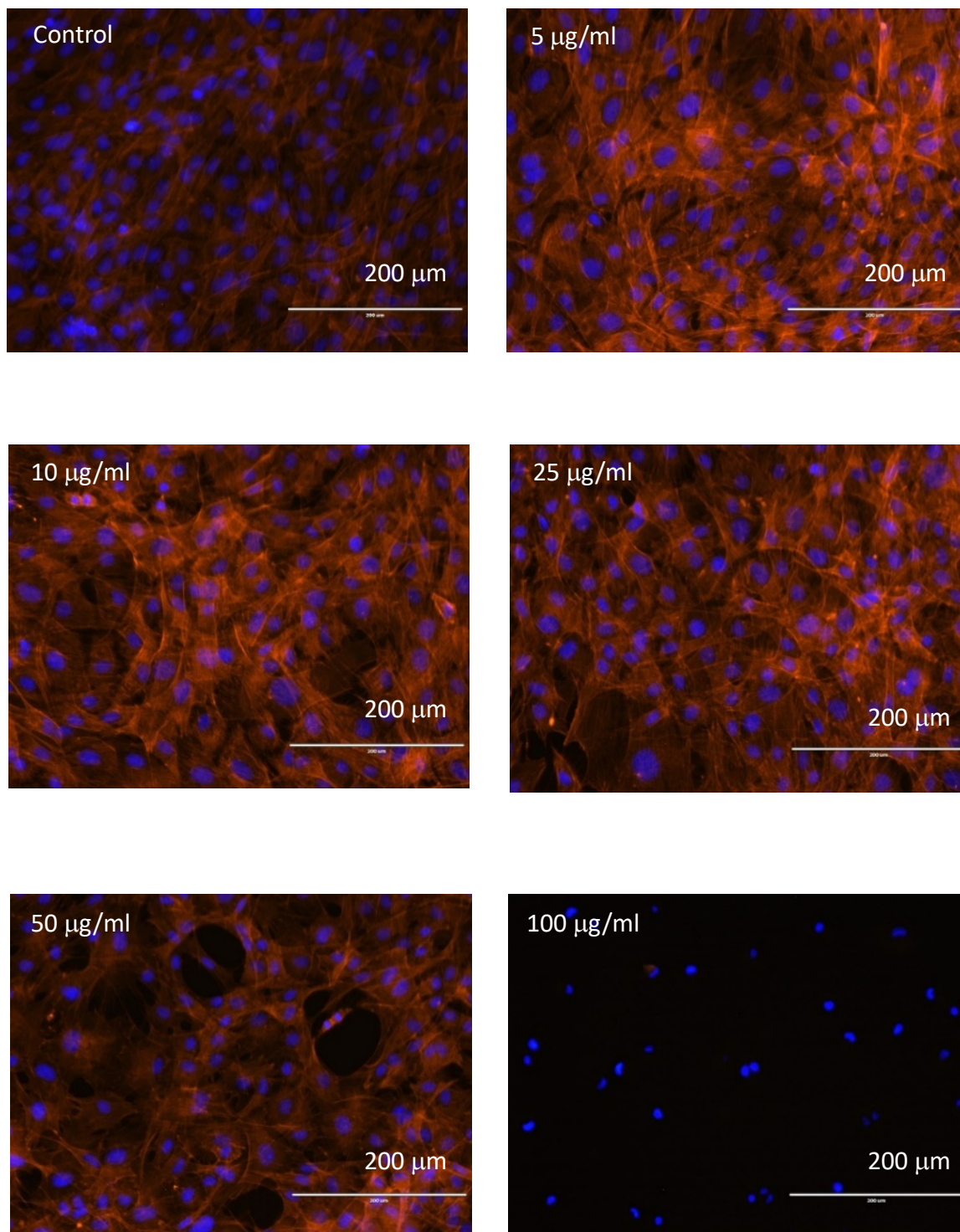


Figure 3.18 Fluorescent microscope images of pre-osteoblasts cultured up to 70 % of confluence after incubation for 4 days with ZnO NPs at different concentrations.

Regarding the functionalized ZnO NPs, this effect is less notable, because the cells in contact with 100 $\mu\text{g/ml}$ show a well-spread morphology, but the grade of confluence is sensibly inferior compared to the control cells. These results have confirmed the previous results, evidencing a good biocompatibility of ZnO up to 50 $\mu\text{g/ml}$. In addition, ZnO-NH₂ resulted more biocompatible, especially for the highest sample concentrations.

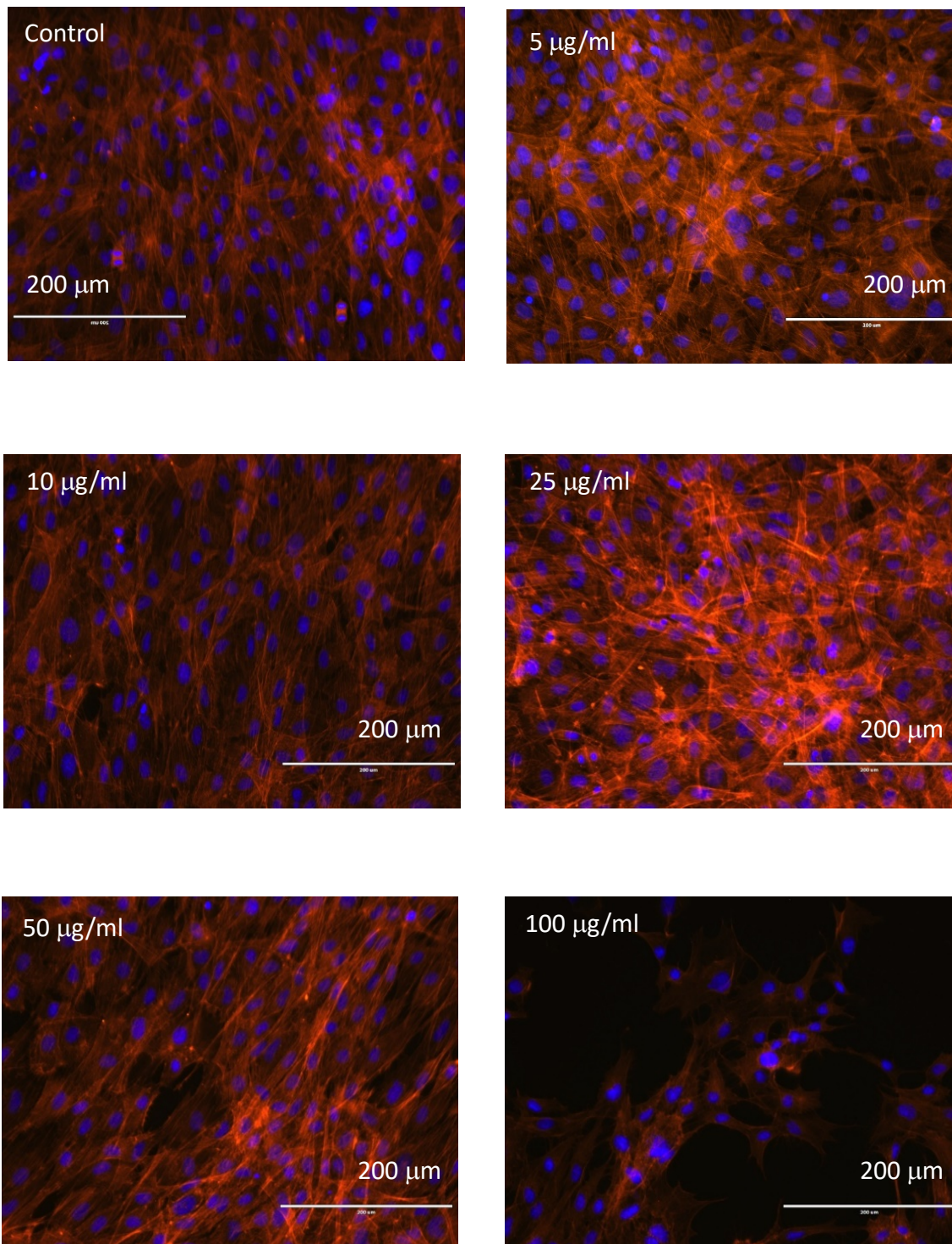


Figure 3.19 Fluorescent microscope images of pre-osteoblasts cultured up to 70 % of confluence after incubation for 4 days with ZnO-NH₂ NPs at different concentrations.

3.3.6 Differentiation assay: Alkaline Phosphatase

Differentiation is a process by which unspecialized cells, pre-osteoblasts, becomes specialized cells with the function to restore the bone. In this assay, ALP and the total protein content were monitored. ALP is a marker enzyme for determining osteoblasts phenotype. ALP activity and total protein amount of ZnO nanostructures was determined after 10 days of incubation. Taking a look at the results of ZnO NPs (Figure 3.20), it is possible to observe a progressive decrease of ALP activity by increasing the concentration of ZnO NPs, and even in this case the lowest value is for 100 µg/ml. Regarding the total protein content, the trend is very similar to ALP activity. No significant differences are observed up to a concentration of 10 µg/ml, while there is a drop from 25 µg/ml to higher concentration values. The total protein content for 100 µg/ml is sensibly low. Therefore, ZnO content negatively affects the process of differentiation, due to the lower ALP activity and total protein content compared to the control cells. On the other side, the ZnO-NH₂ NPs have shown (Figure 3.21) a different behaviour. As it can be observed, there are no significant differences compared to control for the ALP activity, except for the highest concentration of 100 µg/ml.

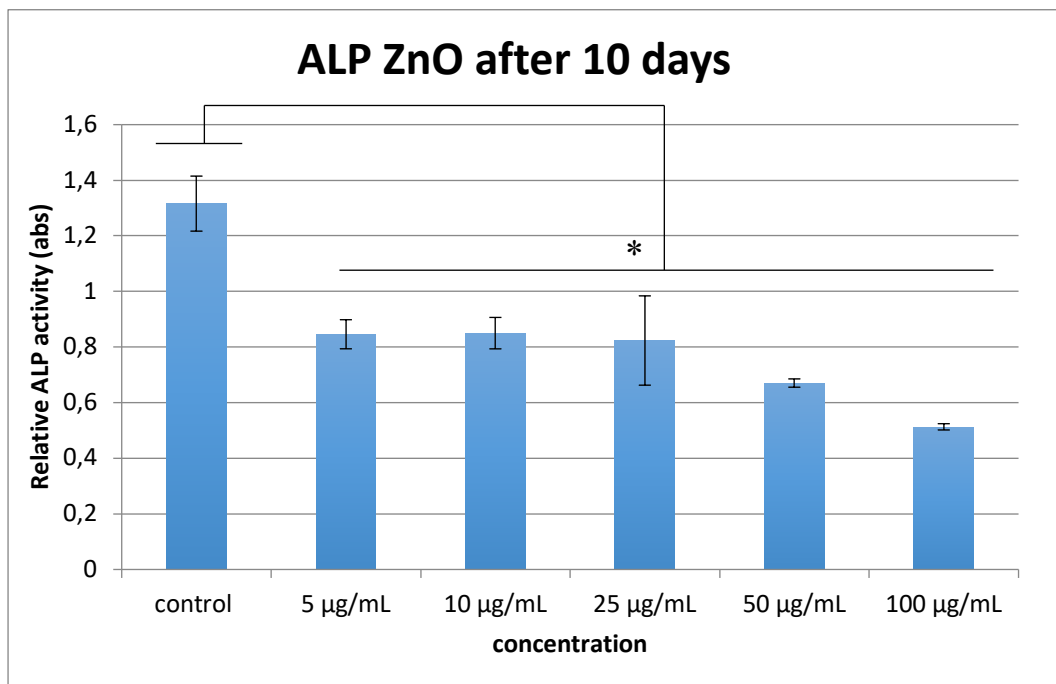


Figure 3.20 Differentiation assays in term of alkaline phosphatase activity (ALP) after 10 days of incubation with ZnO NPs at different concentrations. ($p < 0.05$, significant differences compared to control denoted by an asterisk (*))

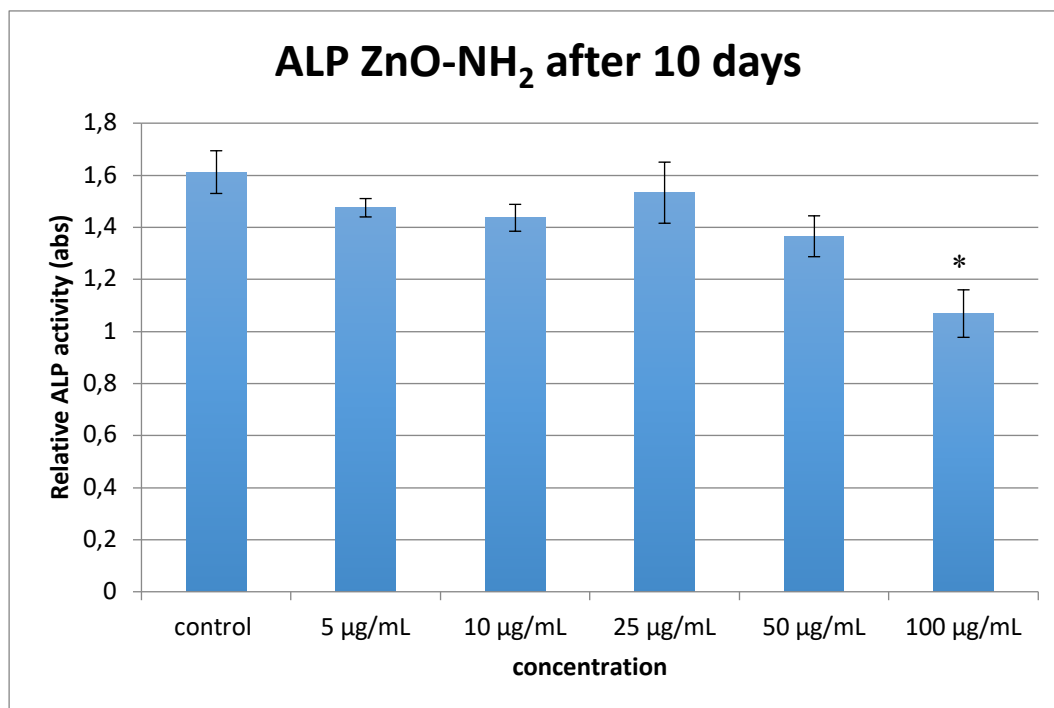


Figure 3.21 Differentiation assays in term of alkaline phosphatase activity (ALP) after 10 days of incubation with ZnO-NH₂ NPs at different concentrations. ($p < 0.05$, significant differences compared to control denoted by an asterisk (*))

3.3.7 Total protein content and cell morphology

The pattern concerning total protein content is comparable with ALP. (Figure 3.22). Therefore, ZnO-NH₂ NPS show a positive behavior up to 50 µg/ml inducing osteoblasts differentiation. In addition, the cell morphology was evaluated by optical microscopy. As it can be seen in the figure 3.24 and 3.25, MC3T3-E1 cells exhibit a well spread morphology, with a high grade of confluence, up to the concentration of 50 µg/ml for pristine ZnO NPs. As observed previously, the cells treated with 100 µg/ml of ZnO NPs present a spherical morphology, with a minor grade of confluence. Regarding the cells treated with ZnO-NH₂ NPs at different concentrations, in all cases a well spread morphology is observed, included the concentration of 100 µg/ml of ZnO-NH₂ NPs. The only difference was a smaller confluence for the most concentrated sample. Optical microscope images have confirmed the results of ALP activity and total protein content. In addition, these results are in agreement with previous experiment, mentioned before.

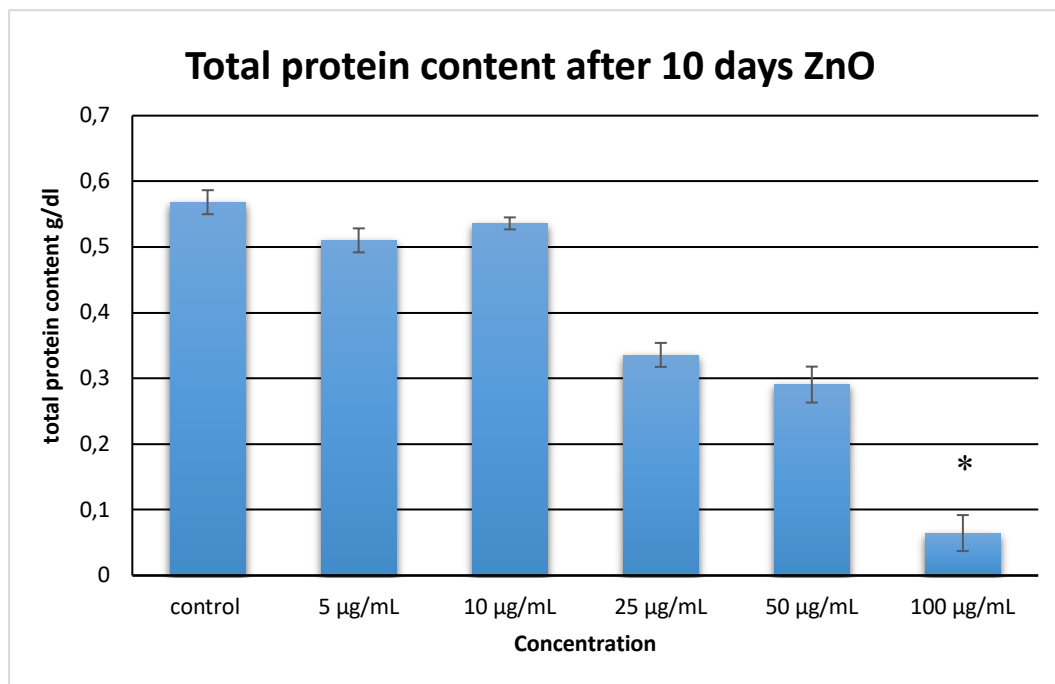


Figure 3.22 Differentiation assays in term of total protein content after 10 days of incubation with ZnO NPs at different concentrations. ($p < 0.05$, significant differences compared to control denoted by an asterisk (*))

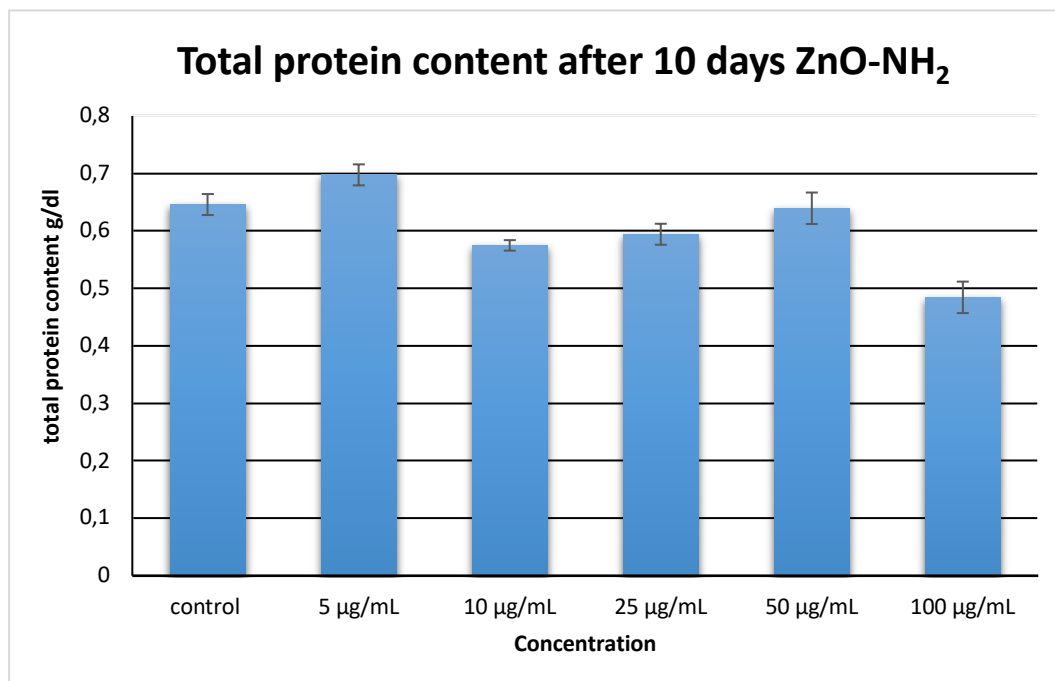


Figure 3.23 Differentiation assays in term of total protein content after 10 days of incubation with ZnO-NH₂ NPs at different concentrations. ($p < 0.05$, significant differences compared to control denoted by an asterisk (*))



Figure 3.24 Cell morphology evaluation by optical microscopy of MC3T3-E1 pre-osteoblast cells after 10 days of incubation with ZnO NPs.

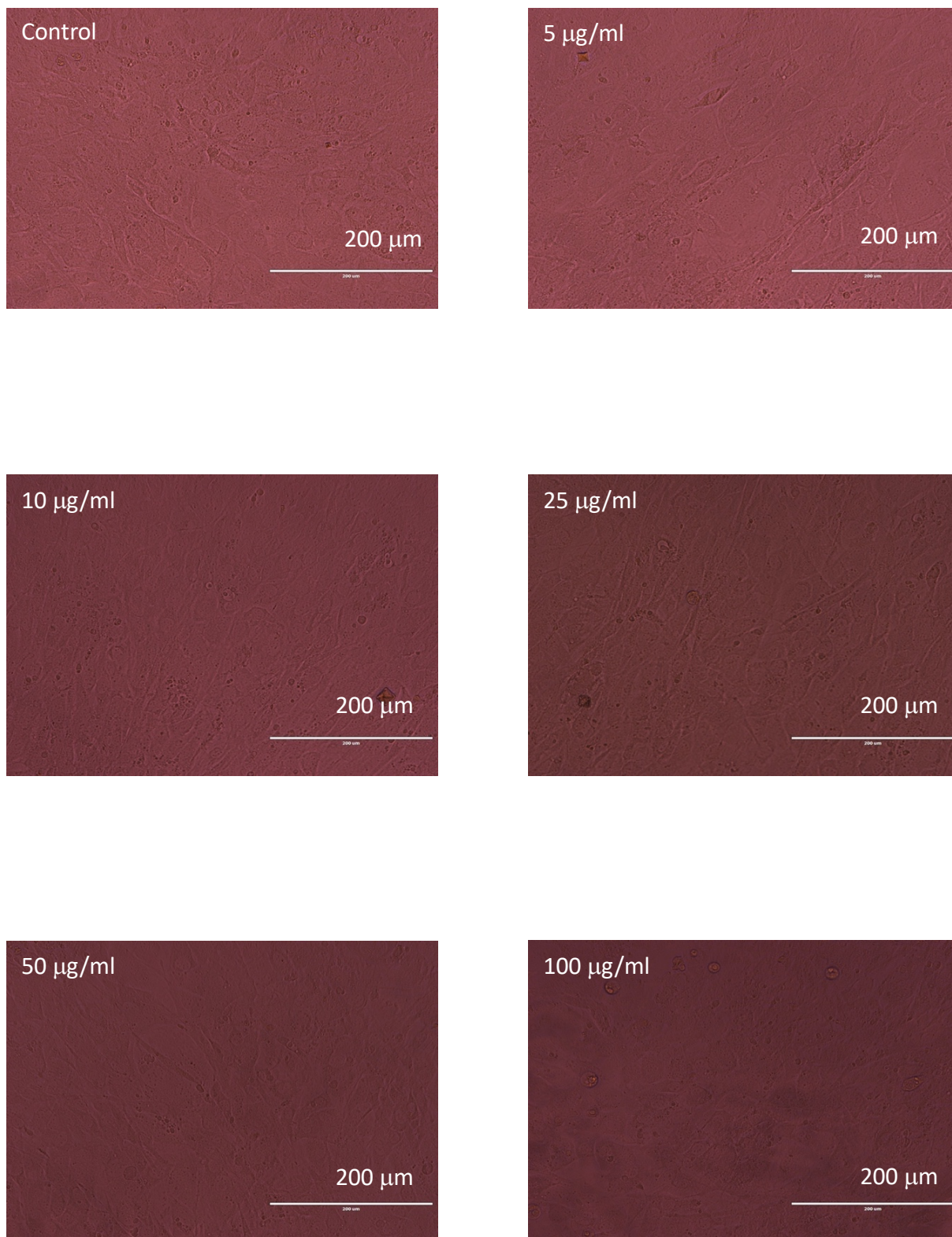


Figure 3.25 Cell morphology evaluation by optical microscopy of MC3T3-E1 pre-osteoblast cells after 10 days of incubation with ZnO-NH₂ NPs.

3.3.8 Differentiation assay for porous ZnO film: Alkaline phosphatase and total protein content

In parallel to the ZnO NPs differentiation studies, the ZnO porous films were studied to understand how a change in morphology affects the differentiation of MC3T3-E1. The ALP activity related to film is deeply different compared to control. In fact, ALP activity with the porous film sample was almost the half compared to the control cells. Moreover, ALP value is comparable to the value of 100 $\mu\text{g/ml}$ in ZnO NPs.

Taking a look at the total protein amount, there was a similar trend (Figure 3.28). The decrease in content compared to the control was sensibly high, and also in this case, similar to the concentration of 100 $\mu\text{g/ml}$ of pristine ZnO NPs. Moreover, optical images in Figure 3.26 by microscope confirm the negative effect on differentiation of the porous thin films, exhibiting a spherical morphology of the cells with a notable reduction in number, whereas a well-spread morphology is shown by the control cells. Therefore, the best performances regarding the differentiation were registered for ZnO-NH₂ NPs.

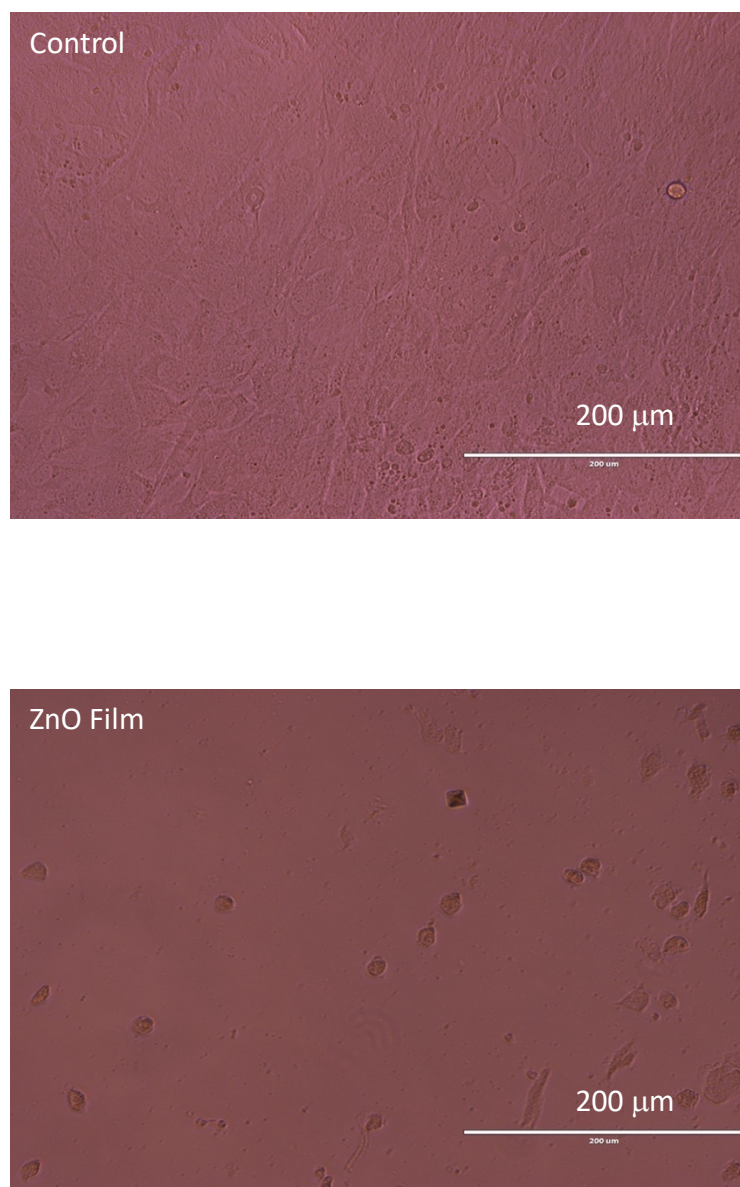


Figure 3.26 Cell morphology evaluation by optical microscopy of MC3T3-E1 pre-osteoblasts after 10 days of incubation with porous ZnO film.

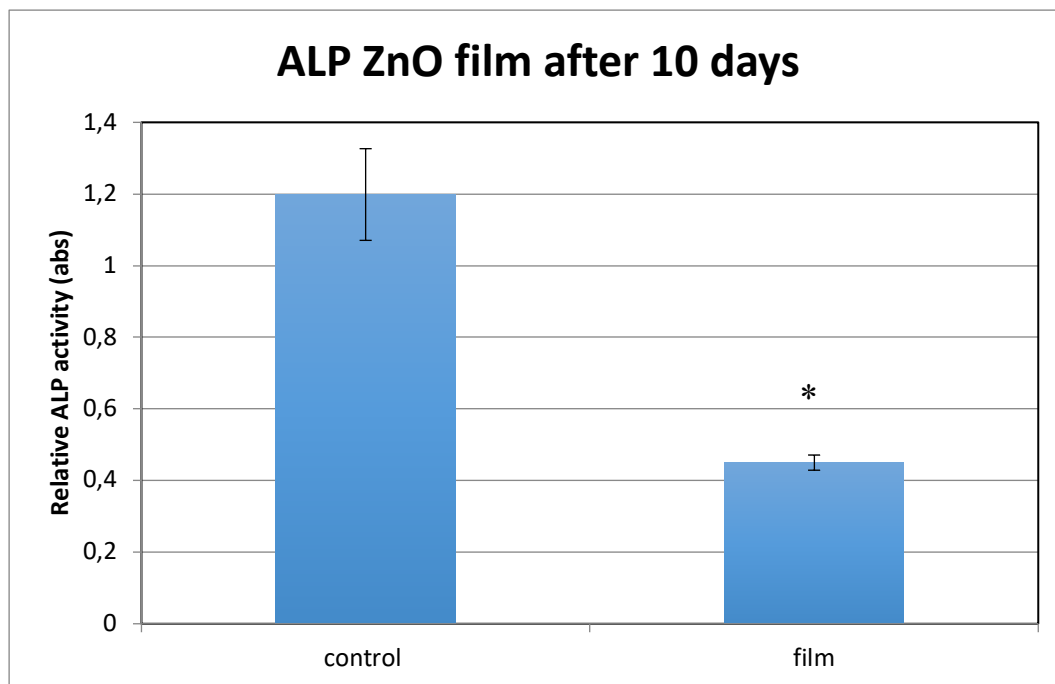


Figure 3.27 Differentiation assays in term of Alkaline phosphatase(ALP) after 10 days of incubation with porous ZnO film . ($p < 0.05$, significant differences compared to control denoted by an asterisk (*))

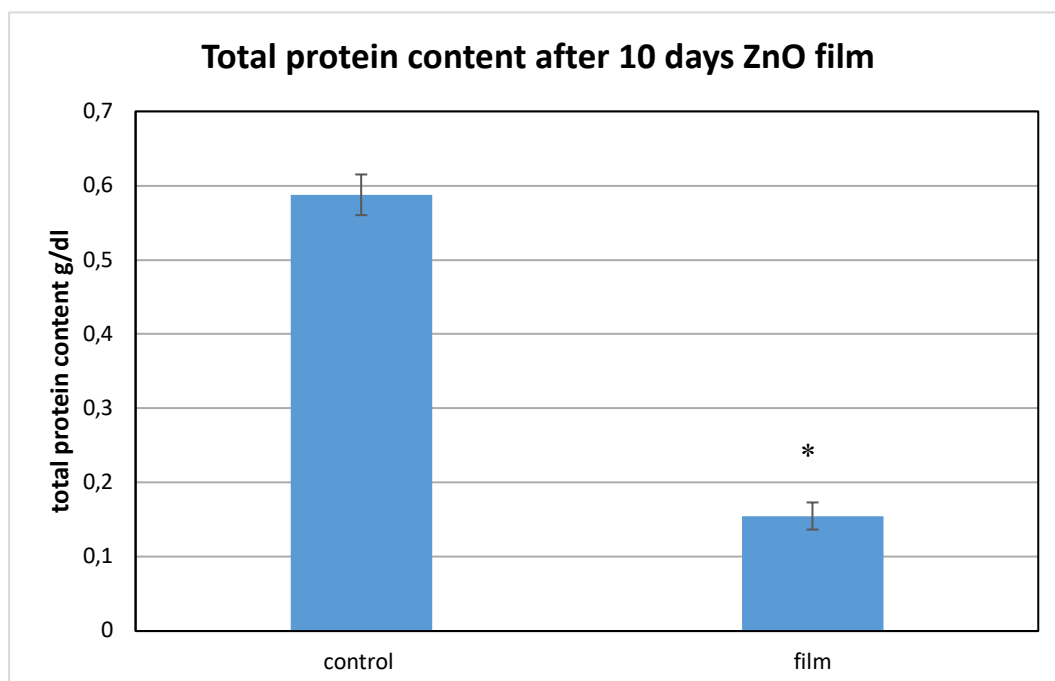


Figure 3.28 Differentiation assays in term of total protein content after 10 days of incubation with ZnO film . ($p < 0.05$, significant differences compared to control denoted by an asterisk (*))

3.4 Antibacterial studies

3.4.1 CFU counting method

The aim of CFU counting method was to probe the antibacterial activity of ZnO and ZnO-NH₂ against Gram positive (*S. aureus*) and Gram negative (*E. coli*) bacteria in planktonic stage.

The incubation time of nanoparticles with bacteria was 1 day and the antibacterial activity was studied as a function of the concentration of NPs. In next pages, the histograms show the results related to samples dilution for three times. Taking a look at these graphs, it is clear the antimicrobial activity of ZnO and ZnO-NH₂ against bacteria, however there are some differences between *E. coli* and *S. aureus*. Regarding the antimicrobial activity against *Escherichia coli*, it is very interesting to notice that there is a complete inhibition of *E. coli* growth. In addition, the results highlight that there are no effect of NPs concentration, because any concentration show a 100 % reduction of bacteria viability. The same behavior was observed both for pristine and functionalized nanoparticles. On the other side, the activity against *S. aureus* was slightly different. The peak of antimicrobial activity is for the concentration of 25 µg/ml because there is a reduction in viability around 97 %, while the smallest activity is for the concentration of 50 µg/ml resulting in 53 % inactivation. In this case, the concentration plays an important role. In particular, there is an increase in activity when the concentration of NPS increases up to 25 µg/ml, while in correspondence of the concentrations of 50 and 100 µg/ml a decrease in activity is observed. This performance can be explained by the aggregation of nanoparticles in PBS as observed by Ancona et al. [33] In fact, by increasing the concentration, there is a greater probability to form huge aggregates, that means a lower surface area to volume ratio. This behavior was not detected with *E. coli* probably because of the different shape and resistance. *E. coli* exhibits an elongated shape while *S. Aureus* a round shape, so aggregated NPs have a major probability to get in touch with *E. coli*. In addition, *S. aureus* is more resistant and pathogenic bacteria compared to *E. coli*. [34]

Concentration	<i>E. coli</i> vs ZnO	<i>E. coli</i> vs ZnO-NH ₂	<i>S. aureus</i> vs ZnO	<i>S. aureus</i> vs ZnO-NH ₂
5 µg/mL	100%	100%	83%	79%
10 µg/mL	100%	100%	93%	88%
25 µg/mL	100%	100%	97%	97%
50 µg/mL	100%	100%	87%	53%
100 µg/mL	100%	100%	92%	62%

Table 3.1 Reduction in bacteria viability after 24 h of incubation with ZnO and ZnO -NH₂ NPs

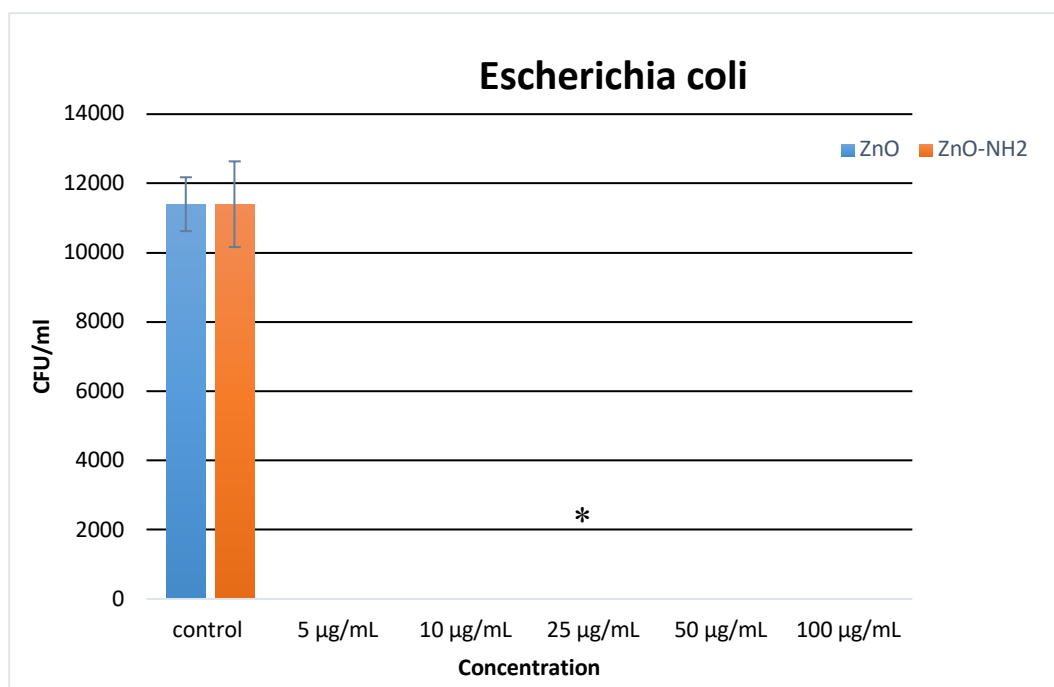


Figure 3.29 CFU per milliliter of *E. coli* in planktonic stage incubated for 24 h in the presence of different concentrations of ZnO and ZnO-NH₂ NPs. ($p < 0.05$, significant differences compared to control denoted by an asterisk (*))

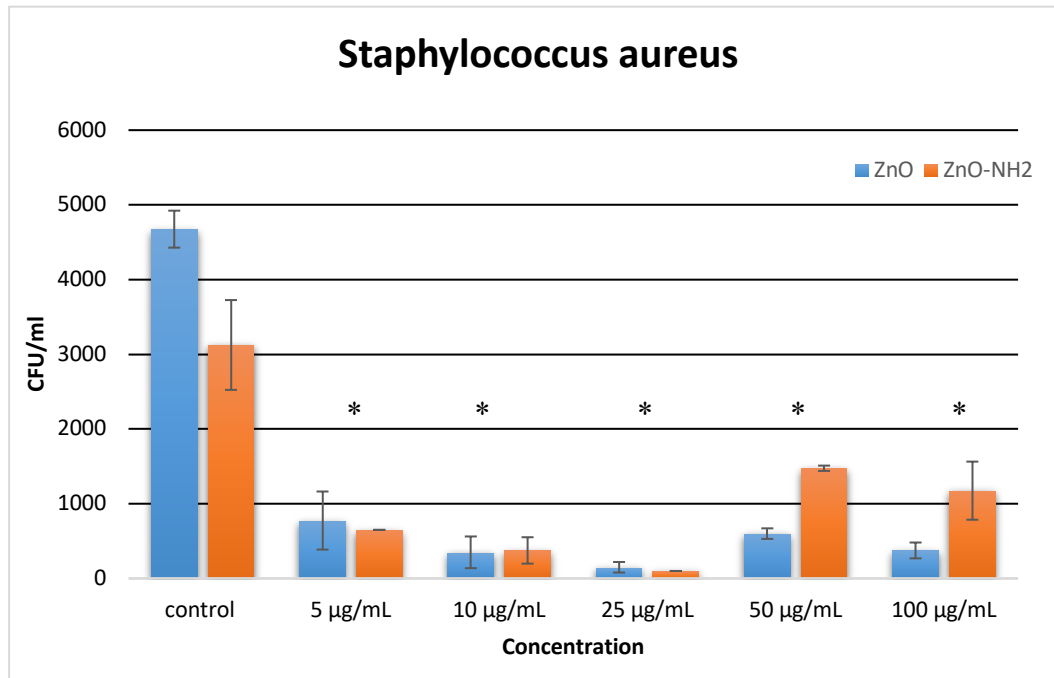


Figure 3.30 CFU per milliliter of *S. aureus* in planktonic stage incubated for 24 h in the presence of different concentrations of ZnO and ZnO-NH₂ NPs ($p < 0.05$, significant differences compared to control denoted by an asterisk (*))

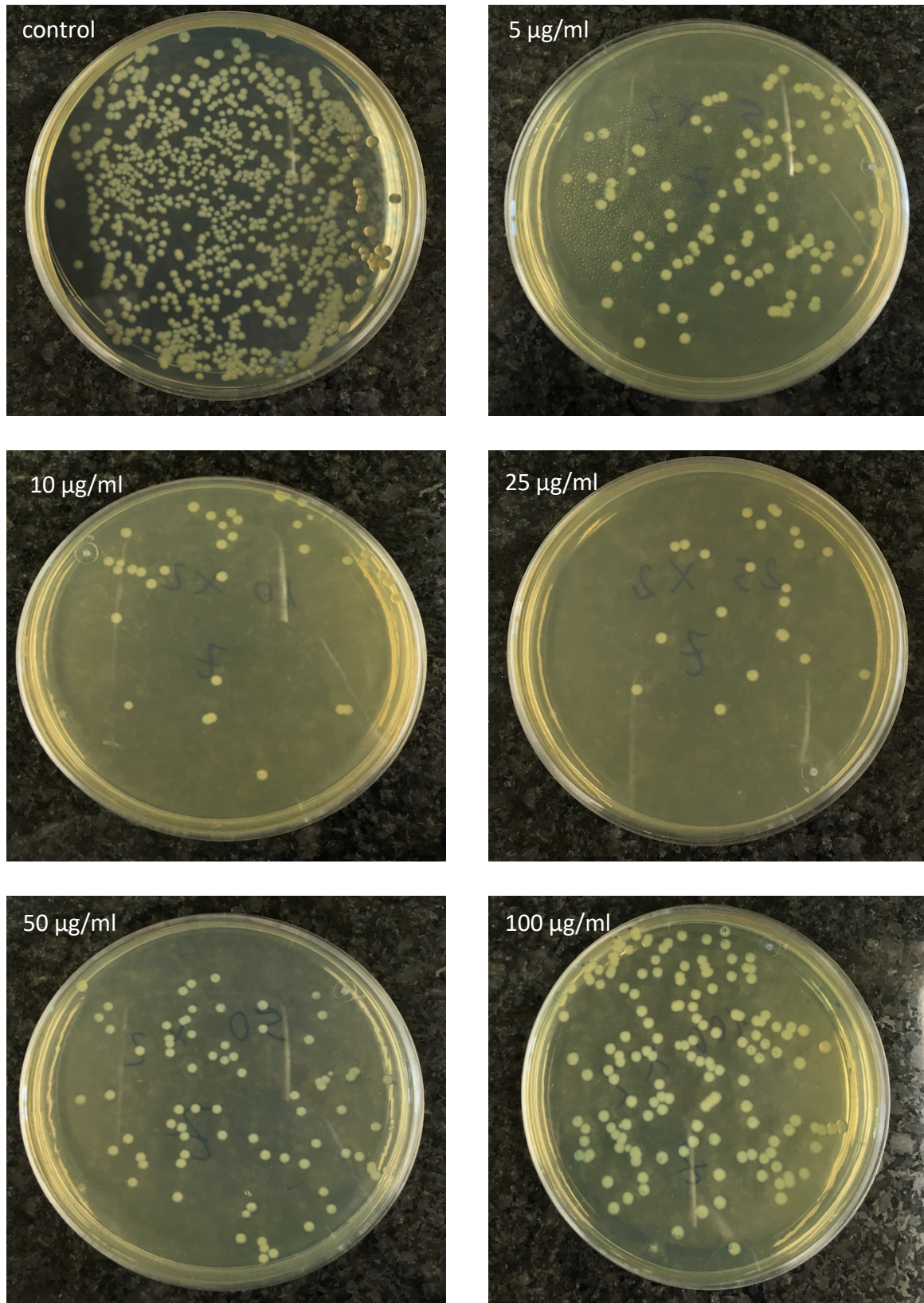


Figure 3.31 Agar plates regarding CFU counting method for *Staphylococcus aureus* after 24 h of incubation with ZnO NPs

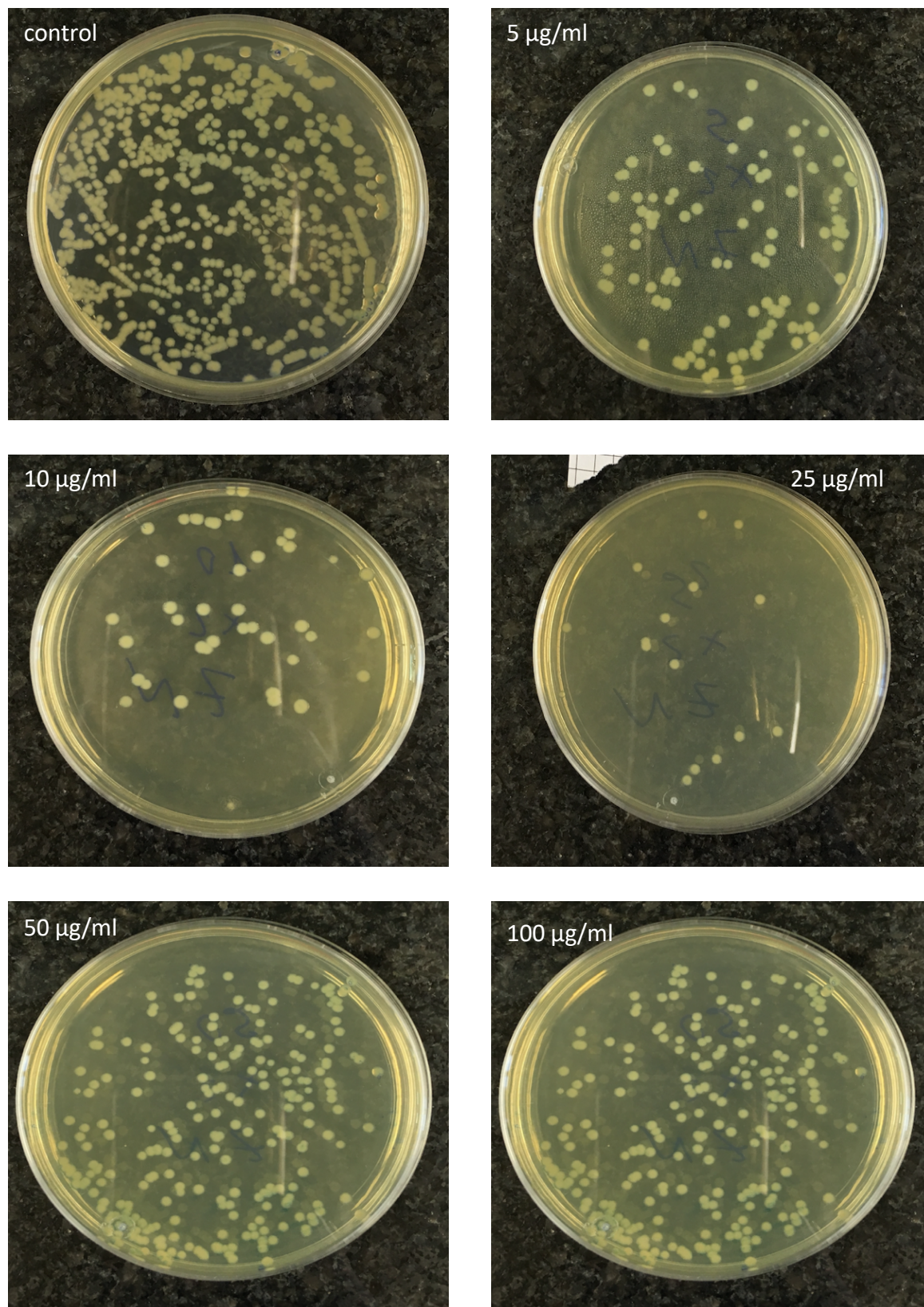


Figure 3.32 Agar plates regarding CFU counting method for *Staphylococcus aureus* after 24 h of incubation with ZnO-NH₂ NPs

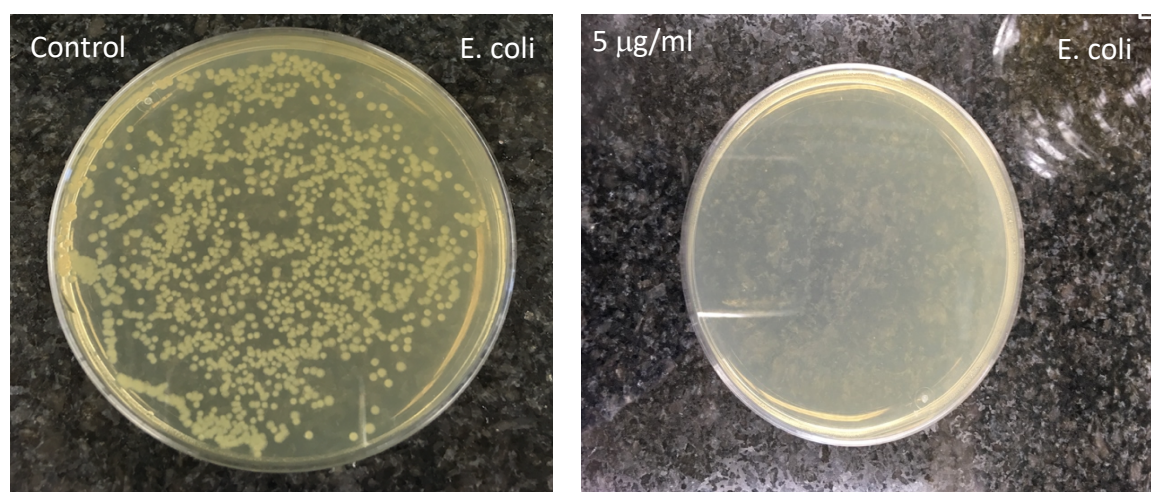


Figure 3.33 Agar plates regarding CFU counting method for *Escherichia coli* after 24 h of incubation with ZnO NPs

3.4.2 Biofilm assay

In the previous experiments the antimicrobial activity of pristine ZnO and ZnO-NH₂ NPs against bacteria in planktonic stage was demonstrated. However, it was necessary to probe their activity against bacteria in a biofilm configuration. As mentioned before, biofilm is a complex polysaccharide matrix which is able to give protection to bacteria from antibiotic. Therefore, it is more difficult and challenging to reduce the bacteria viability. In order to analyze the biofilm formation, it was necessary to image the samples under fluorescence confocal microscopy. This assay was the final experiment of the present work and the most challenging one, due to the difficulties to form a biofilm. In addition, all the previous collected information were utilized in order to have an optimization of process parameters. According to the cellular studies, the concentration of 100 µg/ml is toxic towards the pre-osteoblasts cells, so the chosen option were a concentration smaller than 100 µg/ml. Taking a look at results in planktonic stage, the concentration of 50 µg/ml was the less effective against *S. aureus* due to the sample aggregation in PBS. For these reasons, the concentration of 25 µg/ml was studied in order to perform the biofilm studies in the best conditions. Figure 3.34 shows the control. As we can note there is a high percentage of living bacteria, represented by an intense green color. After one hour of incubation with NPs, the scenario is very different. As it can be observed in Figure 3.34, there is a significant amount of dead bacteria (in red) and only a small amount of living bacteria (in green) both for ZnO and ZnO-NH₂ NPs. It is very interesting to observe that both NPs have shown a good antimicrobial activity after short time incubation and against a pre-formed bacteria colony. This result confirms the planktonic stage activity and highlights the effectiveness of ZnO as antimicrobial agent. However, further investigations are needed, with longer time of incubation, in order to better understand the ZnO (in both pristine and functionalized forms) behavior against biofilm.

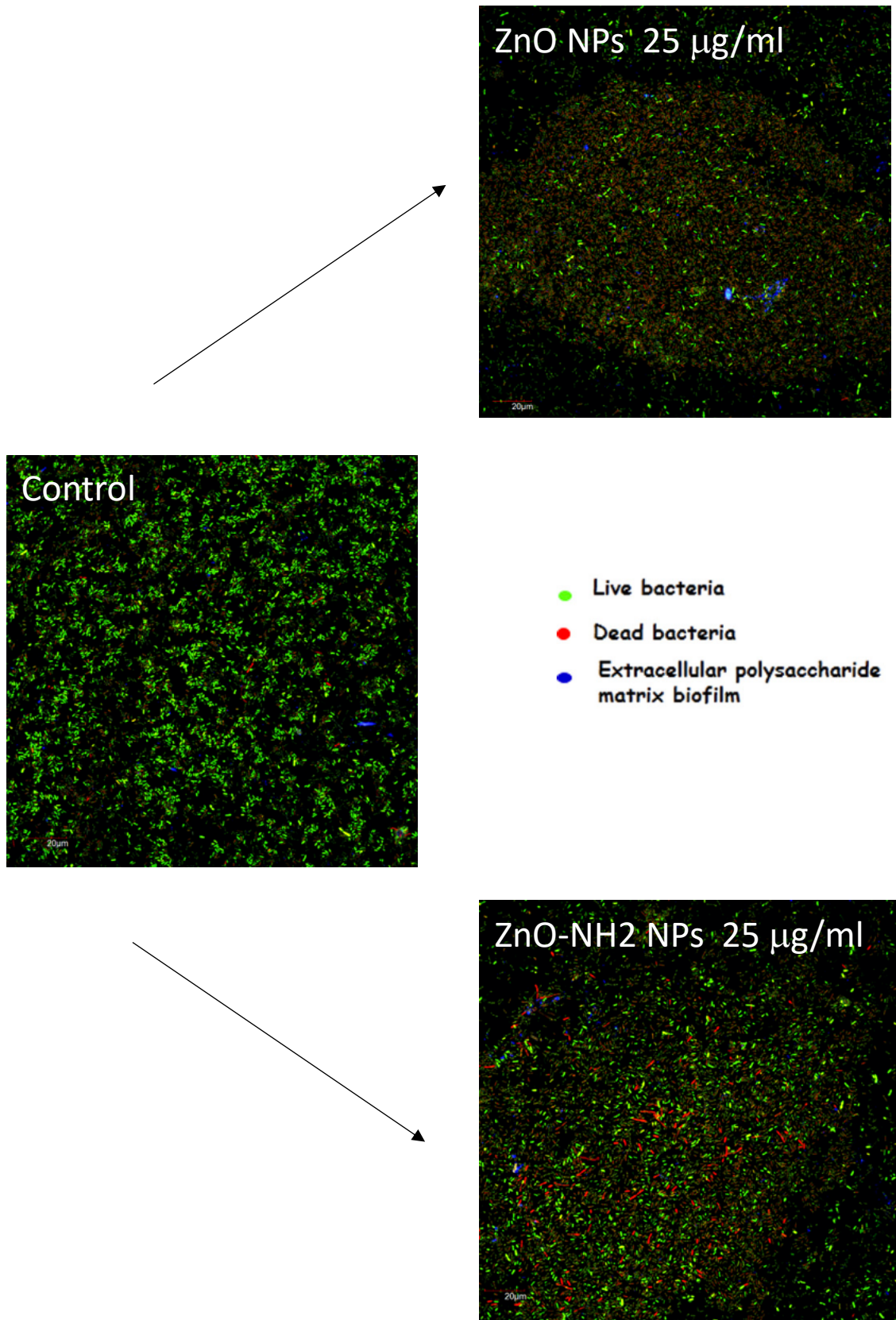


Figure 3.34 Confocal microscopy study concerning the antimicrobial activity of ZnO and ZnO-NH₂ NPs against Gram-negative *E. coli* (EC) biofilm

3.4.3 Bacterial adhesion and biofilm formation

To analyze the performance of porous ZnO films against bacteria, SEM analysis was a preliminary experiment to understand their behavior in contact with bacteria. For this purpose, the film morphology was compared with the initial morphology, therefore it was necessary to study via SEM analysis the ZnO porous films before the incubation with bacteria. SEM micrographs of films at magnification X20 highlights a deep change in the structure. In the film before, the structure is uniform and there are no deficiencies. On the other side, film after the incubation displays a loss of uniformity due to the ZnO dissolution in the bacteria medium. Regarding the magnification of X5000, micrographs have highlighted the highly porous and spongelike structure, composed of randomly oriented crystals, of the pristine films. Moreover, the surface is mainly formed by elongated and branched nanostructures, leading to a nanoporous network in both of them. However, the film after the treatment shows a less dense structure due to the loss of ZnO during the incubations with bacteria, and in addition it is clear the attachment of some *E. coli* to the structure.

Further experiments have been carried out, in particular against biofilm formation. As in the case of NPs, biofilm was analysed under fluorescence confocal microscopy. Biofilm in common infection case is caused by many species, and given that the effectiveness of ZnO porous film, it was studied against *Staphylococcus aureus* and *Escherichia coli*. Biofilm was developed at same time on the surface on the surface of ZnO films during 24 h and of cover glass disks acting as control and. As it can be observed in the fluorescence confocal images (Figure 3.36), the *E. coli* control shows a great number of living bacteria in green. Moreover, there are some areas where the green colour is more intense, representative of bacteria colonies. Taking a look at the control of *S. aureus*, there are some zones characterised by light blue and yellow spots, indicating the biofilm formation. On the other hand, the pictures related to the porous ZnO films, exhibit a very different aspect. The antimicrobial action is notable, because there are no colonies, but bacteria spread out on the surface. Moreover, there is no trace of biofilm formation. The inhibition of bacteria growth in this case could be due to hindered bacteria adhesion performed by the porous film. As seen before, bacterial adhesion is a crucial step in biofilm formation, therefore the bacteria adhesion resistance shown by ZnO film is fundamental against the biofilm formation. In addition, there is another effect of ZnO, which is the inhibition of the proliferation of bacteria and it has been demonstrated by the smaller number of bacteria compared to the control.

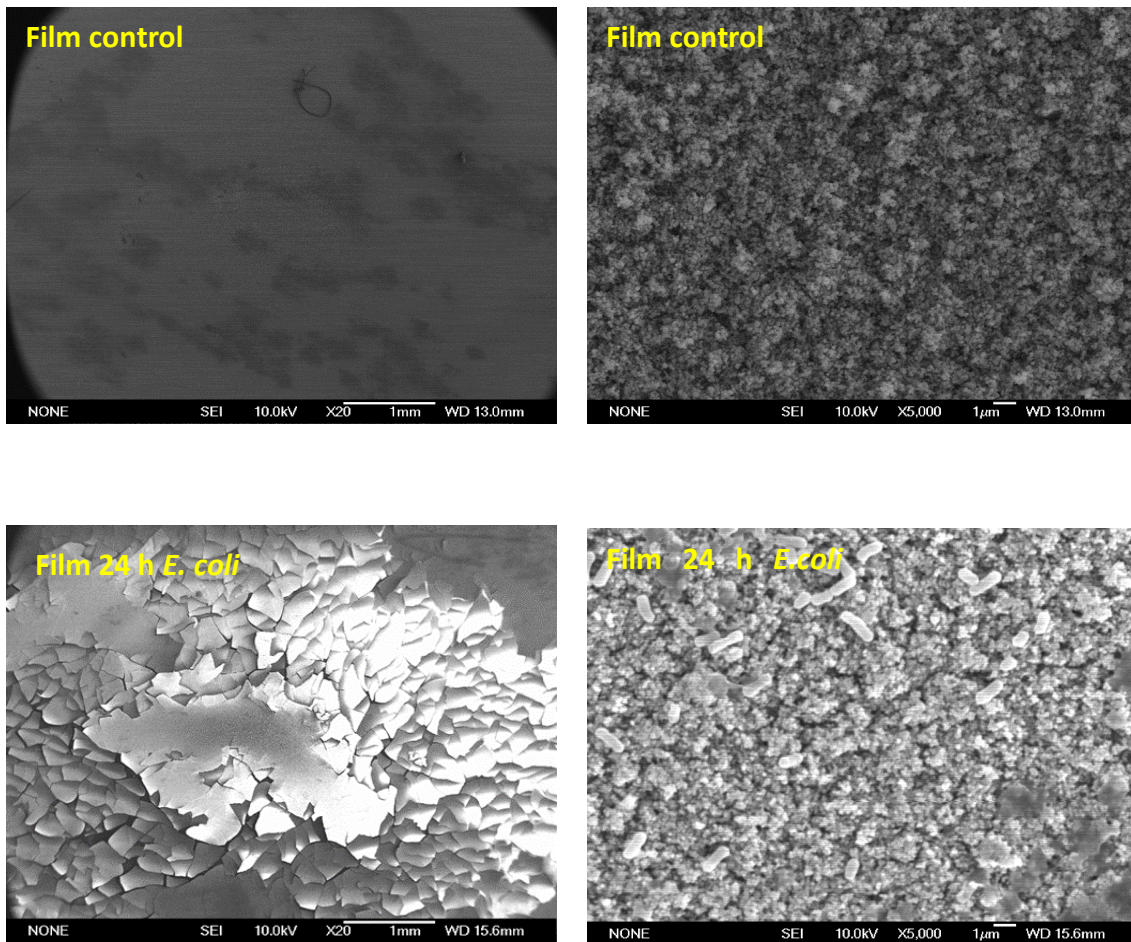


Figure 3.35 SEM micrograph about film morphology before and after the incubation for 24 h with *E. coli*.

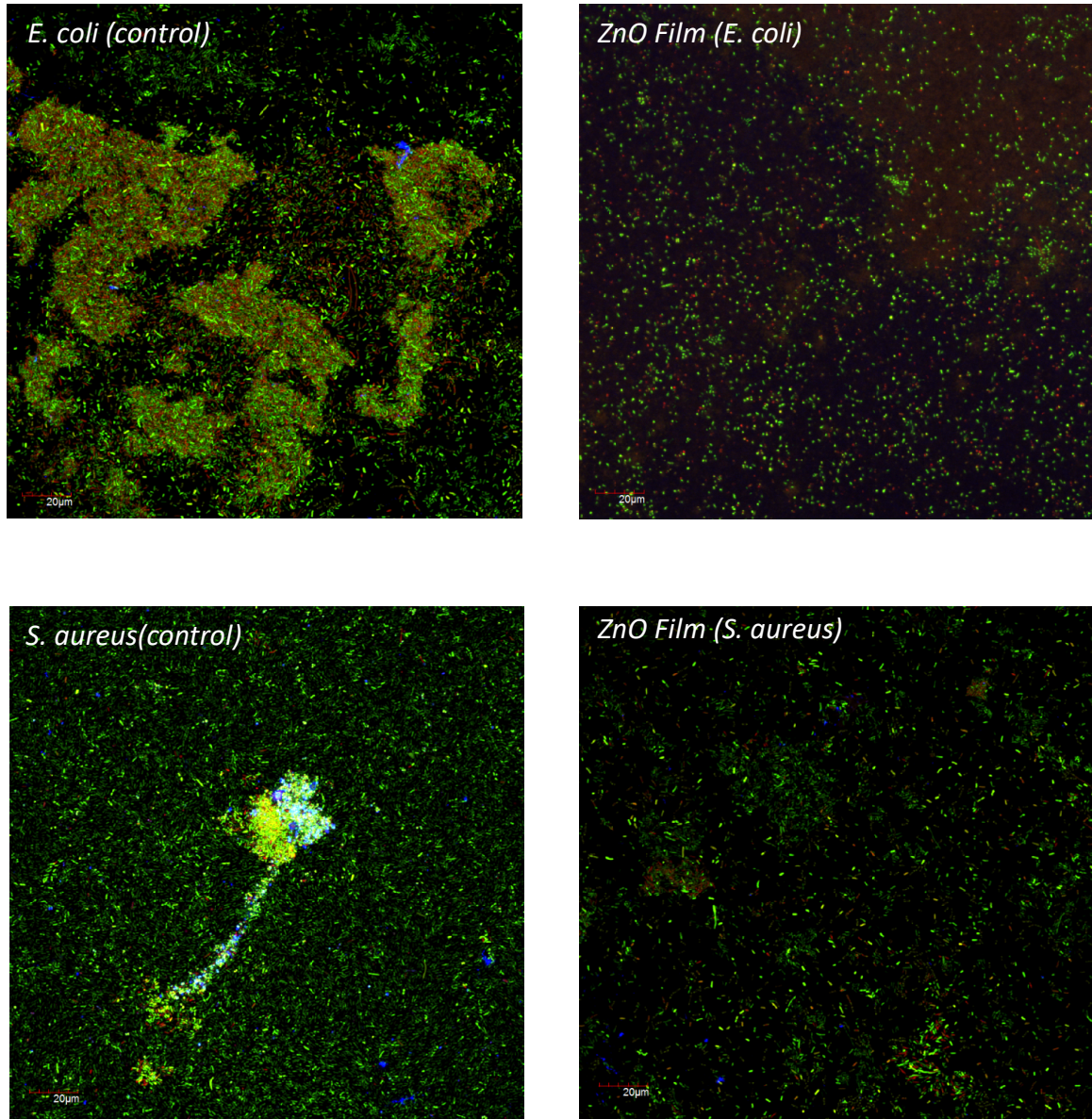


Figure 3.36 Confocal microscopy study concerning the antimicrobial activity of ZnO film against Gram-negative *E. coli* (EC) and Gram positive *Staphylococcus aureus* biofilm.

Conclusions

In the recent years, the use of nanomaterials has found interesting application in the biomedical field. In particular, nanomaterials can be used against the infections as antimicrobial agents in order to solve the problem of antibiotic resistance. Bone tissue engineering implants is a medical field, that deals with infections and antibiotic resistance due to biofilm formation of staphylococci. New approaches are needed to decrease the number of infections in bone implants, and among them nanostructures are promising candidate. ZnO could be a suitable material for these types of applications thanks to its antimicrobial activity and biocompatibility. The aim of this Master Thesis project was to investigate the antimicrobial activity of ZnO nanostructures against *Escherichia coli* and *Staphylococcus aureus* in planktonic stage and biofilm formation. Moreover, ZnO biocompatibility towards pre-osteoblast cells was analyzed. ZnO nanostructures were synthesized by microwave assisted solvothermal synthesis to obtain nanoparticles (NPs) of 20 nm in diameter and by sputtering deposition to get porous thin films. The results have highlighted a great biocompatibility of ZnO NPs, either pristine and functionalized with amino-propyl groups (i.e. ZnO-NH₂ NPs).

The cytotoxicity assay, performed measuring Lactate Hydrogenase, has shown no cytotoxic effect for ZnO and ZnO-NH₂ NPs up to the concentration of 50 µg/ml. The biocompatibility was even confirmed by cell proliferation assays, where no significant differences compared to control cells were observed up to 50 µg/ml. On the other side, the concentration of 100 µg/ml of ZnO NPs and the porous ZnO films have shown an important cytotoxic effect and smaller cell proliferation, leading to an improper biocompatibility.

In order to have a complete scenario about the biocompatibility, cell differentiation was also studied on pre-osteoblasts cells upon incubation with NPs and thin porous films. The differentiation process is a crucial step in bone regeneration and for this purpose, a preliminary study of Alkaline Phosphatase (ALP) was performed. Regarding both pristine ZnO NPs and porous films, a decrease in cell differentiation was observed by increasing the concentration. On the other hand, ZnO-NH₂ NPs exhibit a positive effect on pre-osteoblast differentiation, because the values of ALP activity are more or less in the same order of the control cells. The collected images under fluorescence confocal microscopy have confirmed the results of the previous measurements, evidencing a well spread cell morphology for the biocompatible samples and a spherical morphology with smaller grade of confluence for cytotoxic ones.

Regarding the antimicrobial activity, ZnO has displayed promising results. In fact, both pristine ZnO and ZnO-NH₂ NPs at any concentration resulted in a complete inactivation of *E. coli* activity in the planktonic stage. As regards *S. aureus* in planktonic stage, the ZnO antimicrobial activity depended on the concentration. 25 µg/ml both for both pristine and functionalized ZnO NPs exhibited the best performance, resulting in inactivation of 97 %. As demonstrated in the literature, bacteria in biofilm are more resistant, therefore further experiments will be necessary to confirm such result. ZnO and ZnO-NH₂ NPs at the concentration of 25 µg/ml were tested against bacteria biofilms. They exhibited a good activity, resulting in a diminution of living bacteria after 1 hour. However, further investigations are needed to better understand their behavior against bacteria in biofilm, especially with longer time of incubation with respect of those studied in this thesis. The porous zinc oxide film were also analyzed regarding the bacterial adhesion, a crucial step in biofilm formation. The confocal fluorescence images have highlighted a smaller percentage of bacteria on film surface compared to the control, hindering bacteria proliferation and biofilm formation.

With regard to the obtained results as a whole, the ZnO-NH₂ NPs have shown the most promising results to solve infections disease in bone implants, because of their high biocompatibility toward pre-osteoblast cells and antibacterial activity against both *E. coli* and *S. aureus*. In addition, the optimal interval of concentration ranges from 5 µg/ml to 25 µg/ml. These results have allowed to restrict the field of research on ZnO nanomaterials to specific concentration ranges and two different morphologies. However, further investigations are needed, in particular regarding the biofilm formation and osteoblast differentiation, which are two complex processes. Moreover, the experiments were performed only in vitro, therefore for their future applications in human body, in vivo assays are needed. These results will encourage and help future studies regarding the application of ZnO in bone tissue engineering or the employment of ZnO nanostructures as a new nanoantibiotics.

Bibliography

- [1] Ae Jung Huh, Young Jik Kwon. “Nanoantibiotics”: A new Paaradigm for treating infectious disease using nanomaterials in the antibiotics resistant era. *Journal of Controlled Release* .156, (2011), 128-45
- [2] D. Campoccia, L. Montanaro, C.R. Arciola. The significance of infection related to orthopedic devices and issues of antibiotic resistance, *Biomaterials*, (2006), 27, 2331–2339.
- [3] P. Zhu, ; X. Y. Weng, X. Li, X.M. Liu, S.L.Wu, K.W.K. Yeung, X.B. Wang, Cui Z.D., X.J. Yang, P.K.Chu. Biomedical Applications of Functionalized ZnO Nanomaterials: From Biosensors to Bioimaging. *Adv. Mater. Interfaces* (2016), 3, 1500494 1-30
- [4] V. Cauda, R. Gazia, S. Porro, S. Stassi, G. Canavese, I.Roppolo , A. Chiolerio , Nanostructured ZnO Materials: Synthesis, Properties and Applications. *Handbook of Nanomaterials Properties*. (2014), 137-177, DOI 10.1007/978-3-642-31107-9_32,
- [5] M. Laurenti, S. Stassi, G. Canavese, V. Cauda. Surface Engineering of Nanostructured ZnO Surfaces, *Adv. Mater. Interfaces* (2017), 1600758 1-31
- [6] H. Zazo, C. I. Colino, J. M. Lanao. Current applications of nanoparticles in infection diseases. *Journal of Controlled Release* 224 (2016), 86–102
- [7] A. Sirelkhatim, S. Mahmud, A. Seeni, N. H. M. Kaus , L. C. Ann, S. K. M. Bakhori., H. Hasan, D. Mohamad. Review on Zinc Oxide Nanoparticles: Antibacterial Activity and Toxicity Mechanism. *Nano-Micro Lett.* (2015), 7(3), 219–242
- [8] L. Montanaro, D. Campoccia, C. R. Arciola, Nanostructured materials for inhibition of bacterial adhesion in orthopedic implants: A minireview. *The international Journal of Artificial Organs*. (2008), 9 Vol 31 771-776
- [9] G. Colon, B. C. Ward, T. J. Webster. Increased osteoblast and decreased Staphylococcus epidermidis functions on nanophase ZnO and TiO₂. *Journal of Biomedical Materials Research Part A* (2006), 595-604DOI 10.1002/jbm.a
- [10] Memarzadeh K., Sharili A. S., Huang J., Rawlinson S. C. F., Allaker P. R. Nanoparticulate zinc oxide as a coating material for orthopaedic and dental implants. *Journal of biomedical material research* (2015), 103A, issue 3, 981-989 DOI: 10.1002/jbm.a.35241
- [11] V. Pokropivny, V. Skorokhod. Classification of nanostructures by dimensionality and concept of surface forms engineering in nanomaterial science. *Mater Sci Eng C* (2007), 27, 990–993
- [12] J. W. Rasmussen. Zinc oxide nanoparticles for selective destruction of tumor cells and potential for drug delivery applications. *Expert Opinion on Drug Delivery* (2010) ,7 (9):1063-1077

- [13] K. Ocakoglu, S.A. Mansour, S. Yildirimcan, A. Ahmed Al-Ghamdi, F. El-Tantawy, F. Yakuphanoglu. Microwave-assisted hydrothermal synthesis and characterization of ZnO nanorods. *Spectrochimica Acta Part A: Molecular and Biomolecular Spectroscopy* 148 (2015), 362–368
- [14] B. Dumontel, M. Canta, H. Engelke, A. Chiodoni, L. Racca, A. Ancona, T. Limongi, G. Canavese, V. Cauda. Enhanced biostability and cellular uptake of zinc oxide nanocrystals shielded with a phospholipid bilayer. *J.Mater.Chem.B*, (2017), 5, 8799-8813.
- [15] P. Dobrowolska, A. Krajewska, M. Gajda-Raczka, B. Bartosewicz, P. Nyga, B. Jankiewicz, Application of Turkevich Method for Gold Nanoparticles Synthesis to Fabrication of SiO₂ Au and TiO₂ Au Core-Shell Nanostructure, *Materials*, (2015), 8 (6), 2849-2862
- [16] R. Gazia G. Canavese, A. Chiodoni, A. Lamberti, S. Stassi, A. Sacco, S. Bianco, A. Virga, E. Tresso, C.F. Pirri R. Novel spongelike nanostructured ZnO films: Properties and applications. *Journal of Alloys and Compounds*. (2014), 331-335
- [17] <https://www.lucideon.com/testing-characterization/techniques/x-ray-diffraction-xrd>
- [18] <http://www.horiba.com/scientific/products/particle-characterization/technology/dynamic-light-scattering/>
- [19] <https://www.nobelprize.org/educational/physics/microscopes/tem/>
- [20] http://www.vcbio.science.ru.nl/public/pdf/fesem_info_eng.pdf
- [21] <https://www.thermofisher.com/es/es/home/technical-resources/media-formulation.93.html>
- [22] <http://www.thermofisher.com/es/es/home/technical-resources/media-formulation.160.html>
- [23] http://www.spinreact.com/files/Inserts/Bioquimica/BEIS16_LDH_02-2015.pdf
- [24] V. Kuete, O. Karaosmanoğlu, H. Sivas, Anticancer Activities of African Medicinal Spices and Vegetables. *Medicinal Spices and Vegetables from Africa* (2017), 10, 271-297.
- [25] R. García-Alvarez, I. Izquierdo-Barba, M. Vallet-Regí. 3D scaffold with effective multidrug sequential release against bacteria biofilm. *Acta Biomaterialia* 49, (2017), 113–126.
- [26] A. Rutkovskiy, K. O. Stensløyken, I. J. Vaage. Osteoblast Differentiation at a Glance. *Med Sci Monit Basic Res*, (2016), 22, 95-106
- [27] https://www.promocell.com/fileadmin/knowledgebase/pdfxls/Osteoblast_Differentiation_and_Mineralization.pdf
- [28] http://www.spinreact.com/files/Inserts/Bioquimica/BEIS01_ALP-AMP_BUFFER_2015.pdf
- [29] http://www.spinreact.com/files/Inserts/Bioquimica/BSIS30_PROT_TOT_02-2015.pdf

- [30] <https://www.sigmaaldrich.com/content/dam/sigma-aldrich/docs/Sigma-Aldrich/Datasheet/1/T1438dat.pdf>
- [31] <https://www.sigmaaldrich.com/content/dam/sigma-aldrich/docs/Sigma-Aldrich/Datasheet/1/22091dat.pdf>
- [32] T. R. Garrett, M. Bhakoo, Z. Zhang. Bacterial adhesion and biofilms on surfaces. *Progress in Natural Science*. 18, (2008), 1049–1056.
- [33] A. Ancona, B. Dumontel, N. Garino, B. Demarco, D. Chatzitheodoridou, W. Fazzini, H. Engelke, V. Cauda. Lipid-Coated Zinc Oxide Nanoparticles as Innovative ROS-Generators for Photodynamic Therapy in Cancer Cells. *Nanomaterials* (2018), 8, 143-150.
- [34] A. Stankovic, S. Dimitrijevic, D. Uskokovic. Influence of size scale and morphology on antibacterial properties of ZnO powders hydrothermally synthesized using different surface stabilizing agents. *Colloids and Surfaces B: Biointerfaces* 102 (2013), 21–28
- [35] G. Applerot, A. Lipovsky, R. Dror, N. Perkas, Y. Nitzan, R. Lubart, A. Gedanken. Enhanced Antibacterial Activity of Nanocrystalline ZnO Due to Increased ROS-Mediated Cell Injury. *Adv. Funct. Mater.* (2009), 19, 842–852
- [36] T. Jan, J. Iqbal, M. Ismail, M. Zakauallah S. H. Naqvi, N. Badshah. Sn doping induced enhancement in the activity of ZnO nanostructures against antibiotic resistant *S. aureus* bacteria. *International Journal of Nanomedicine* (2013), 8 3679–3687
- [37] V. Schwartz, F. Thétiot, S. Ritz, S. Pütz, L. Choritz, A. Lappas, R. Förch, K. Landfester, U. Jonas. Antibacterial Surface Coatings from Zinc Oxide Nanoparticles Embedded in Poly(N-isopropylacrylamide) Hydrogel Surface Layers. *Adv. Funct. Mater.* (2012), 22, 2376–2386
- [38] K. M. Reddy, K. Feris, J. Bell, D. G. Wingett, C. Hanley, A. Punnoosea. Selective toxicity of zinc oxide nanoparticles to prokaryotic and eukaryotic systems. *Applied physics letters* (2007), 90, 213-215
- [39] R. Brayner,† R. Ferrari-Iliou, N. Brivois, S. Djediat, M. F. Benedetti, F. Fievet. Toxicological Impact Studies Based on *Escherichia coli* Bacteria in Ultrafine ZnO Nanoparticles Colloidal Medium. *Nanoletters* (2006), 6, 4, 866-870.
- [40] E. H. Abdulkareema, K. Memarzadeh, R.P. Allakerb, J. Huangc, J. Prattena, D. Spratta. Anti-biofilm activity of zinc oxide and hydroxyapatite nanoparticles as dental implant coating materials. *Journal of Dentistry* 43 (2015), 1462–1469.
- [41] S. Dwivedi, R. Wahab, F. Khan, Y. K. Mishra, J. Musarrat, A. A. Al-Khedhairi. Reactive Oxygen Species Mediated Bacterial Biofilm Inhibition via Zinc Oxide Nanoparticles and Their Statistical Determination. *Plos one*. (2014), Vol 9, issue 11, 1-9.
- [42] B. Sevinc, L. Hanley. Antibacterial activity of dental composites containing zinc oxide nanoparticles. *Journal of biomedical material*. (2010), Vol 94B, Issue 122-131
- [43] G. Applerot, J. Lellouche, N. Perkas, Y. Nitzan, A. Gedanken, E. Banin. ZnO nanoparticle-coated surfaces inhibit bacterial biofilm formation and increase antibiotic susceptibility. *Royal Society Chemistry Adv.*, (2012), 2, 2314–2321

- [44] B. Park, Y. J. Kim, J. Yeom, J. H. Jeon, G. C. Yi, J. H. Je, S. K. Hahn. The Topographic Effect of Zinc Oxide Nanoflowers on Osteoblast Growth and Osseointegration. *Adv. Mater.* (2010), 22, 4857–4861.
- [45] K. S. Suh, Y. S. Lee, S. H. Seo, Y. S. Kim, E. M. Choi. Effect of Zinc Oxide Nanoparticles on the Function of MC3T3-E1 Osteoblastic Cells *Biol. Trace. Elem. Res.* (2013), 155, 287–294.
- [46] M. Laurenti, V. Cauda. ZnO Nanostructures for Tissue Engineering Applications. *Nanomaterials*, (2017), 7, 374, 1-35

Ringraziamenti

Innanzitutto, desidero ringraziare la professoressa Valentina Cauda per la grande disponibilità e per l'enorme opportunità concessomi di studiare all'estero. Inoltre, ringrazio il Dott. Marco Laurenti e la Dott.ssa Nadia Garino per l'aiuto prezioso nel corso di questo lavoro. Visto il mio periodo di permanenza all'estero non posso che ringraziare i dottorandi e i professori che mi hanno sostenuto e aiutato nel laboratorio di Madrid, in particolare Nati, Noemi, Anna e Adrian. Il grazie più grande va però ai miei genitori, a mia sorella e mia zia Gisella che sono stati fondamentali per la riuscita e il completamento di questo percorso. Oltre all'amore che mi date ogni giorno, vi ringrazio per la fiducia e la serenità che mi trasmettete nelle mie scelte. Tra le persone da ringraziare, non posso dimenticare Enzo, praticamente un fratello acquisito, fonte di ispirazione e di rassicurazione. Grazie agli amici conosciuti in questi 2 anni e mezzo a Torino, in particolare Danilo, Antonio, Fabrizio, Tonia, Federica, che in ogni occasione mi hanno mostrato il loro affetto e mi hanno sopportato e supportato nei momenti bui. Grazie a Rosaria, per l'ospitalità, per l'affetto, per le nottate a studiare insieme, in pratica una mamma, una sorella, una amica. Grazie agli amici di sempre, Annino, Marco, Carmen, Luigi che anche stando molto lontani si sono mostrati più vicini che mai. Ringrazio ancora una volta la professoressa Patrone che non mi fa mancare mai la sua fiducia e la sua sopravvalutazione nei miei confronti. Grazie Edisu per il pasto ridotto, per la casa gratis, ma soprattutto per avermi fatto conoscere tante belle persone provenienti da parti diverse, tutte con una storia da raccontare. Grazie ping pong perchè nonostante tutto mi hai permesso di pagare gli studi e di incontrare dei ragazzi fantastici come Andrea, Paolo, Luca, Vincenzo, Stefano ed Alfonso. Infine ringrazio tutti quelli che ho incontrato e che mi hanno saputo donare sempre un qualcosa in più.

List Of Figures

Figure 1.1 Antimicrobial mechanisms of inorganic nanostructures (modified from [1]).....	5
Figure 1.2 ZnO crystal structures [4]	6
Figure 1.3 Antimicrobial mechanisms of ZnO nanostructures.....	9
Figure 2.1 ZnO functionalization with amino groups (modified from [15]).....	10
Figure 2.2 Cover glasses of ZnO film before (left) and after thermal oxidation (right)	12
Figure 2.3 24-well plates used in the assays.....	17
Figure 2.4 Scheme of osteoblasts differentiation and mineralization (modified from [27])....	20
Figure 2.5 24 well-plates used in the assays.....	25
Figure 3.1 XRD pattern for ZnO NPs	27
Figure 3.2 XRD pattern for ZnO-NH ₂ NPs	28
Figure 3.3 Distribution curves deriving from DLS measurement for ZnO NPs.....	29
Figure 3.4 Distribution curves deriving from DLS measurement for ZnO-NH ₂ NPs	29
Figure 3.5 - Tem micrographs of ZnO -NH ₂ NPs at different magnification	30
Figure 3.6 - Tem micrographs of ZnO NPs at different magnification.....	30
Figure 3.7 XRD pattern of porous ZnO thin film	31
Figure 3.8 FESEM micrographs of porous ZnO thin film	32
Figure 3.9 FESEM micrograph (cross section) of porous ZnO film.....	33
Figure 3.10 Cytotoxicity by lactate dehydrogenase (LDH) released into the medium after 3 days of incubation with different concentrations of ZnO NPs. (p < 0.05, significant differences compared to control denoted by an asterisk (*)).....	34
Figure 3.11 Cytotoxicity by lactate dehydrtheogenase (LDH) released into the medium after 3 days of incubation with different concentrations of ZnO-NH ₂ NPs (p < 0.05, significant differences compared to control denoted by an asterisk (*)).....	35
Figure 3.12 Proliferation results in terms of mitochondrial activity (MTT) after 3 days of incubation and with different concentrations of ZnO NPs. (p < 0.05, significant differences compared to control denoted by an asterisk (*)).....	36
Figure 3.13 Proliferation results in terms of mitochondrial activity (MTT) after 3 days of incubation and with different concentrations of ZnO-NH ₂ NPs. (p < 0.05, significant differences compared to control denoted by an asterisk (*)).....	36

Figure 3.14 Cytotoxicity by lactate dehydrogenase (LDH) released into the medium after 3 days of incubation with porous ZnO film. ($p < 0.05$, significant differences compared to control denoted by an asterisk (*)).....	37
Figure 3.15 Proliferation results in terms of mitochondrial activity (MTT) after 3 days of incubation with porous ZnO film. ($p < 0.05$, significant differences compared to control denoted by an asterisk (*)).....	38
Figure 3.16 Proliferation results in terms of mitochondrial activity (MTT) of MC3T3-E1 (at 70% of confluence) and incubated for 1 day with different concentrations of ZnO NPs. ($p < 0.05$, significant differences compared to control denoted by an asterisk (*)).....	39
Figure 3.17 Proliferation results in terms of mitochondrial activity (MTT) of MC3T3-E1 (at 70% of confluence) and incubated for 1 day with different concentrations of ZnO-NH ₂ NPs. ($p < 0.05$, significant differences compared to control denoted by an asterisk (*)).....	39
Figure 3.18 Fluorescent microscope images of pre-osteoblasts cultured up to 70 % of confluence after incubation for 4 days with ZnO NPs at different concentrations.....	40
Figure 3.19 Fluorescent microscope images of pre-osteoblasts cultured up to 70 % of confluence after incubation for 4 days with ZnO-NH ₂ NPs at different concentrations.....	41
Figure 3.20 Differentiation assays in term of alkaline phosphatase activity (ALP) after 10 days of incubation with ZnO NPs at different concentrations. ($p < 0.05$, significant differences compared to control denoted by an asterisk (*)).....	42
Figure 3.21 Differentiation assays in term of alkaline phosphatase activity (ALP) after 10 days of incubation with ZnO-NH ₂ NPs at different concentrations. ($p < 0.05$, significant differences compared to control denoted by an asterisk (*)).....	43
Figure 3.22 Differentiation assays in term of total protein content after 10 days of incubation with ZnO NPs at different concentrations. ($p < 0.05$, significant differences compared to control denoted by an asterisk (*)).....	44
Figure 3.23 Differentiation assays in term of total protein content after 10 days of incubation with ZnO-NH ₂ NPs at different concentrations. ($p < 0.05$, significant differences compared to control denoted by an asterisk (*)).....	44
Figure 3.24 Cell morphology evaluation by optical microscopy of MC3T3-E1 pre-osteoblast cells after 10 days of incubation with ZnO NPs.	45
Figure 3.25 Cell morphology evaluation by optical microscopy of MC3T3-E1 pre-osteoblast cells after 10 days of incubation with ZnO-NH ₂ NPs.	46
Figure 3.26 Cell morphology evaluation by optical microscopy of MC3T3-E1 pre-osteoblasts after 10 days of incubation with porous ZnO film.....	47
Figure 3.27 Differentiation assays in term of Alkaline phosphatase(ALP) after 10 days of incubation with porous ZnO film . ($p < 0.05$, significant differences compared to control denoted by an asterisk (*)).....	48

Figure 3.28 Differentiation assays in term of total protein content after 10 days of incubation with ZnO film . (p < 0.05, significant differences compared to control denoted by an asterisk (*)).....	48
Figure 3.29 CFU per milliliter of E. coli in planktonic stage incubated for 24 h in the presence of different concentrations of ZnO and ZnO-NH ₂ NPs. (p < 0.05, significant differences compared to control denoted by an asterisk (*)).....	50
Figure 3.30 CFU per milliliter of S. aureus in planktonic stage incubated for 24 h in the presence of different concentrations of ZnO and ZnO-NH ₂ NPs (p < 0.05, significant differences compared to control denoted by an asterisk (*)).....	50
Figure 3.31 Agar plates regarding CFU counting method for Staphylococcus aureus after 24 h of incubation with ZnO NPs.....	51
Figure 3.32 Agar plates regarding CFU counting method for Staphylococcus aureus after 24 h of incubation with ZnO-NH ₂ NPs.....	52
Figure 3.33 Agar plates regarding CFU counting method for Escherichia coli after 24 h of incubation with ZnO NPs.....	53
Figure 3.34 Confocal microscopy study concerning the antimicrobial activity of ZnO and ZnO-NH ₂ NPs against Gram-negative E. coli (EC) biofilm	54
Figure 3.35 SEM micrograph about film morphology before and after the incubation for 24 h with E. coli.....	56
Figure 3.36 Confocal microscopy study concerning the antimicrobial activity of ZnO film against Gram-negative E. coli (EC) and Gram positive Staphylococcus aureus biofilm.....	57

List Of Tables

Table 2.1 – Sputtering synthesis conditions	12
Table 2.2 - Composition of α -MEM [21].....	17
Table 2.3 - Composition of PBS 1x [22].....	17
Table 2.4 Reagents of LDH measurement [23]	18
Table 2.5 Reagents for ALP measurement [28].....	21
Table 2.6 Reagents for total protein content measurement[29].....	22
Table 2.7 Composition of Todd Hewitt Broth [30].....	23
Table 2.8 Composition of Tryptic Soy Agar (Sigma Aldrich) [31].....	24
Table 3.1 Reduction in bacteria viability after 24 h of incubation with ZnO and ZnO -NH ₂ NPs	49